Miocene carbonate platform slopes

Dissertation
with the aim of achieving a doctoral degree
at the Faculty of Mathematics, Informatics and Natural Sciences
Department of Geology
of Universität Hamburg

Submitted by

Jesús Reolid Pérez

from
Granada

Hamburg
2016

Eidesstattliche Versicherung

Declaration on oath

Hiermit erkläre ich an Eides statt, dass ich die vorliegende Dissertationsschrift selbst verfasst und keine anderen als die angegebenen Quellen und Hilfsmittel benutzt habe.

I hereby declare, on oath, that I have written the present dissertation by my own and have not used other than the acknowledged resources and aids.

Hamburg, den *Unterschrift*

Day of oral defense: 19th of October 2016

The following evaluators recommend the admission of the dissertation:

Prof. Dr. Christian Betzler

Prof. Dr. Juan Carlos Braga Alarcón

Summary

This thesis aims to unravel the factors controlling the geometries, the facies composition and distribution, as well as the diagenesis of tropical carbonate platform slopes. To achieve these goals, different Miocene tropical carbonate platform slopes from Almería (SE Spain) were mapped, sampled, and digitalized with LIDAR. Field observations were backed up by microfacies analysis, cathodoluminescence, SEM, EDX, and isotopic analysis. The case studies dealing with Neogene deposits are complemented with a data set from the Holocene carbonate platform slopes from the Bahamas.

The tropical carbonate platforms of SE Spain in cross-section exhibit progradational patterns with steep clinoform bodies showing a downslope decrease of grain size, from reef-framework blocks and breccia to fine-grained packstone, and a basinward thinning and flattening. Previously, this facies distribution was assumed to be static when performing architecture analyses of the carbonate platform showing the vertical shifts of reef-slope facies during reef progradation following sea-level oscillations. Slope facies distribution and composition, however, are the result of the interaction of several factors such as coral growth, in-situ slope carbonate production, rockfalls and sediment gravity flows, hemipelagic rain, reworking of reef-slope facies and siliciclastic input. The relative impact of these factors was controlled by changes in accommodation related to sea-level fluctuations. Sea-level fluctuations may also change the hydrographical conditions of the basins controlling water stratification and upwelling, which prevailed during relative highstand and promoted the abundance of *Halimeda* algae, the main component of the proximal slope facies. Upwelling conditions did not occur during late stages of sea-level fall and lowstand and accordingly *Halimeda* algae are absent in the facies.

Therefore this study shows the dynamic behaviour of slope facies changes related to sea-level fluctuations, in contrast to the classic static models. Reef-slope facies may also vary their content in *Halimeda* algae and serpulids in response to changes of the amount of siliciclastics. Fluctuating terrigenous influx triggers a greater facies variability compared to pure carbonate systems. In mixed systems, the patchy distribution of reef-framework debris, *Halimeda* accumulations, serpulids build-ups, and alluvial fans indicates that a new model, more accurate than the classical and static facies belts, is needed for understanding the facies distribution in such carbonate platform slopes. Thus this research adds an element to the ongoing discussion about the validity of the concept of facies belts versus the concept of facies mosaics.

Past sea-level changes are also found to control the diagenetic history of the tropical carbonate platforms. The last episodes of platform progradation in the Cariatiz carbonate

platform (Almería, SE Spain) present a complex diagenetic history related to karst development during the late Miocene. The diagenetic overprint in two successive clinoform packages and a lowstand wedge forms distinct zones linked to different positions of past sea-level stands. The study of the diagenetic evolution together with classic pinning points of reef slopes has here been proven to be an accurate tool to calibrate the amplitude of sea-level fluctuations revealing a complete cycle of sea-level fall (23 ± 1 m) and rise (31 ± 1 m) between 5.89 and 5.87 Ma. The analysed outcrop is the first example where amplitudes of sea-level fall and rise related to precessional frequency during the Miocene can be precisely reconstructed. This allows the direct comparison to amplitude values of sea-level fluctuations inferred from proxies in pelagic sequences.

The steep angles, over 35°, of the tropical carbonate platform slopes of SE Spain are the result of extensive microbial binding as is the case in Palaeozoic and Triassic settings. The microbial coating and binding of the slope sediment prevented the shear failure of the steep slope deposits and allowed the conservation of the original angles of repose for these materials at an early stage. The extensive microbial influence on the slope deposition of the Miocene carbonate platform slopes of SE Spain raises the question if this is a singular case, or if this process affects slope deposition in Neogene or younger carbonate platforms elsewhere. Similar angles of deposition were observed in slopes from the Holocene of Tongue of the Ocean (Bahamas) that present similar facies to Miocene platform slopes, including the extensive microbial binding. The occurrence of microbial binding in the normal-marine Holocene slopes from the Tongue of the Ocean as well as in the Miocene Cariatiz carbonate platform therefore proves that the significance of microbial stabilization in carbonates slopes does not exclusively affect Palaeozoic and Triassic slopes. It is therefore proposed that microbial binding is a previously underestimated factor of slope stabilization in Neogene and Holocene carbonate platform slopes.

Zusammenfassung

Die Untersuchung der Kontrollfaktoren für Geometrie, Fazieskomposition und –verteilung sowie Diagenese von tropischen Karbonatplattformhängen stellen das Ziel dieser Forschungsarbeit dar. Hierfür wurden verschiedene miozäne tropische Karbonatplattformhänge in der Region Almeria (SO Spanien) kartiert, beprobt und mit Hilfe von terrestrischem Laserscanning (Lidar) digitalisiert. Die Geländedaten wurden hierbei durch die Analyse der Mikrofazies, REM, EDX sowie Isotopenmessungen verifiziert. Diese Fallstudien über neogene Ablagerungen wurden mit einem Datensatz eines holozänen Karbonatplattformhanges auf den Bahamas komplettiert.

Die tropischen Karbonatplattformen in Südostspanien sind als steil einfallende progradierende Klinoformkörper aufgeschlossen, deren Korngrößen, Schichtmächtigkeiten sowie Hangwinkel hangabwärts und beckenwärts abnehmen. Die Korngrößen variieren hierbei von Riffgerüstblöcken und Brekzien bis hin zu einem beckenwärtig abgelagerten feinkörnigem Packstone. In der Vergangenheit wurde diese Faziesverteilung, hervorgerufen infolge vertikaler Verlagerungen der Hangfazies durch Meeresspiegelschwankungen während der Riffprogradation, als statisch angenommen. Die Verteilung der Hangfazies ist jedoch das Ergebnis der Interaktion von unterschiedlichen Faktoren wie Korallenwachstum, In-situ Karbonatproduktion am Hang, Felsstürze und gravitatives Sedimentfließen, hemipelagischer Regen, Sedimentaufarbeitung der Hangfazies und siliziklastischer Eintrag. Der relative Einfluss dieser einzelnen Faktoren wurde kontrolliert durch die mit Meeresspiegelschwankungen im Zusammenhang stehenden Änderungen im Akkomodationsraum. Des Weiteren werden Meeresspiegelschwankungen als Ursache für die Änderungen von hydrographischen Bedingungen im Becken angenommen. So kam es während Meeresspiegelhöchstständen zu Auftrieb von Tiefenwässern sowie zur Stratifizierung der Wassersäule. Diese Annahme wird bestätigt durch das häufige Auftreten der Grünalge *Halimeda*, Hauptkomponent der proximalen Hangfazies. Bei fallendem Meeresspiegel sowie bei Meeresspiegeltiefständen kam es nicht zum Auftrieb von Tiefenwässern, was die Abwesenheit von *Halimeda* zur Folge hat.

Im Gegensatz zum klassischen statischen Modell, zeigt diese Studie ein dynamisches Verhalten von Änderungen der Hangfazies im Zusammenhang mit Meerespiegelschwankungen auf. Änderungen des siliziklastischen Eintrags haben ebenso Einfluss auf das Auftreten von *Halimeda* und Serpuliden. Ein sich ändernder terrigener Eintrag führt zu einer größeren Faziesvariabilität im Vergleich zu reinen karbonatischen Systemen. In gemischten Systemen kommt es zur fleckenhaften Verteilung von Riffschutt, *Halimeda* und Serpulid Akkumulation, und Schwemmfächern, was darauf schließen lässt,

dass das neue Modell präziser ist als das klassische statische Modell und benötigt wird, um die Faziesverteilung in Karbonatplattformhängen zu verstehen. Diese Studie liefert ein weiteres Argument in der andauernden Diskussion über die Richtigkeit des Konzepts des Faziesgürtels gegenüber dem Konzept des Faziesmosaiks.

Die Diagenese von tropischen Karbonatplattformen ist ebenso kontrolliert durch vergangene Meeresspiegelschwankungen. Die letzte Episode der Progradation der Cariatiz Karbonatplattform (Almería, SO Spanien) weist eine komplexe diagentische Entwicklung auf, die auf eine Abfolge von mehreren Verkarstungsereignissen während des Oberen Miozäns schließen lässt. Die diagenetische Überprägung von zwei aufeinanderfolgenden Klinoformkörpern sowie einer *lowstand wedge* führt zur Ausbildung von individuell ausgeprägten Bereichen, die vergangenen Meeresspiegelständen zugeordnet werden konnten. Die diagenetische Evolution der Plattform zusammen mit den *classic pinning points* des Plattformhanges stellen ein akkurates Werkzeug dar, um die Amplituden von Meeresspiegelschwankungen eines kompletten Zyklus von Meeresspiegelfallen (23 ± 1 m) und Wiederanstieg (31 ± 1 m), zwischen 5,89 und 5,87 Ma Jahren, zu rekonstruieren. Der untersuchte Aufschluss repräsentiert das erste Beispiel, bei dem die Amplitude von präzessionsbedingtem Meeresspiegelanstieg und –abfall des Miozäns rekonstruiert werden konnte. Dies ermöglicht den direkten Vergleich zu den Amplitudenwerten der Meeresspiegelschwankungen, wie sie auch von Proxies in pelagischen Sequenzen abzuleiten sind.

Mikroben als Bindemittel, wie sie ebenfalls in paläozoischen und triassischen Ablagerungen vorkommen, sind verantwortlich für die steilen Hänge (>35°) der tropischen Karbonatplattformen im Südosten Spaniens. Mikrobielle Umhüllungen und das Zusammenbinden der Sedimente in der Hangfazies verhindern ein Rutschen der steilen Hangablagerungen und erlauben die Erhaltung des originalen Reibungswinkel im frühen Stadium. Der ausgeprägte mikrobielle Einfluss auf die, während des Miozäns entstandenen, Karbonatplattformhänge in Südostspanien lässt die Frage aufkommen, ob es sich hier um einen Einzelfall handelt oder ob dieser Prozess auch neogene oder jüngere Karbonatplattformen andernorts beeinflusst. Ähnliche Ablagerungswinkel sowie von Mikroben dominierte Fazies, wie in den miozänen Plattformhängen, wurden auch an den holozänen Hängen der "Tongue of the Ocean" auf den Bahamas beobachtet. Das Auftreten von Mikroben als Bindemittel in den marinen Hängen der holozänen „Tongue of the Ocean“, ebenso wie in der miozänen Cariatiz Karbonatplattform, bestätigt, dass die Stabilisierung von Karbonathängen durch Mikroben nicht nur während des Paläozoikums und der Trias erfolgte. Es wird angenommen, dass das Zusammenbinden durch Mikroben ein unterschätzter Faktor ist, der zur Stabilisierung von neogenen und holozänen Karbonatplattformhängen beiträgt.

Acknowledgements

This thesis is the result of all the help I received from the people who were with me during this adventure. First of all, I want to thank my supervisor (although I prefer the term Doktorvater, because he is my father in sedimentology), Prof. Dr. Christian Betzler. He proposed the idea of the NEOCARPS (Neogene Carbonate Platform Slopes) project, searched for the financial support for its development, and chose me to carry out this research. I also want to thank him the countless hours of discussion in field, ocean, or office, and the numerous proof-readings, comments on figures, and especially for pushing me to accomplish nothing but the best I can do. Thank you for your patience with my German-English issues and my Andalusian lateral thinking.

I sincerely want to thank Prof. Dr. Juan Carlos Braga of the University of Granada for his help at every step of this research. I would have never met Christian and applied for the PhD position without him. I also want to thank Juan Carlos for introducing me to the Cariatiz Reef during my master studies and for numerous scientific discussions and advices during my PhD research. My sincere thanks go to Prof. Dr. José Manuel Martín for introducing me to the world of sedimentology, and for his comments to improve the second chapter of this thesis. It was always a pleasure to talk to both of you every time I was back in Granada.

I truly thank Dr. Sebastian Lindhorst for helping me with my, more than often, problems with informatics, his support during the LIDAR campaigns in Almería and his comments for the improvement of the second chapter of this dissertation. I also thank Prof. Dr. John Reijmer of VU University Amsterdam and Carlos Acevedo of Hafen City University for helping in the acquisition and the representation of LIDAR data used in Chapter II. I also want to thank Prof. Dr. Gregor Eberli for the chance to visit the Rosenstiel School of Marine and Atmospheric Science, University of Miami, and for everything I learnt from him in field, ocean, and office. I want to thank you for make me improve from Mr. Packstone to El Hombre. I would also like to thank Prof. Dr. Michael Grammer, Oklahoma State University, for his inestimable help for the realisation of the Chapter IV of this thesis. Thank you for your samples from TOTO and your e-mails answering every question that I had.

Special thanks go to Victoria Singler and Christiane Stange, the best team I could ever imagine. Thank you for your help in the field from dawn till dusk, the great job in Polopos, the awesome driving-backwards skills, the burgers, and milnos. Thanks to Prof. Dr. Gerhard Schmiedl for the literature and for the metal boxes he provided me when I needed them. Thanks to Mark Theodor for his guidance in SEM and EDX analysis, and Eva Vinx

for the support producing thin sections. I also want to acknowledge the support of my colleagues at the Institute of Geology: Juliane (for helping me with almost every paperwork and language problem that I had), Huaqing (always taking care of my avocado plant while I was abroad), Khurram and Marco (for the great times in the field), Dirk and Annemarie (for all the logistic and paperwork), Martin Clark (for the English check), Doro (for the work, work, work), and Martin Hinke (for the work with Arcmap). I want to thank Dr. Isabel Sánchez-Almazo for the isotopic analyses and Christine Laurin and Dr. Matt Fentem for English editing. I also want to thank the CSL team (Jara, Viviana, Ergin, Emanuelle, Kim, and especially Annita) for making me feel at home while I was in Miami.

I also want to express my gratitude to Chantal, Ivan, Claudia and Iria for their help and support when I was starting my life in Hamburg. I thank Manuel, Canario, Juadri and particularly Oscar for their help during the fieldwork in Níjar and especially in the Cariatiz karst. I also want to thank my friends and colleagues for their support and interest in my work (Dr. Julio Aguirre, Dr. Or Bialik, Dr. Montse Alonso, Dr. Cell, Javi, Miguelón, Bruno, Víctor, Antonio, Nacho and Juanma). And my sincere thanks to Melani Cazorla for leaving Granada to start a life with me in Hamburg.

I am eternally grateful to my family for the support in the distance and for their care when I visited Granada or they visited me. Thank you, Isabel, for your advice. Thank you, Eli, for always asking about my red eye and always suffering the same bad jokes. Gracias Mamá por ser mi todo. Gracias Papá por pasarte los días conmigo picando piedras en Cariatiz o por llevarme al afloramiento en año nuevo para ver si el karst seguía en su sitio. But I especially thank my brother Matías. Thank you for taking me to the field when I was a child, for teaching me the secrets of the stones, for your guidance at every step of my degree and PhD, thank you for your time in Rambla de la Mora and for your proof readings. Thank you for being my brother, my father, my teacher, my supervisor and my model. I would never be who I am without you.

Finally, I also would like to acknowledge the Deutsche Forschungsgemeinschaft for financial support through the grant Be 1272/21-1 (NEOCARPS). This financial support has allowed me to travel to the study areas several times, to prepare and analyse the numerous samples as well as to participate in international meetings. The International Association of Sedimentologists is thanked for funding of the research I developed at the Rosenstiel School of Marine and Atmospheric Science, University of Miami, through the IAS Post-graduate Scheme Grant.

This is just a tribute to all the people who have been by my side these years. To all of you:
Danke, Thank you, Gracias.

Table of contents

Summary 3
Zusammenfassung 5
Acknowledgements 7

1. Chapter I: Introduction 11
1.1 Carbonate platform slopes 12
1.2 Study area 13
1.3 Aim of the thesis 14
1.4 Outline of the thesis 15

2. Chapter II: Reef-slope geometries and facies distribution: controlling factors 17
2.1 Introduction 18
2.2 Geological setting 19
2.3 Methods 21
2.4 Results 22
2.4.1 Clinoform Body 1 23
2.4.2 Clinoform Body 2 26
2.4.3 Conglomerate body 26
2.5 Discussion 27
2.5.1 Facies Interpretation 27
2.5.2 Clinoform development and sea-level change 31
2.5.3 Composition and sea-level change 33
2.5.4 Geometry of clinoform bodies 35
2.6 Conclusions 38

3. Chapter III: Amplitude of late Miocene sea-level fluctuations from karst development in reef-slope deposits 39
3.1 Introduction 40
3.2 Geological setting 40
3.3 Methods 42
3.4 Results 44
3.4.1 Lower Clinoform Body 44
3.4.2 Lowstand Wedge 45
3.4.3 Upper Clinoform Body 45
3.5 Interpretation and discussion 47
3.5.1 Diagenetic zones 47
3.5.2 Sea level and diagenesis 47

3.5.3 Amplitude of sea-level changes 50
3.6 Conclusions 51

4. Chapter IV: Microbial binding: controlling factor of slope angles in post-Triassic carbonate slopes? 53
4.1 Introduction 54
4.2 Geological setting 55
4.3 Methods 55
4.4 Results 56
4.4.1 Tongue of the Ocean slopes 56
4.4.2 Cariatiz slopes 62
4.5 Discussion 65
4.5.1 Origin of steep slopes 65
4.5.2 Microbial influence on the steep slopes 68
4.6 Conclusions 70

5. Chapter V: Facies variability in mixed carbonate-siliciclastic platform slopes 71
5.1 Introduction 72
5.2 Geological setting 72
5.3 Methods 74
5.4 Results 74
5.4.1 Carbonate slope facies 74
5.4.2 Cariatiz carbonate platform: slope facies distribution 77
5.4.3 Polopos carbonate platform: slope facies distribution 82
5.5 Discussion 83
5.5.1 Miocene carbonate platform slopes from SE Spain 83
5.5.2 Siliciclastic input and facies variability 87
5.5.3 Facies belts or facies mosaics? 89
5.6 Conclusions 92

6. Chapter VI: Conclusions 93

7. References 97

Chapter I

Introduction

1.1 Carbonate platform slopes

Carbonate platform slopes form the transition between shallow-water shelf carbonates and deep-water basinal deposits. The slopes of carbonate platforms are of the greatest interest to sedimentologists, stratigraphers, palaeontologists, and petroleum geologists. Carbonate platform slopes may contain reservoirs for oil and gas, their configuration often influences processes on the platform and on the distal areas around them, they contain significant variability in biological assemblages, lithologies, and depositional and diagenetic processes compared to those of the platform itself (Ginsburg, 2001). The slope features are closely linked to sea-level changes, however, there are no integrated studies for analysing variations in components and fabrics, geometries and diagenesis in successive slopes affected by relative sea-level fluctuations during the Miocene. The focus of this thesis is to discuss the nature, importance, and extent of all the factors affecting slope geometries, diagenesis, and facies composition distribution as well as how they evolve in a fluctuating sea-level context.

Dynamics of carbonate platform slope sedimentation and architecture were analysed in terms of sediment production and processes of transport to the basin, slope geometry, and stratigraphic architecture. Alongslope facies distribution in carbonate platform slopes develops as a result of the combination of several intrinsic factors such as initial bathymetry, biological, and sedimentary processes that affect the carbonate factory (Wright and Burgess, 2005). But carbonate slopes are not uniform factories and the carbonate production areas may occur in lateral and alongslope patchworks (Wright and Burgess, 2005). Many of these patchworks are not depth dependent and can change through time because of external factors (Wright and Burgess, 2005), as the input of siliciclastics in the carbonate factory. Aside from the effects of unpredictable external factors, the main control over carbonate assemblages and the resulting depositional facies on short time scales are temperature, nutrients, and salinity of the water masses in which the organisms live (Mutti et al., 2010). The biota in carbonate slope facies records the effects of distinct environmental conditions and in this respect variations in carbonate platform slope facies can be related to climatic changes, such as sea-level fluctuations. Sea-level fluctuations expose the slope deposits to freshwater and associated diagenetic alteration (Swart, 2015). These alterations involve dissolution of components and precipitation of meteoric cements that result in porosity changes and therefore changes of the reservoir potential of the slope.

The platform slope geometry is related to the composition of the sediment produced on the platforms, and on the slope itself, as well as the amount of sediment exported downslope. The geometrical aspects of carbonate slopes were analysed in detail by Kenter (1990) and Adams et al. (2002). Factors controlling the slope geometry are the volume of sediment

and platform height (Schlager, 1981), the erosion-deposition balance (Schlager and Camber, 1986), and the grain size (Kirkby, 1987). In slopes with steep angles of repose additional factors were proposed including the response to great shear strengths in fine-grained carbonate slope sediments (Kenter, 1990; Kenter et al., 2005; Schlager, 2005; Playton et al., 2010), processes of early lithification and cementation of the slope sediments (Grammer et al., 1993a; 1993b), and in-situ stabilization (Kenter, 1990; Della Porta et al., 2003; 2004; Kenter et al., 2005). Wind and currents were reported as major controlling factors of slope geometry along the flanks of Great Bahama Bank, in which a strong windward-leeward asymmetry of the slope shape was identified (Grammer and Ginsburg, 1992). Alongslope currents are a further controlling factor of slope geometry and slope sediment texture (Betzler et al., 2015; Principaud et al., 2015). The significance of sequence stratigraphy of the carbonate platform slopes was highlighted by seismic profiles (Eberli and Ginsburg, 1989) and detailed outcrop mapping (Pomar and Ward, 1994; Braga and Martín, 1996). Accordingly, an important influence in platform slope geometry is therefore due to the fluctuation in sea-level position, as it exerts a strong control on the distribution and composition of the facies belts, the stacking patterns, and the morphology of the depositional profile.

1.2 The study area

Miocene carbonate platform slopes are well exposed in the Neogene basins of the Betic Cordillera in SE Spain and accordingly have been extensively studied (Esteban, 1980; Dabrio et al., 1981; 1985; Riding et al., 1991; Martín and Braga, 1994; Braga and Martín, 1996; Esteban, 1996; Franseen and Goldstein, 1996; Cornée et al., 2004, Warrlich et al., 2005; Cuevas-Castell et al., 2007; Sánchez-Almazo et al., 2007; Rodríguez-Tovar et al., 2013). Miocene carbonate platform slopes of SE Spain offer unique study conditions for analysing the relative influence of the different tectonic (Martín and Braga, 1994; Braga et al., 2003), sedimentological (Esteban, 1980; Dabrio et al., 1981; Riding et al., 1991), hydrographic (Mankiewicz, 1988), ecological (Mankiewicz, 1988; Jiménez and Braga, 1993) and eustatic (Braga and Martín, 1996; Cuevas-Castell et al., 2007) controls on slope facies and geometries. Miocene carbonate platform slopes of Mediterranean regions also offer an excellent stratigraphic resolution for the study of high-frequency stratigraphic cycles (Braga and Martín, 1996; Cuevas-Castell et al., 2007, Sánchez-Almazo et al., 2007; Rodríguez-Tovar et al., 2013). Miocene carbonates have generally suffered from minor burial and multiple diagenetic overprints compared to older carbonates, and in this respect diagenesis and porosity evolution are more easily studied and timing of diagenetic events more easily determined (Goldstein et al., 1994; Franseen et al., 1996; Li et al., 2014). The similarity of Miocene outcrops with modern carbonates facilitates the detailed analysis of depositional facies and ecology.

Several Miocene and Holocene carbonate platforms were selected to develop this research due to their established stratigraphy, extensive knowledge of the general climatic conditions, and superb outcrop conditions. The Messinian Cariatiz carbonate platform in the Sorbas Basin (Almería, SE Spain) is a tropical platform with steep angles and complex facies distribution and diagenetic history. The slopes from Cariatiz were compared to other Messinian tropical slopes of SE Spain as the Níjar and Polopos carbonate platforms in the Níjar Basin, and to Holocene carbonate platform slopes from the Tongue of the Ocean in Bahamas (Fig. 1.1).

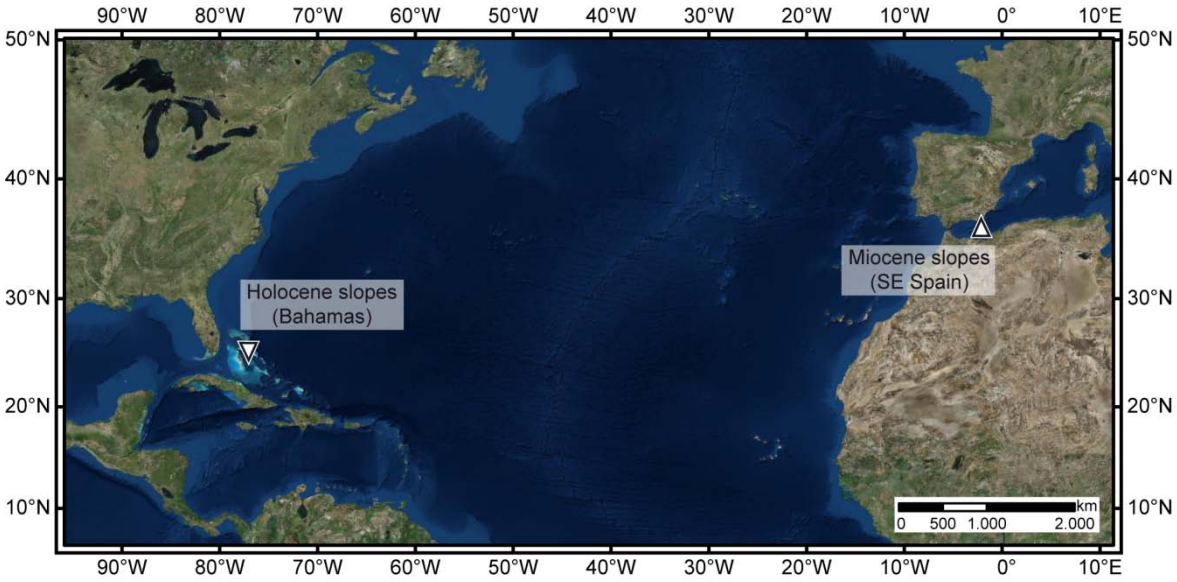

Fig. 1.1: Geographical position of the Miocene and Holocene slopes discussed in this thesis.

1.3 Aim of the thesis

The goal of this study is to unravel intrinsic and extrinsic controlling factors which shape Miocene tropical carbonate platform slopes. The hypothesis to test is that although platform slopes forming in successive stages of platform progradation have a similar appearance, controlling factors of slope depositional processes may differ as a consequence of the impact of sea-level fluctuations on carbonate production, transport, and deposition. Primary investigations are focused on the Cariatiz carbonate platform (Messinian, SE Spain), and others Messinian carbonate platform slopes from the Sorbas and Níjar Basin (SE Spain). The Holocene carbonate platform slopes from the Tongue of the Ocean in Bahamas are secondary study areas for comparing the main findings achieved during the research in SE Spain. The geometrical data obtained by laser scanning and the facies and microfacies analysis of slope deposits shed new light on slope geometries, lateral and

alongslope facies distribution, palaeowater-depth related sediment compositional variations, and alongslope differentiation of diagenetic processes.

1.4 Outline of the thesis

This thesis is subdivided into six chapters. Chapter I introduces the aim of the research.

Chapter II focuses on one of the platforms studied (Cariatiz carbonate platform). The reef slopes during the last progradation episodes of this platform show a complex facies distribution within clinoform bodies with different geometries. In this chapter, the factors controlling the facies distribution and geometries are defined as well as how these factors are linked to sea-level fluctuations. Additionally it is shown that the steep carbonate platform slopes are stabilized by microbial binding. This chapter was published as "Reef-slope geometries and facies distribution: controlling factors (Messinian, SE Spain)" in Facies (2014), volume 60, pages 737 to 753.

Chapter III focuses on the role of diagenesis in affecting slope deposits. Different diagenetic zones, including a level of palaeokarst, provide a precise gauge for measuring the amplitude of high-frequency sea-level changes. In this case, the precise age assignment of the deposits allows the comparison of the values of sea-level change as recorded in the neritic deposits with the values as deduced from stable oxygen isotope variations in pelagic sequences. This chapter was submitted to the International Journal Sedimentary Geology as the manuscript entitled: "Amplitude of late Miocene sea-level fluctuations from karst development in reef-slope deposits (SE Spain)".

Chapter IV discusses the role of microbial binding in Neogene carbonate platform slopes. Comparing the flanks of the Tongue of the Ocean in the Bahamas with the Miocene carbonate platform of Cariatiz it is shown that in all cases extensive occurrence of microbial textures indicates an early stabilization of the carbonate platform slopes. Therefore this chapter first proposes that a microbial influence plays a leading role in controlling Holocene and Neogene carbonate platform slopes geometries. This is relevant, as previous researches identify microbial processes to only affect slopes which formed during the Triassic or earlier.

Chapter V introduces a general model to document the different outcrops of Miocene carbonate platform slopes from SE Spain. By comparing different sections through three platforms, the facies variability is discussed with a particular focus on the role of siliciclastics. Siliciclastic influx apparently resulted in an increase of the facies variability, mostly related to the extensive occurrence of serpulids and red algae. This study therefore

contributes to the ongoing discussion about the application of the concept of facies belts versus the concept of facies mosaics. The chapter was submitted to the journal Facies as the manuscript entitled "Facies variability in mixed carbonate-siliciclastic platform slopes (Miocene)".

Chapter VI finally presents the conclusions of this study.

All the chapters were written by the author, Jesús reolid, and are based on original fieldwork and microfacies analysis, as well as the LIDAR data obtained by Prof. Dr. Christian Betzler, Dr. Sebastian Lindhorst, Victoria Singler, and Christiane Stange. Chapter IV is additionally based on the slope samples provided by Prof. Dr. Michael Grammer and Prof. Dr. Gregor Eberli.

Chapter II

Reef-slope geometries and facies distribution: controlling factors

Abstract

Sea-level fluctuations and changes in sediment grain size are widely thought to be the main factors controlling carbonate platform slope geometries. Two successive clinoform bodies from the Upper Miocene Cariatiz carbonate platform (SE Spain) were selected to analyse geometry and facies distribution in relation to sea-level oscillations. Facies occurring in these clinoform bodies are from top to bottom reef framework, reef-framework debris, *Halimeda* breccia, *Halimeda* rudstone, and bioclastic packstone, as well as siltstone and marl. Slope geometry and facies, composition and distribution, are significantly different in each clinoform body. These differences are the result of the interaction of several factors such as coral growth, in-situ slope carbonate production, rockfalls and sediment gravity flows, hemipelagic rain, reworking of reef-slope facies, and siliciclastic input. Changes in accommodation were related to sea-level fluctuations and controlled the relative impact of these factors. A sea-level fall took place in the time between deposition of the selected clinoform bodies and changed the hydrographical conditions of the basin. These changes influenced the presence of *Halimeda* and the grain-size distribution, and consequently the slope geometries. Reef-slope geometry is not exclusively controlled by changes in grain size. The stabilization by organic binding is proposed to be a significant factor controlling the slope deposition.

This chapter is based on **Reolid, J., Betzler, C., Braga, J.C., Martín, J.M., Lindhorst, S., and Reijmer, J.J.G.** (2014) Reef slope geometries and facies distribution: controlling factors (Messinian, SE Spain). *Facies*, 60, 737–753. DOI 10.1007/s10347-014-0406-4

2.1 Introduction

Sea-level changes are reported as the main factor controlling productivity, reef-slope geometry, and stacking patterns of clinoform bodies in carbonate platforms (Kendall and Schlager, 1981; Bosellini, 1984; Eberli and Ginsburg, 1989; Pomar and Ward, 1994). According to Kenter (1990), carbonate platform slope angles are also closely linked to the sediment grain size. This was expanded by Adams and Schlager (2000) and Schlager and Adams (2001) relating the geometry of the slope to the sediment type and consequently to the hydrodynamic energy. Schlager and Reijmer (2009) showed that the type of carbonate mud, i.e. loose needles vs. sand-sized mud clasts, also plays a role in determining the slope of clinoform bodies. In order to test the applicability of these models to Upper Miocene carbonate platforms, two successive clinoform bodies from the latest episodes of reef progradation were selected in the Cariatiz carbonate complex (SE Spain) to calibrate facies distribution and grain-size variations in relation to sea-level oscillations.

Messinian coral reefs are well exposed in the Neogene basins of the Betic Cordillera in southeastern Spain and have been the subject of extensive research (Esteban, 1980; Dabrio et al., 1981; 1985; Riding et al., 1991; Martín and Braga, 1994; Braga and Martín, 1996; Esteban, 1996; Franseen and Goldstein, 1996; Cornée et al., 2004, Warrlich et al., 2005; Cuevas-Castell et al., 2007; Sánchez-Almazo et al., 2007; Rodríguez-Tovar et al., 2013). The Cariatiz carbonate platform in the Sorbas Basin (Almería) in cross-section exhibits a progradational pattern with well-developed clinoform bodies. These clinoform bodies show a downslope decrease of grain size, from reef-framework blocks and breccia to fine-grained packstone, and a basinward thinning and flattening. This facies distribution was assumed to be static when performing architecture analyses of the carbonate platform showing the vertical shifts of reef-slope facies during reef progradation following sea-level oscillations (Braga and Martín, 1996; Cuevas-Castell et al., 2007). Up to now, however, no attempts were made to study variations in components and fabrics in successive reef-slope clinoform bodies affected by relative sea-level changes.

Mapping of facies distribution, with the support of terrestrial LIDAR data and microfacies analysis, shows that the two selected clinoform bodies exhibit different slope geometries and completely different facies distribution patterns. Changes in slope geometries are linked to changes in grain size and facies distribution. In the clinoform bodies, facies distribution is the result of the interaction of different factors related to carbonate production and its distribution along the reef slope. These factors seem to be linked to sea-level fluctuations. A sea-level fall appears as the main cause for facies variations in the studied clinoform bodies but it cannot completely explain reef-slope geometries. The aim of this research is to discuss the nature, importance and extent of all the factors affecting

the geometry of clinoform bodies and to contribute to the ongoing discussion on carbonate slope systems and their controls.

2.2 Geological setting

The studied outcrop is located in the Barranco de los Castaños ravine near the village of Cariatiz, at the northern margin of the Sorbas Basin (SE Spain) (Fig. 2.1). The Sorbas Basin is elongated in an E-W direction, and is bound by metamorphic rocks from the Internal Betic Zone cropping out in the Sierra de los Filabres to the north and in the Sierra Alhamilla and Sierra Cabrera to the south.

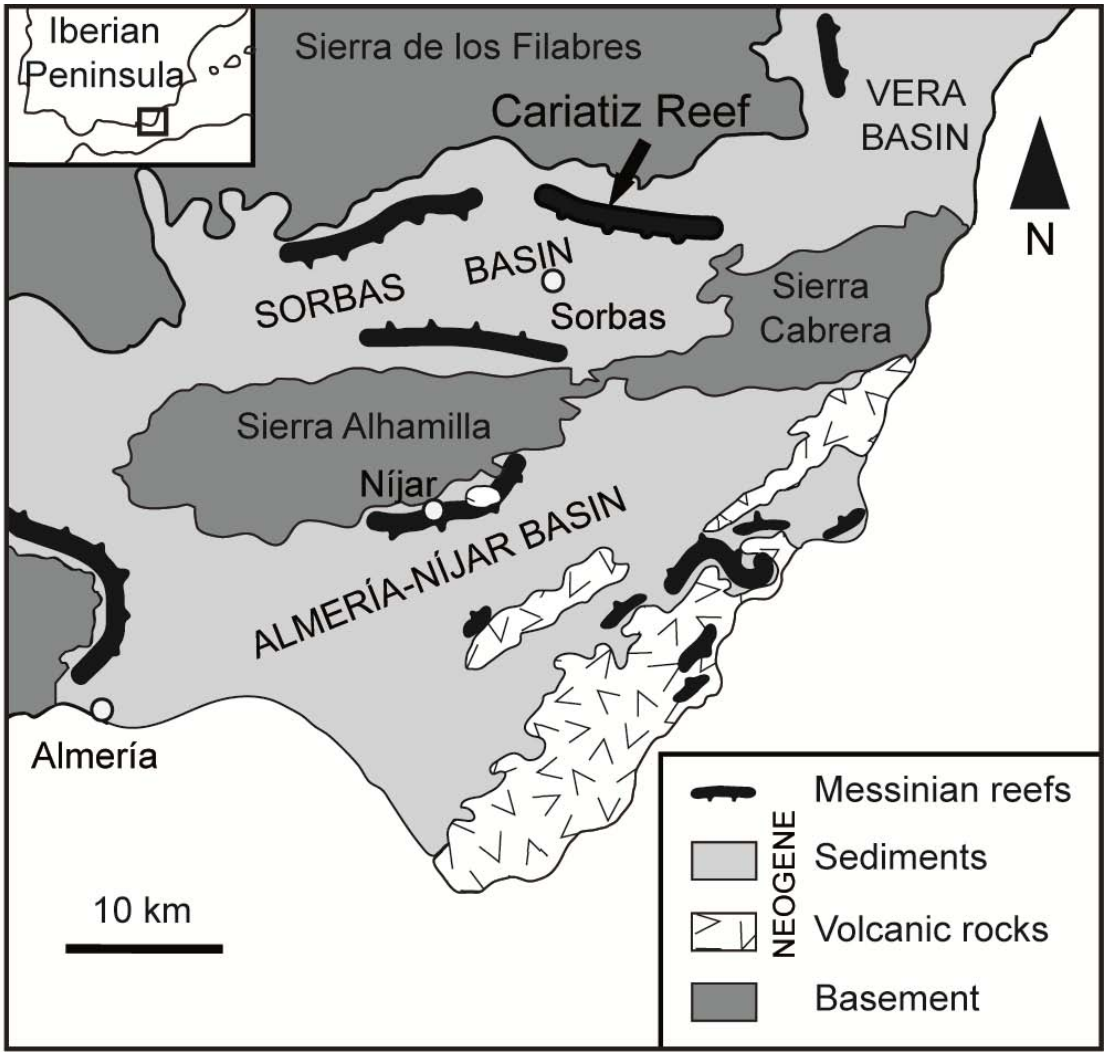

Fig. 2.1: Regional setting of the Sorbas Basin and the Cariatiz Reef in SE Spain (modified from Braga and Martín, 1996).

The basin-fill is up to 700 m thick and consists of several stratigraphic units ranging from Middle Miocene to Quaternary in age (Martín and Braga, 1994). These stratigraphic units are separated by unconformities (Fig. 2.2A). The Upper Tortonian Unit comprises neritic

to deep-sea siliciclastics and carbonates (Kleverlaan, 1989; Martín and Braga, 1994). The overlying Azagador Member (Völk and Rondeel, 1964) consists of platform packstone and bioclastic sandstone. Basinward, the Azagador Member grades into fine-grained packstone and marl of the Lower Abad Member (Martín and Braga, 1994), deposited close to the Tortonian-Messinian boundary (Sierro et al., 1993). The lowest Messinian reef deposits constitute the Bioherm Unit (Martín and Braga, 1994) which contains coral and algal bioherms among packstone background deposits grading basinward into silty marl and marl with intercalated diatomite. The unconformably overlying Messinian Fringing Reef Unit is the scope of this study. It comprises carbonate platform deposits and related basinal silty marl, marl and diatomite from the Upper Abad Member (Martín and Braga, 1994). The southern end of the Barranco de los Castaños section is located at the transition from reef carbonates to basinal marl and silty marl (Fig. 2.2A). A basin-wide erosional surface, with signs of subaerial exposure, bounds the top of the Fringing Reef Unit. The Upper Abad marl and the distal Fringing Reef deposits are onlapped by a series of evaporite, carbonate and siliciclastic deposits (Ruegg, 1964; Riding et al., 1998; 1999).

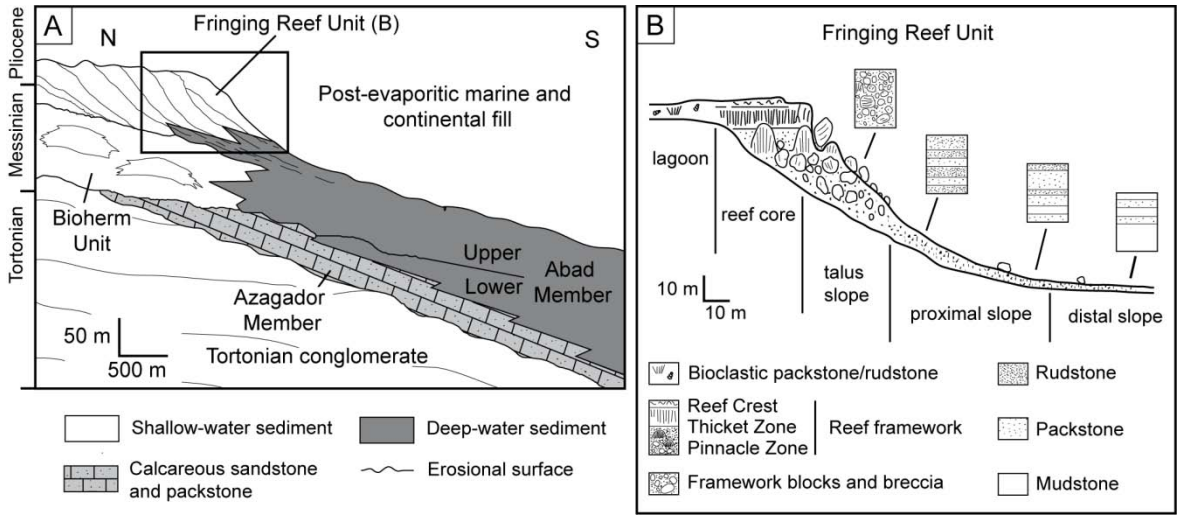

Fig. 2.2: A Neogene lithostratigraphy of the Sorbas Basin (modified from Sánchez-Almazo et al., 2007). **B** facies model for the Cariatiz fringing reef (after Riding et al., 1991 and Braga and Martín, 1996).

In the carbonate platform of the Fringing Reef Unit, Riding et al. (1991) and Braga and Martín (1996) differentiated a series of facies belts. From the inner platform to the basin these are (Fig. 2.2B):

1) Lagoon. Deposits from this belt are parallel beds of packstone to rudstone with coral, coralline algal, foraminifera, and mollusc remains. Siliciclastic grains also occur, usually mixed with carbonates. Small patches of the coral *Porites* occur near the reef crest at the outer margin of lagoon sediments. Lagoonal beds dip 3° to southwest (N216E).

2) Reef framework. Deposits from this belt are about 20 m thick including from bottom to top: (a) a Pinnacle Zone dominated by columnar *Porites* connected by bridges of laminar

growths. Coral colonies are grouped in up to 15 m high pinnacles separated by areas of reef debris. *Porites* skeletons are covered by thin coralline algal-foraminiferal crusts overgrown by thick stromatolitic crusts. A bioclastic matrix fills in the remaining spaces. (b) A Thicket Zone with a framework similar to the Pinnacle Zone but with more lateral continuity of the coral growths; and (c) a reef crest made up of *Porites* colonies with platy to irregular shape.
3) Reef slope. These deposits consist of three different facies belts including from upper to lower slope: (a) the reef-talus slope, immediately in front of the Pinnacle Zone, consists of a breccia made up of framework blocks (the size of which decreases downslope) with *Halimeda* plates, bivalves, serpulids, and coralline algae. The proximal reef-slope (b) with packstone and rudstone that are made up of coralline algae, serpulids, and molluscs (*Halimeda* bioclasts can be locally abundant); and the distal reef-slope (c), which consists of silty marl and mudstone to packstone intercalated with basinal marl and diatomite.

Reef-framework and reef-slope facies are arranged into depositional wedges thinning downslope and basinward (Fig. 2.2B). These wedges, here referred as clinoform bodies, represent different phases of reef growth. In the Cariatiz carbonate platform it is possible to identify distinct stacking patterns of the clinoform bodies starting with lowstand deposits recorded by inverted wedges. These deposits consist of onlapping rudstone with bivalves, serpulids, and red algae. Inverted wedges are overlain by an aggrading systems tract and highstand systems tract followed by a downstepping-offlapping systems tract (Pomar and Ward, 1994; Braga and Martín, 1996). Along with this progradation of the reef system, facies shifts occurred in response to sea-level fluctuations.

2.3 Methods

The study of the reef-slope facies and architecture relies on detailed outcrop mapping of reef clinoform bodies. This mapping was performed using panoramic photomosaics of the best-exposed parts of the succession. The study was carried out over a distance of more than 1100 m along reef progradation, but this work focuses on the youngest part of the prograding carbonate platform, which is the most accessible. Two clinoform bodies were selected due to their good exposure. The different reef facies within the two clinoform bodies were described and sampled. A petrographic analysis of 43 thin sections was conducted to identify microfacies and components. Polished slabs were additionally used for analysing large bioclasts, as well as sedimentary fabrics and structures.

The quantification of slope dimensions and slope geometries of the selected clinoform bodies was achieved by laser scanning with an Optech Laser Imaging ILRIS 3D terrestrial LIDAR of the Institute for Geology at Hamburg University. LIDAR data were processed

using 3D-Reconstructor (Gexcel). Bedding planes and facies limits were mapped in the digital model. The resulting polylines were exported into Autocad for body-dimensions and slope-angle measurements. Autocad was also used for converting the 3D model into 2D by projecting the system onto a plane positioned parallel-to-progradation.

2.4 Results

Clinoform bodies in the Barranco de los Castaños are intercalated with inverted wedges and fan-delta deposits (Braga and Martín, 1996), as shown in Fig. 2.3. This study is focused on the last episodes of reef advance, which include two clinoform bodies, herein defined as Clinoform Body 1 (CB1) and Clinoform Body 2 (CB2), separated by a conglomerate body (Fig. 2.4A). The detailed analysis shows the differences in clinoform body geometries (Fig. 2.4B). Diverse facies in the clinoform bodies are documented in Table 2.1. Facies distribution is shown in Fig. 2.4C.

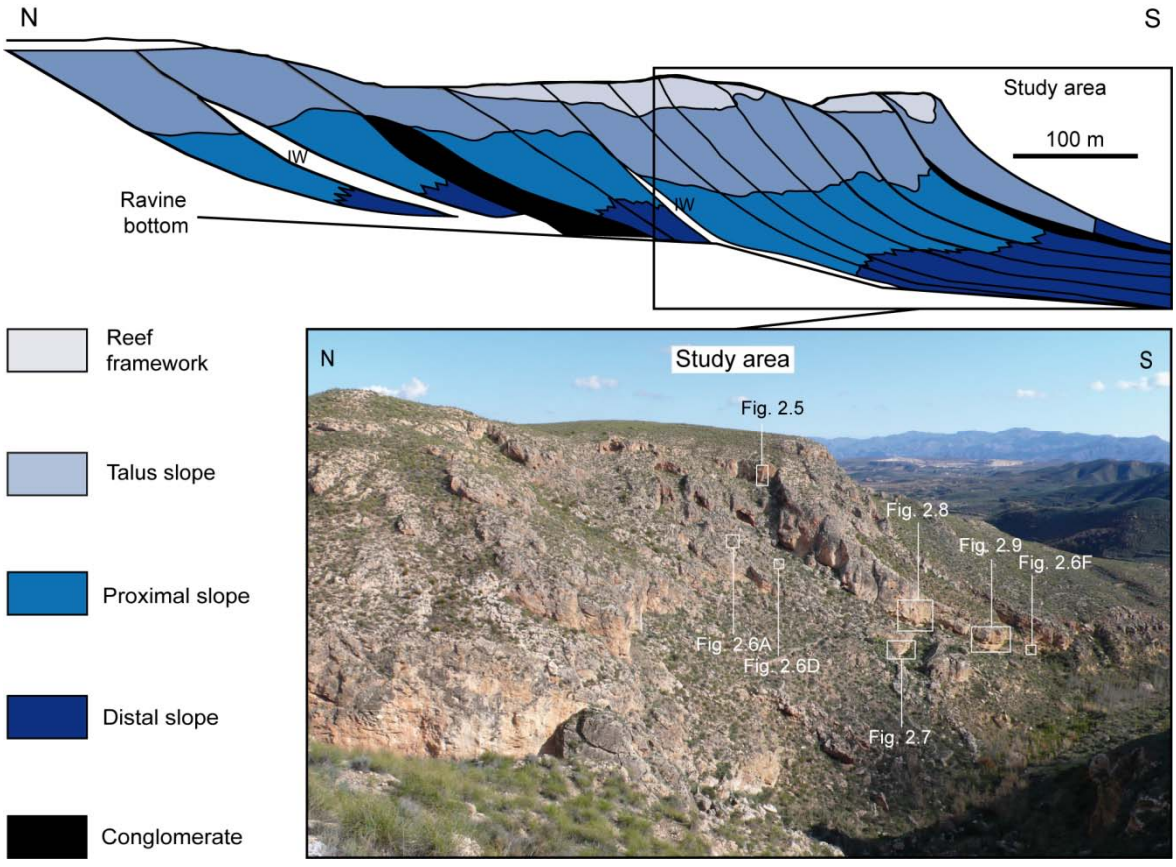

Fig. 2.3: Barranco de los Castaños section, IW= Inverted wedges (modified from Braga and Martín, 1996). Numbers indicate location of outcrops shown in the corresponding figures.

2.4.1 Clinoform Body 1

This clinoform body is 80 m high. In the direction of progradation (N160E) it extends for nearly 200 m (Fig. 2.4B). According to Adams and Kenter (2014), this body has a concave-upward linear profile, including three segments with different angles. The upper segment comprises the upper reef-talus slope with an approximate inclination of 60°. The middle segment includes the lower reef-talus slope and the proximal reef-slope with angles between 40° and 30°. The lower segment corresponds to the distal slope with angles between 15° and 10°.

The uppermost part of the body consists of a ~10 m thick package of reef framework which has a lateral extension of 35 m in the direction of progradation. The main volume of preserved reef framework corresponds to the Pinnacle Zone (Fig. 2.5). The Thicket Zone and the reef crest are only locally preserved. The reef-framework debris facies is 22 m thick. The size and the amount of the debris decrease downslope from the outermost reef framework (Fig. 2.4C). The reef-framework debris gradually changes into the reef-talus slope breccia (*Halimeda* breccia), which is approximately 20 m thick and spreads basinward 15 m from the last large blocks (Fig. 2.6A). Up to 1 mm thick and 6 to 10 mm long *Halimeda* plates usually make up more than 20% of the rock (Fig. 2.6B). Plates are usually oriented subparallel to bedding but locally they accumulate in patches with a random orientation. Sediments are floatstone and rudstone with varying amounts of micritic matrix. Within the *Halimeda* breccia, some patches occur which are formed by serpulid-tube clusters and red algae in a micritic matrix (Fig. 2.6C).

The good exposure of this clinoform body allows the facies change to be traced from the reef-talus slope into the proximal reef-slope, in a transition zone characterized by interdigitation of *Halimeda* breccia and *Halimeda* rudstone facies, involving a change in the degree of lithification (Fig. 2.6D). The change in the degree of lithification parallels the basinward decrease of patches of encrusting organisms. The *Halimeda* rudstone is bedded in the proximal reef-slope. Beds range in thickness from 5 to 30 cm and are grouped into an up to 15 m thick package. Patches of oysters, with some articulated individuals, occur at the top of this interval.

The transition between the *Halimeda* rudstone and the basinal facies is gradual. It occurs in an area with an alternation of 5-10 cm thick *Halimeda* rudstone beds and 15-25 cm thick siltstone and marl (Fig. 2.7). Deposits in this part of the slope are bioturbated. Low-angle tabular cross lamination pointing upslope occurs in the *Halimeda* rudstone beds (Fig. 2.7). The alternation of *Halimeda* rudstone and fine-grained beds in this area is a 15 m thick fining- and thickening-upward sequence. Siltstone and marl with diatomite layers appear at

the top of this alternation. The upper boundary of this sequence is an erosional surface at the base of the conglomerate body. The upper beds are deformed by the loading effect of overlying decametre-scale CB2 reef-framework blocks (Fig. 2.8).

Facies	Components	Matrix	Fabric	Coatings	Position	Dip
Reef framework (Fig. 2.5)	*Porites* skeletons (sticks and laminar forms) encrusted by thin coralline algal-foraminiferal coatings covered by thick stromatolitic crusts. Bivalves, echinoids, red algae, brachiopods, and gastropods (in gaps).	Microbial (stromatolitic) micrite. Bioclastic matrix.	In-situ *Porites* growths. Reef debris (bioclastic rudstone) between *Porites* colonies.	mm-size red algal-foraminiferal coatings. cm- to dm-size stromatolitic crusts.	Platform edge.	--
Reef-framework debris (Fig. 2.8)	Reef-framework blocks (up to 10 m in size). Echinoids, bivalves (pectinids), brachiopods, and gastropods. Intraclasts.	Microgranular (locally microbial micrite matrix).	Chaotic. Poorly bedded in CB1. Reef-framework block size decrease basinward.	--	Reef-talus slope (CB1 and CB2) and proximal reef-slope (CB2).	60°-55° CB1. 80°-60° (Reef-talus slope CB2) and 45°-30° (proximal reef-slope CB2).
Halimeda breccia (Fig. 2.6A-C) (floatstone to rudstone)	cm-dm reef-framework blocks. *Halimeda* plates. Bivalves (pectinids), gastropods, serpulids, red algae, echinoid spines, and benthic foraminifera. Intraclasts and minor siliciclastics.	Microgranular (locally microbial micrite matrix).	Chaotic. Poorly bedded (beds up to 40 cm thick). Local serpulid-red algal patches up to 1 m wide.	Fossils with micritic envelopes, locally connecting bioclasts. Red algal crusts around some bioclasts.	Reef-talus slope (CB1).	55°-45° CB1.
Halimeda rudstone (Fig. 2.6D)	*Halimeda* plates. Bivalves (pectinids and oysters), gastropods, serpulids, and red algae.	Microbial micrite matrix.	5-30 cm thick beds. Bioturbation. In the upper proximal slope 15-25 mm thick red algal nodule beds. In the lower proximal slope low-angle cross-lammination (5 cm high and 20 cm long sets).	Micritic envelopes.	Proximal reef-slope (CB1).	35°-30° CB1.
Bioclastic packstone (Fig. 2.6E)	Bivalves (pectinids), gastropods, serpulids, benthic foraminifera, red algae, and echinoid spines. Siliciclastic grains (7-10%).	Microbial micrite matrix.	10 - 30 cm thick beds with 1-5 cm thick layers. Bivalve shells parallel to bedding (equal concave/convex-up orientation). Locally intercalated with basinal silts and marls.	Micritic envelopes with a major development on one side of the grain (no preferred orientation).	Distal reef-slope (CB2).	20°-15° CB2.
Basinal siltstone and marl (Fig. 2.6F)	Red algae. Diatoms.	Silts and marls.	15-35 cm thick beds thickening upward to 40-60 cm thick beds. Alternation of mm-cm diatomite beds. Significant bioturbation.	--	Distal reef-slope (CB1 and CB2).	15°-10° CB1. 20°-15° CB2.

Table 2.1: Reef-framework and reef-slope facies of Barranco de los Castaños section.

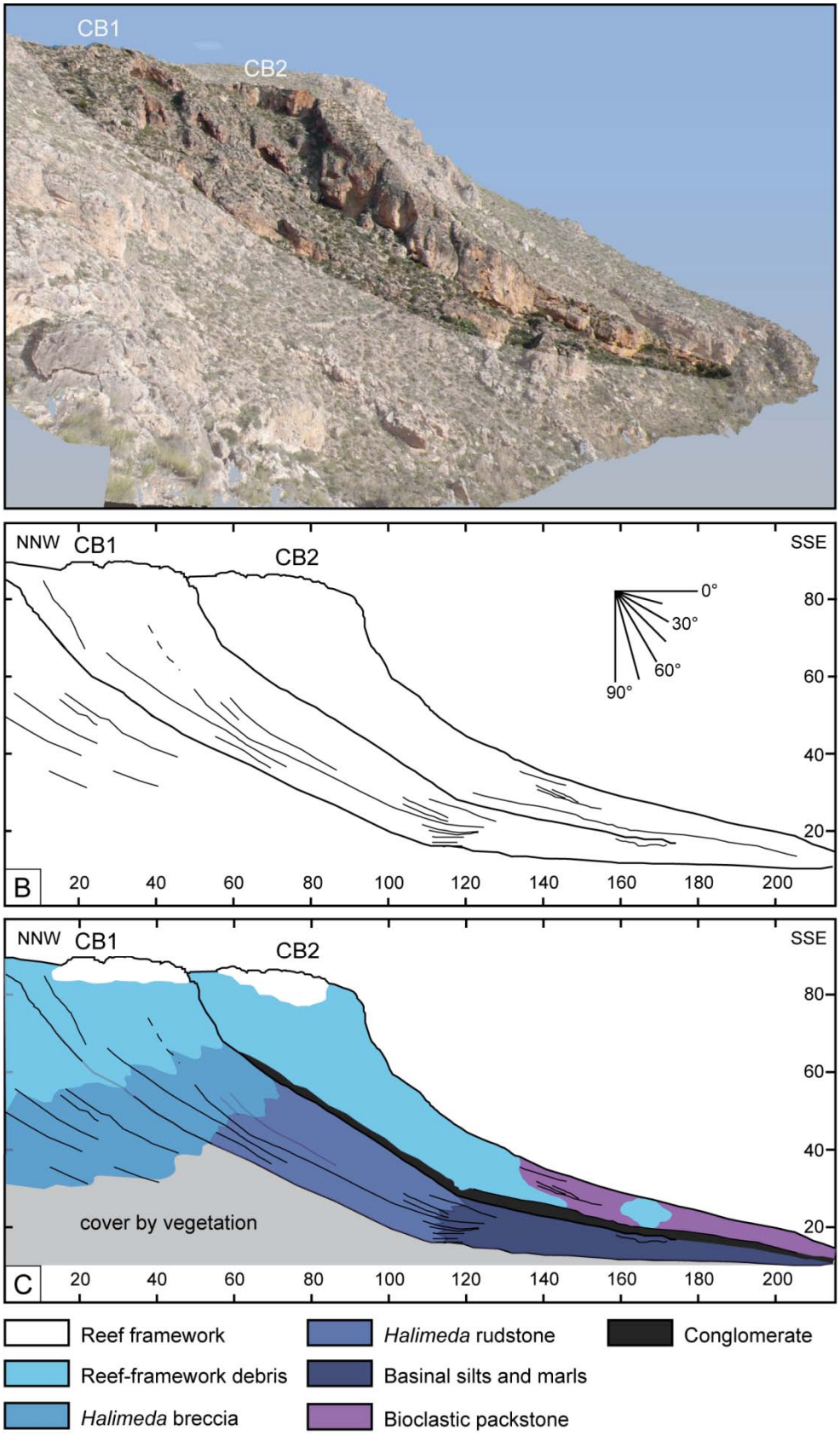

Fig. 2.4: A 3D model (point cloud) of studied clinoform bodies in Barranco de los Castaños section. **B** 2D projection of main surfaces, external and internal bedding, onto a plane oriented parallel to the progradation direction (N160E). **C** Facies distribution in CB1 and CB2.

2.4.2 Clinoform Body 2

Clinoform Body 2 has a height of nearly 80 m. In the direction of progradation (N160E) it extends for 170 m (Fig. 2.4B). This body has a concave-upward exponential profile, according to the scheme of Adams and Kenter (2014). The reef-slope angles are approximately 80°-60° in the reef-talus slope, 45°-30° in the proximal reef-slope, and 20°-15° in the distal reef-slope.

The uppermost part of CB2 consists of a 10 m high reef framework (Fig. 2.5) with a lateral extension of 30 m in the direction of progradation. The preserved framework facies are similar to those in CB1. The transition from the reef framework to the reef-talus slope is gradual. In the uppermost reef-talus slope facies, there are decametre- to metre-scale reef-framework blocks. The abundance of stick-like *Porites* colonies indicates that most of the reef-framework blocks are derived from the Pinnacle or Thicket Zones. Locally there are some patches with bioclastic rudstone to packstone made up of bivalves mostly preserved as molds of articulated valves, gastropods, brachiopods, and coral fragments. The reef-framework debris spreads basinward for 60 m from the lower limit of the reef framework and to the proximal to distal reef-slope (Fig. 2.4). The average thickness of this facies is approximately 17 m.

A bioclastic packstone (Fig. 2.6E) occurs at the transition from the proximal to the distal reef-slope, where bedding is locally deformed by decametric reef-framework debris (Fig. 2.9). Between the large blocks there are also some metre- to centimetre-scale reef-framework blocks. In the distal reef-slope, 20 cm thick siltstone and marl units are interbedded with 20-30 cm thick bivalve packstone beds. Some layers, usually red to ochre in colour, are very rich in coralline algae represented by sand-sized fragments and minor rhodoliths up to 15 cm in size. The entire package of alternating siltstone-marl and bivalve packstone is up to 5 m thick. Marl contains pebbles of quartz, schist, and serpentinite at the most distal reef-slope. These deposits are in part intensely bioturbated (Fig. 2.6F).

2.4.3 Conglomerate body

A 50-100 cm thick and 110 m wide conglomerate unit separates CB1 and CB2. The conglomerate comprises up to 20 cm large clasts of quartzite, micaschist, marble, amphibolite, and serpentine, which are derived from the Betic basement in the Sierra de los Filabres to the north. Clasts are supported by a microconglomeratic to sandy matrix. This body spreads from the uppermost part of the CB1 reef-slope to the most distal (lowest) point of the studied section. The largest clasts are located in the upper part of the slope and grain size decreases downward where deposits change into sandstone, basinal

siltstone and marl. The thickness of the conglomerate changes from 50 cm in the upper slope to 100 cm downslope. In the proximal to distal reef-slope, CB1 siltstone and marl occur above and below the conglomerate body. The conglomerate base is an erosional surface over the underlying siltstone and marl (Fig. 2.7).

Fig. 2.5: *Porites* with vertical growth forms in the reef-framework facies. Example is from CB2.

2.5 Discussion

2.5.1 Facies interpretation

It is proposed that the facies distribution in the clinoform bodies is controlled by the effects of the interaction of several processes. These processes are: a) carbonate production, linked to coral-reef growth and in-situ skeletal generation at the reef slope; b) physical

processes such as rock falls, downslope gravity flows and current reworking; and c) sediment input from suspension or continental supply.

2.5.1.1 Coral-reef growth

Reef growth is water-depth limited and therefore restricted to the uppermost part of the slope in the shallow part of the photic zone. *Porites* colonies were early encrusted by stromatolites which are volumetrically and structurally important components of the reef framework (Riding et al., 1991). The presence of these crusts was crucial to protect and enforce the relatively delicate *Porites* colonies. The early lithification by stromatolitic crusts is thought to have exerted some sort of control on the way reef-framework facies broke and detached as individual blocks. The reef framework was preferentially broken along the planes of weakness provided by the vertical *Porites* sticks and the horizontal, laminar coral growths (Riding et al., 1991).

2.5.1.2 In-situ slope carbonate production

Halimeda plates are the main component in the reef-slope facies. Their major occurrence is in the reef-talus slope. This has also been described from the Messinian Níjar carbonate complex (Fig. 2.1). Mankiewicz (1988) and Martín and Braga (1989) showed that the most abundant *Halimeda* algal production area was in the reef-talus slope. Reef-framework blocks located in the reef-talus slope were suggested as ideal substrates for *Halimeda* growth (Riding et al., 1991). *Halimeda* plates either accumulated in-situ or were exported downslope by sediment flows, forming parautochthonous to allochthonous accumulations. These accumulations were syndepositionally encrusted by microbial biofilms that precipitated micrite contributing to the early lithification of the deposits (Adams and Kenter, 2014). This is similar to *Halimeda* mounds from the Bioherm Unit (Martín et al., 1997). The presence of isolated specimens and clusters of articulated oyster shells in life position, with encrusting serpulids and coralline red algae, indicates that the reef-talus slope was the main skeletal production area together with the reef framework.

2.5.1.3 Rockfalls and gravity flows

The Pinnacle and Thicket Zones at the base of the reef framework were areas of potential instability by slumping and sliding of the underlying unconsolidated sediment at the top of the reef slope (Riding et al., 1991). Under these conditions, the collapse of the reef framework originating rocks and debris falls was a frequent phenomenon at the reef front (Hime et al., 1992; Martinsen, 1994; Drzewievcki and Simó, 2002; Berra et al., 2007; Playton et al., 2010). This resulted in the accumulation of blocks and debris on the reef-talus slope. These accumulations occur as discrete tongues (Playton et al., 2010). These tongues reach metre thickness in CB1 and decametre thickness in CB2. Rockfalls and debris falls involved the sediment produced on the reef-talus slope and triggered sediment

flows spreading basinward to the distal reef-slope. The transport capacity of these sediment flows decayed with increasing distance from the uppermost part of the slope (Adams et al., 1998). The progressive energy decrease in these sediment gravity flows as they moved down slope is proposed to control the grain-size reduction which occurs in the reef-slope sediments.

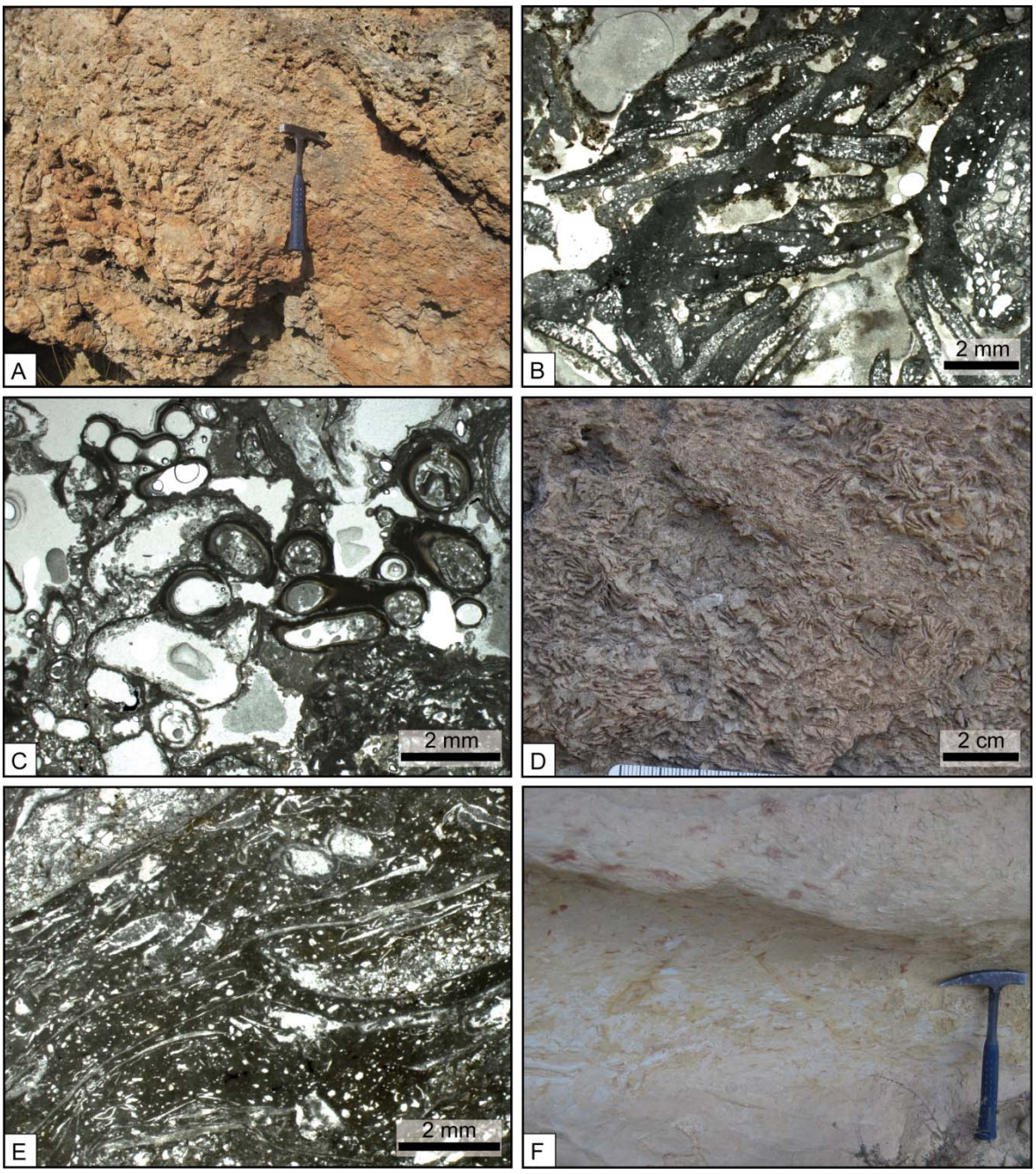

Fig. 2.6: Barranco de los Castaños facies. **A** Outcrop picture of centimetric framework debris in the *Halimeda* breccia. **B** Photomicrograph of *Halimeda* plates embedded in microbial micrite in the *Halimeda* breccia. **C** Photomicrograph of red algal nodule and serpulid clusters from patches within the *Halimeda* breccia. **D** Outcrop view of *Halimeda* rudstone. **E** Photomicrograph of bivalve accumulation in the bioclastic packstone. **F** Outcrop picture of bioturbated siltstone and marls.

2.5.1.4 Hemipelagic rain

The abundance of siltstone and marl in the distal reef-slope reflects the prevalence of deposition from suspension under quiet-water conditions (Drzewievcki and Simó, 2002). Quiet-water conditions are also indicated by the extensive bioturbation of the distal reef-slope deposits. Thin diatomite layers in the basinal sectors are interpreted as the suspension fall-out of planktic-diatom blooms (Saint Martin et al., 2001).

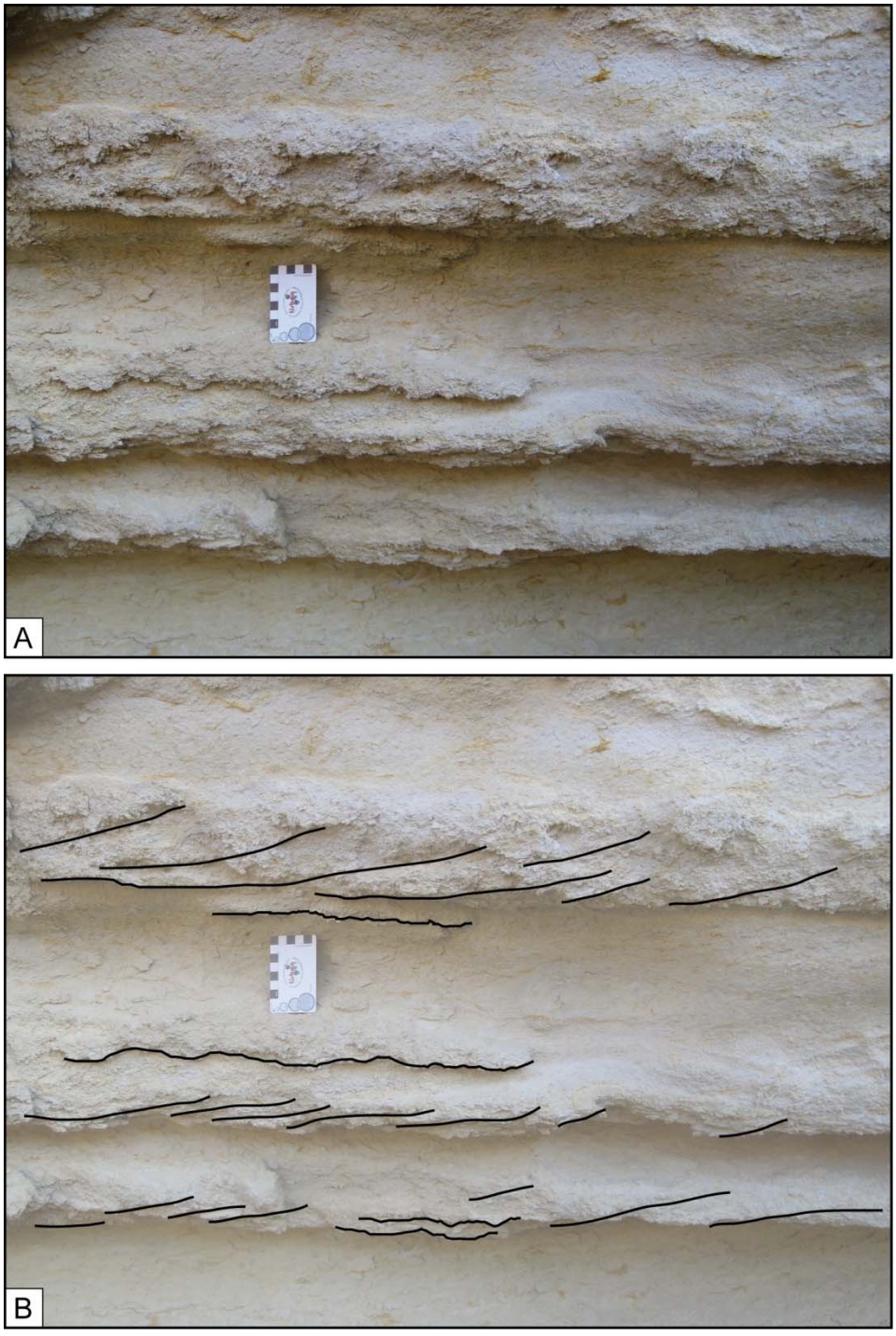

Fig. 2.7: A Outcrop view of the alternation of cross-laminated *Halimeda* rudstone beds with bioturbated marl beds in the distal reef-slope of CB1. **B** sedimentary structures interpreted over the outcrop view.

2.5.1.5 Reworking of reef-slope facies

The presence of climbing-slope cross lamination in the distal reef-slope points toward the existence of upslope directed northward-flowing bottom currents at the distal reef-slope. These upslope currents were not acting continuously as cross-laminated coarse sediment alternates with bioturbated siltstone and marl. The change from cross lamination in CB1 to parallel lamination in CB2 suggests that bottom currents became less significant through time.

2.5.1.6 Siliciclastic input

The advance of the conglomerate body to the south is coeval with the continuous input of hemipelagic rain. This resulted in the mixture of terrigenous grains and basinal sediments in the distal reef-slope. Braga and Martín (1996) identified this conglomerate as part of the middle-fan facies of a fan delta prograding southward from the Sierra de los Filabres and juxtaposed to the reef at some points.

2.5.2 Clinoform development and sea-level change

The facies distribution and depositional geometries along the 1100 m Cariatiz carbonate platform section reveal that a long-term cycle of relative sea-level rise and fall took place throughout reef advance (Braga and Martín, 1996; Cuevas-Castell et al., 2007). According to Braga and Martín (1996) and Rodríguez-Tovar et al. (2013) the relative sea-level cycles reflect glacio-eustatic sea-level changes, as tectonic oscillations of the substrate can be discarded. Obliquity and precession controlled sea-level fluctuations are superimposed onto this general long-term trend (Rodríguez-Tovar et al., 2013). Precessional cycles (C2 cyclicity of Braga and Martín, 1996; and RGP in Cuevas-Castell et al., 2007) are separated by lowstand deposits represented by the inverted wedges. Clinoform bodies reflect a higher-frequency cyclicity within the precessional cycles.

Clinoform Body 1 occurs at the beginning of a sea-level fall in the last precession-forced cycle of the Cariatiz carbonate platform (C2.7 in Braga and Martín, 1996; and RGP 8 in Cuevas-Castell et al., 2007). Rockfalls, in-situ carbonate production, gravity flows and hemipelagic rain were the main processes controlling facies distribution (Fig. 2.10A). Despite the relative sea-level fall and the decreasing accommodation space, the reef slope was large enough for the development of different subenvironments and successive facies belts, as in the examples shown by Adams et al. (1998; 2004) and Playton et al. (2010). At the distal reef-slope, hemipelagic rain and upslope-directed bottom currents were the factors controlling the facies distribution. The occurrence of upslope-directed bottom currents alternates with quiet periods of basinal deposition (Fig. 2.10B). There was a period of bottom current inactivity recorded by bioturbated siltstone and marl during the

last stages of development of CB1.The conglomerates reached the reef slope while the siltstone and marl accumulated in the basin (Fig. 2.8).

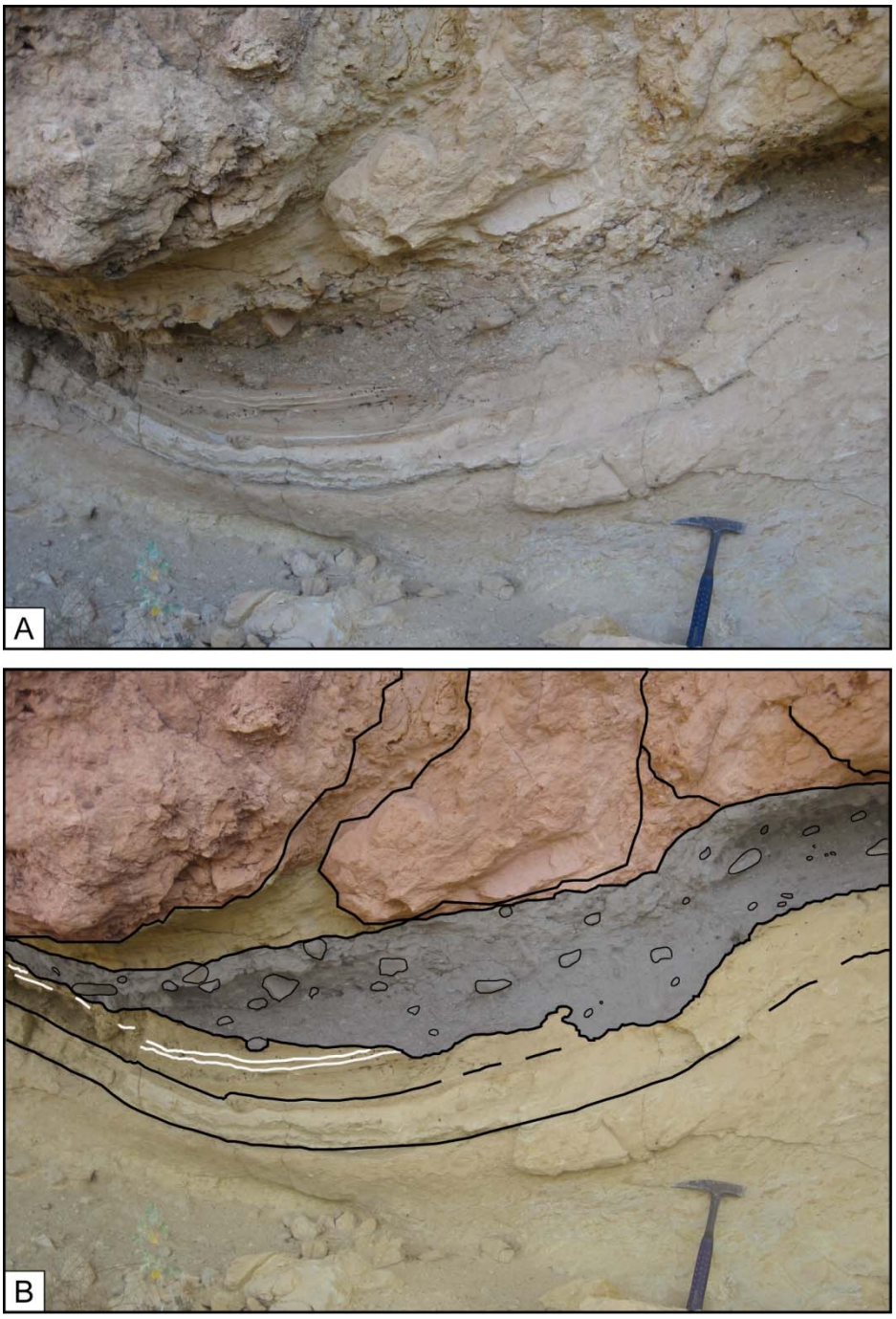

Fig. 2.8: A Outcrop view of the conglomerate body intercalated between CB1 and CB2. **B** facies interpretation of the outcrop view with conglomerate body (gray) among basinal sediments (yellow). The conglomerate erosional base cuts diatomite-rich beds (white) and basinal siltstone and marl. The overlying framework blocks and debris (red) are deforming the conglomerate body and the basinal sediments.

A significant sea-level fall marked the end of CB1 and the beginning of CB2 development. This sea-level fall caused a major exposure of CB1, which resulted in increasing erosion and breakage of CB1 reef-framework. Rockfalls dominated the sedimentation and reef-

framework debris piled up on the CB1 reef-slope (Fig. 2.10C). The upper part of the reef-framework debris is the substrate, where CB2 reef-framework developed. As a result of a lower sea level this new reef framework grew downslope with respect to the position of reef growth in CB1. The downstepping trend of the reef-framework base (Fig. 2.4C) indicates a continuous sea-level fall during the development of CB2. Whereas the accommodation during CB1 formation was enough to allow for a classical reef-slope facies partitioning, this was significantly reduced in CB2 where the facies distribution exhibits a completely different pattern. The proximity of the source area of the debris and a shorter reef-slope did not allow for an adequate energy decay (Schlager and Adams, 2001), and the reef-framework debris could be more easily exported, spreading down to the distal reef-slope (Fig. 2.10D). Facies distribution at the distal reef-slope therefore was controlled by sediment gravity flows and eventual rockfalls (Fig. 2.10E). These sediment gravity flows resulted in well-laminated bioclastic packstone in the distal reef-slope. Hemipelagic rain affected the distal reef-slope but was less significant than in CB1.

2.5.3 Composition and sea-level change

Halimeda is a major component in CB1 and is absent, or almost absent, in CB2. In general, the facies with high concentrations of *Halimeda* (*Halimeda* breccia and *Halimeda* rudstone) are common in most of the Cariatiz reef-slope deposits including CB1. The amount of *Halimeda* algae in reef-slope facies increased during reef progradation reaching its maximum value during the highstand and beginning of sea-level fall of the last precession-forced cycle (C2.7 of Braga and Martín, 1996).

Facies with a high proportion of *Halimeda* plates also occur in other Messinian carbonate platforms (Esteban, 1980; Mankiewicz, 1988; Franseen and Mankiewicz, 1991; Braga et al., 1996; Franseen and Goldstein, 1996; Martín et al., 1997). Most of the Messinian *Halimeda* facies are found in the coral-bearing fringing-reef slope. *Halimeda* was also the main constituent in some bioherms located on non-rimmed platform slopes as in the bioherms described by Martín et al. (1997). Widespread and extensive *Halimeda* growth needs a relatively high nutrient environment (Drew and Abel, 1983; Franseen and Mankiewicz, 1991; Martín et al., 1997), which can ultimately be related to upwelling currents (Mankiewicz, 1988).

Sánchez-Almazo et al. (2007) described stable oxygen and carbon isotope variations in shells of benthic and planktic foraminifera from the distal reef-slope and basinal deposits adjacent to the analysed Cariatiz carbonate platform. In deposits laterally equivalent to CB1, planktic and benthic $\delta^{13}C$ values are different, which was interpreted to reflect a pronounced water stratification. Up-section, in deposits coeval to CB2, the carbon isotope

signals converge. According to Sánchez-Almazo et al. (2007) this indicates an important nutrient-content decrease and the disappearance of water stratification as a result of the mixing of deeper and shallower water masses.

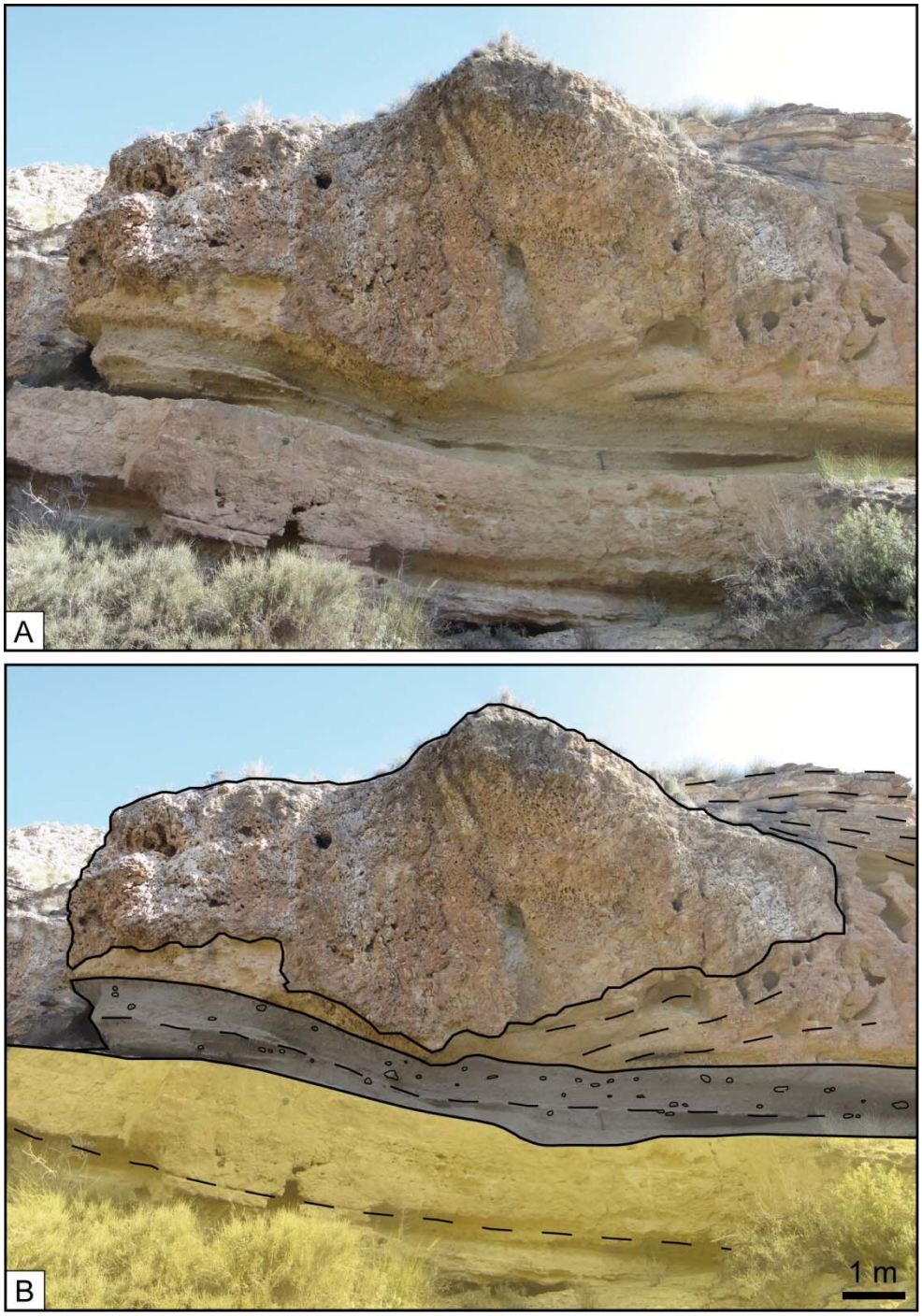

Fig. 2.9: A Outcrop view of a framework block deforming the distal reef-slope deposits of CB2. **B** facies interpretation of the outcrop view with distal reef-slope deposits of CB2 (red), conglomerate body (gray) and distal reef-slope deposits of CB1 (yellow).

This change in water stratification can be linked to the falling sea level during the last precession-forced cycle (Sánchez-Almazo et al., 2007). Gill and Clarke (1974) related the occurrence of upwelling in modern equatorial areas to sea-level fluctuations: upwelling takes place in stratified-water conditions during sea-level rise and highstand. Therefore, it is proposed that upwelling of nutrient-rich waters during sea-level rise and highstand stages also promoted the flourishing of *Halimeda* in the analysed carbonate platform. These upwelling conditions persisted at the beginning of sea-level fall in the last precession-forced cycle, as recorded by the presence of *Halimeda* breccia and *Halimeda* rudstone facies in CB1. This is corroborated by upslope-pointing, low-angle cross lamination indicating the occurrence of upslope-directed bottom currents at the CB1 distal reef-slope. The decreasing water depth with continued sea-level fall finally caused water mixing and consequently the interruption of upwelling. The end of upwelling conditions probably explains the absence of *Halimeda* algae in CB2 facies.

2.5.4 Geometry of clinoform bodies

The factors that control the geometry of carbonate platform slopes are summarised in Schlager (2005). These are the volume of sediment and platform height (Schlager, 1981), the grain size (Kirkby, 1987), and the erosion-deposition balance (Schlager and Camber, 1986). Schlager (1981) pointed out that the volume of sediment must decrease with decreasing height of the platform to keep the same geometry of the slope. At the studied section, platform height changed as a response to falling sea level, but the volume of sediment, as deduced from clinoform body size (Fig. 2.4), does not varies significantly from CB1 to CB2. The variation in the platform height from CB1 to CB2 seems to be more significant for changing the erosion-deposition balance and, consequently, facies distribution. Schlager and Camber (1986) described variations in slope geometries as a result of changes in the erosion-deposition balance during slope evolution. Erosional and depositional processes, as described in the previous section, were approximately the same in both clinoform bodies but acted with different intensity. Depositional processes are dominant during CB1 formation while erosion is more relevant in CB2, at least during the first stages of clinoform body development. Changes in the erosion-deposition balance therefore explain the different facies distribution, but not CB1 and CB2 geometries. Kirkby (1987) suggested that grain size controls the angle of stability of the slope. Our study shows that facies, and subsequently grain-size patterns, are completely different in each segment of the linear slope of CB1, explaining changes in angles of these segments. These slope-angle changes related to grain size are also recorded in the transition from reef-framework debris to bioclastic packstone and basinal deposits in CB2.

Adams and Kenter (2014) proposed additional factors controlling the steep angles in carbonate slopes. The major factors are the response to high shear strengths in fine-grained carbonate slope sediments (Kenter, 1990; Kenter et al., 2005; Schlager, 2005; Playton et al., 2010), processes of early lithification and cementation of the slope sediments, and in-situ carbonate production and stabilization (Kenter, 1990; Della Porta et al., 2003; 2004; Kenter et al., 2005).

Several factors contribute to the studied clinoform geometries in Barranco de los Castaños. In CB1, with a linear profile, the different slope segments are characterized by different facies, with different grain-sizes, and consequently different angles of repose (Kenter, 1990; Adams and Schlager, 2000). The uppermost segment consists of an accumulation of reef-framework debris. The large debris blocks were nearly deposited in-situ and their imbrication allowed the high angle accumulation of 60°. The slope angles of 40°-30° in the proximal and 15°-10° in the distal reef-slope correspond to the angles of repose of sand-gravel and mud respectively (Kenter, 1990). Although these angles of repose are theoretically possible, field and seismic examples usually show lower angles than those described for CB1 (see Table 1 in Kenter, 1990; and Adams and Schlager, 2000).

Carbonates slopes with angles steeper than 30°-45°, as in the studied section, were described by Kenter (1990) as the result of stabilization by organic framebuilding or by early lithification. That is the case of CB1, where patches of serpulids and red algae as well as the abundant microbial micrite matrix and micritic envelopes in most of the bioclasts definitely contributed to the stabilization of the steep reef-slope. This binding favoured the sediment accumulation in such steep angles of repose (Adams and Kenter, 2014). Stabilization by microbial micrite was also suggested as an important factor controlling slopes geometries in Palaeozoic and Triassic platforms (Keim and Schlager, 2001; Della Porta et al., 2003; 2004; Kenter et al., 2005; Schlager and Reijmer, 2009). In these platforms, organic binding is more significant than grain size to determine the slope geometry.

In CB2, decametric reef-framework blocks are the main component of the reef slope. The accumulation of blocks at the base of CB2 occurred on top of the inherited CB1 steep reef-slope. The imbrication of such large blocks and the development of reef framework on top contributed to stabilize the reef slope despite its high angle. When the steep slope collapsed, reef debris reached the proximal to distal reef-slope (Adams and Kenter, 2014). Inheritance of substrate topography was suggested by Franseen and Goldstein (1996) as the dominant factor controlling slope geometries in Messinian reefs in the Molata de las Negras, coeval with the Cariatiz reef.

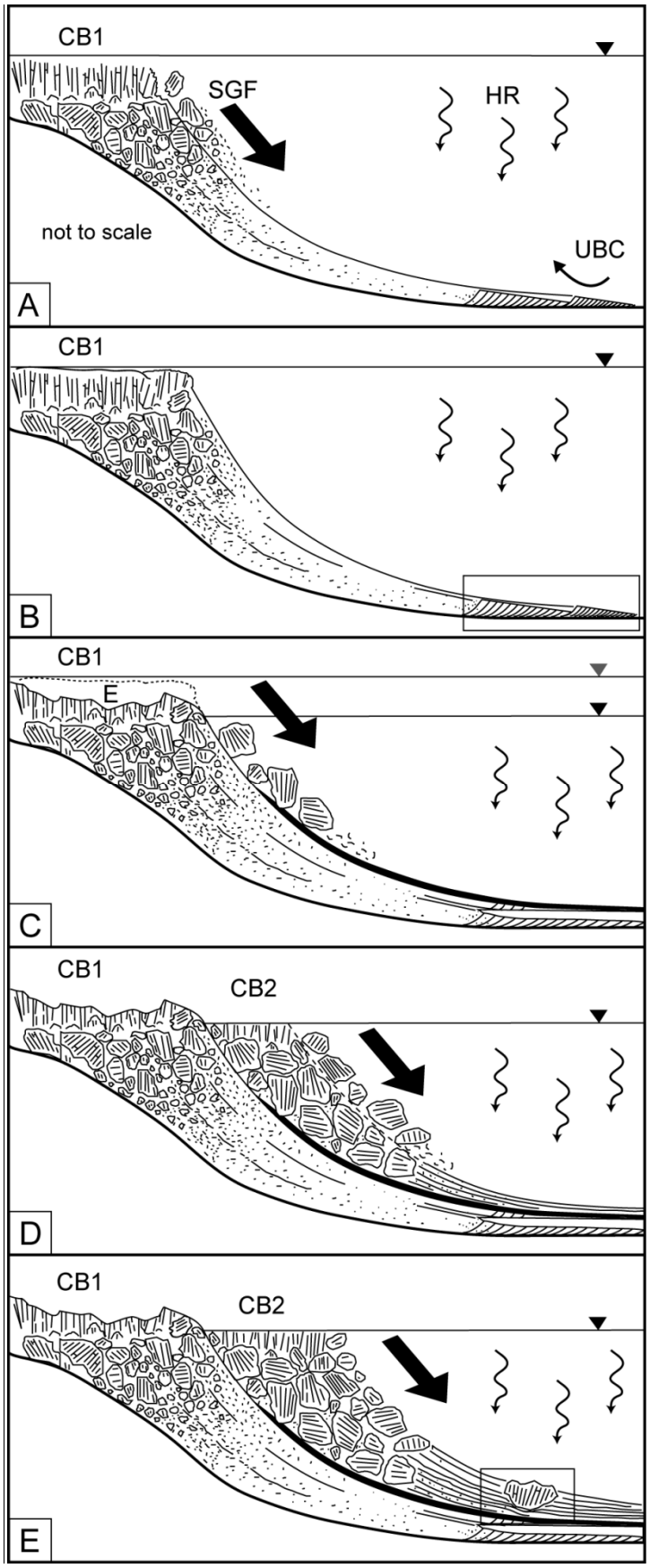

Fig. 2.10: Model showing the development of CB1 and CB2: **A** instability and collapse of the reef framework produces rockfalls and sediment gravity flows (SGF). Grain-size distribution reflects the progressive energy decay of these flows along the slope. The sediments in the distal reef-slope are reworked by upslope-directed bottom currents (UBC). Hemipelagic rain (HR) occurs at the distal reef-slope. **B** Phases of upslope bottom currents alternate with quiet periods (Fig. 2.7 in box). **C** A sea-level fall exposes CB1 triggering erosion (E) of CB1 deposits. Rockfalls are significant. Conglomerates occur at the base of the framework debris. **D** The CB2 reef grows on top of framework debris reworked from CB1. The new framework was in a lower position compared to CB1 reefs. Fallen blocks extend further down slope into a now shallower basin. **E** During CB2 growth, sediment gravity flows are stronger as reflected by the persistent parallel lamination in distal reef-slope deposits. Fallen reef-framework blocks deformed these distal deposits (Fig. 2.9 in box).

2.6 Conclusions

Two clinoform bodies, CB1 and CB2, were studied in the Messinian carbonate platform of Cariatiz. Clinoform Body 1 has a concave-upward linear slope with facies represented by reef framework, reef-framework debris and *Halimeda* breccia in the reef-talus slope deposits. A *Halimeda* rudstone characterizes the proximal reef-slope, and bioclastic packstone together with siltstone and marl the distal reef-slope. Microbial micrite and micritic envelopes are common in this clinoform body. Clinoform Body 2 has an exponential profile and its facies consist of reef framework, reef-framework debris from the reef-talus to distal reef-slope, and bioclastic packstone and hemipelagic sediment in the distal reef-slope.

This facies distribution is the response to the interaction of coral-reef growth, in-situ slope carbonate production, rockfalls, sediment gravity flows, hemipelagic rain, reworking of reef-slope facies, and siliciclastic input from the basement cropping out to the north. Changes in accommodation space, ultimately related to sea-level fluctuations, controlled the relative impact of these processes as well as their intensity, and, in this respect the type of sediment that finally accumulated along the reef slope. The vertical shift of facies shows that a sea-level fall took place from CB1 to CB2. This sea-level fall also changed the hydrographical conditions of the basin eliminating water stratification and upwelling, which prevailed during formation of CB1 and promoted the abundance of *Halimeda* algae that do not occur in CB2.

Facies distribution and changes in grain size are widely thought to be the main factors controlling slope geometries. However, geometry and facies analysis of CB1 and CB2 suggest that additional factors are needed to explain the steep angles of these slopes. The presence of microbial micrite, micritic envelopes and patches of encrusting organisms such as red algae and serpulids in CB1 stabilized the steep angle of the reef slope. In CB2, the heavy decametric reef-framework blocks deposited on top of an inherited, steep, prior topography were fixed there by the reef framework that settled and grew on top of them.

This study propose two new considerations to the ongoing discussion on carbonate slope systems: a) The dynamic behaviour of slope facies changes related to sea-level fluctuations, in contrast with the classic static models; and b) the importance of organic binding in Neogene reef-slope geometries, similar to Palaeozoic and Triassic examples.

Chapter III

Amplitude of late Miocene sea-level fluctuations from karst development in reef-slope deposits

Abstract

With the aim to increase accuracy of the reconstruction of past sea-level changes, a prograding upper Miocene carbonate platform in southern Spain revealing different sea-level pinning points was analysed. These levels are distinct diagenetic zones (DZ) and the position of reef crest deposits. DZ1 is defined by the dissolution of bioclastic components and DZ2 by calcitic cement precipitation in dissolution pores. Calcite cements are granular, drusy, and radiaxial fibrous, of meteoric origin as deduced from cathodoluminescence, EDX spectroscopy, as well as $\delta^{13}C$ and $\delta^{18}O$ isotope analyses. DZ3 has moldic porosity after aragonite bioclasts with minor granular calcitic cements. DZ1 and DZ2 indicate karstification and the development of a coastal palaeoaquifer during a sea-level lowstand. DZ3 diagenetic features are related to the final exposure of the section. Facies and diagenetic data reveal a complete cycle of sea-level fall (23 ± 1 m) and rise (31 ± 1 m). A solid age model for these deposits places this cycle between 5.89 and 5.87 Ma. Therefore, for the first time, this work allows a direct comparison of an outcrop with a pelagic marine proxy record of a specific Neogene sea-level fluctuation.

This chapter is based on **Reolid, J., Betzler, C., and Braga, J.C.** (submitted) Amplitude of late Miocene sea-level fluctuations from karst development in reef-slope deposits (SE Spain).

3.1 Introduction

Past sea-level stands or fluctuations in sea level may be reconstructed using: (1) sedimentologically defined pinning points, that is, points of quantitative constraint of ancient sea-level positions relative to an arbitrarily defined, geologically useful starting elevation (Goldstein and Franseen, 1995), (2) the interpretation of seismostratigraphic relationships (Zhong et al., 2004), and (3) the $\delta^{18}O$ analysis of deep-water benthic foraminifera as an ice-volume proxy (Miller et al., 2005; 2011). Several curves showing Neogene sea-level fluctuations were developed using these proxies (Haq et al., 1987; Miller et al., 2011), but these curves show discrepancies and some uncertainties for the amplitudes of sea-level fluctuations, especially for high-frequency changes.

In nearshore carbonate deposits, there were several attempts to reconstruct past sea-level changes based on coastal karst marine sedimentary infilling, which can change from meteoric-vadose to meteoric-phreatic or to marine environments in response to sea-level fluctuations (Van Hengstum et al., 2011), and on the occurrence and distribution of calcitic cement fabrics (Meyers, 1978; Li et al., 2014). Such studies provide accurate values for the Quaternary (Van Hengstum et al., 2011) but show high uncertainties for Neogene and older deposits.

In this paper, a test is proposed to verify and reconcile postulated amplitudes of late Miocene (5.89 to 5.87 Ma) high-frequency sea-level changes defined by oxygen isotopes with those recorded in shallow water deposits. The superbly exposed Cariatiz carbonate platform in southern Spain (Braga and Martín, 1996; Sánchez-Almazo et al., 2007; Cuevas-Castell et al., 2007; Reolid et al., 2014) is well dated (Rodríguez-Tovar et al., 2013), and both highstand and lowstand sea-level positions can be traced in the outcrop. The present research, based on combined LIDAR and outcrop mapping (Reolid et al., 2014) as well as petrographic and isotopic analyses, uses the position of coral reefs and distinct early diagenetic zones to trace sea-level change during the formation of a single high-frequency sequence. Thus, a unique opportunity arises for testing the validity of the amplitudes of global sea-level fluctuations recorded by proxies in pelagic sequences.

3.2 Geological setting

The Cariatiz carbonate platform is located at the northern margin of the Sorbas Basin in southeast Spain, which is bounded by metamorphic rocks from the Internal Betic Zone of the Betic Cordillera (Fig. 3.1). During the Messinian, the basin was rimmed by carbonate platforms, such as the Cariatiz location, changing basinwards to marls and diatomites

(Martín and Braga, 1994). The carbonate-platform top is an unconformity onlapped by a sequence of evaporites, carbonates, and siliciclastics (Riding et al., 1999).

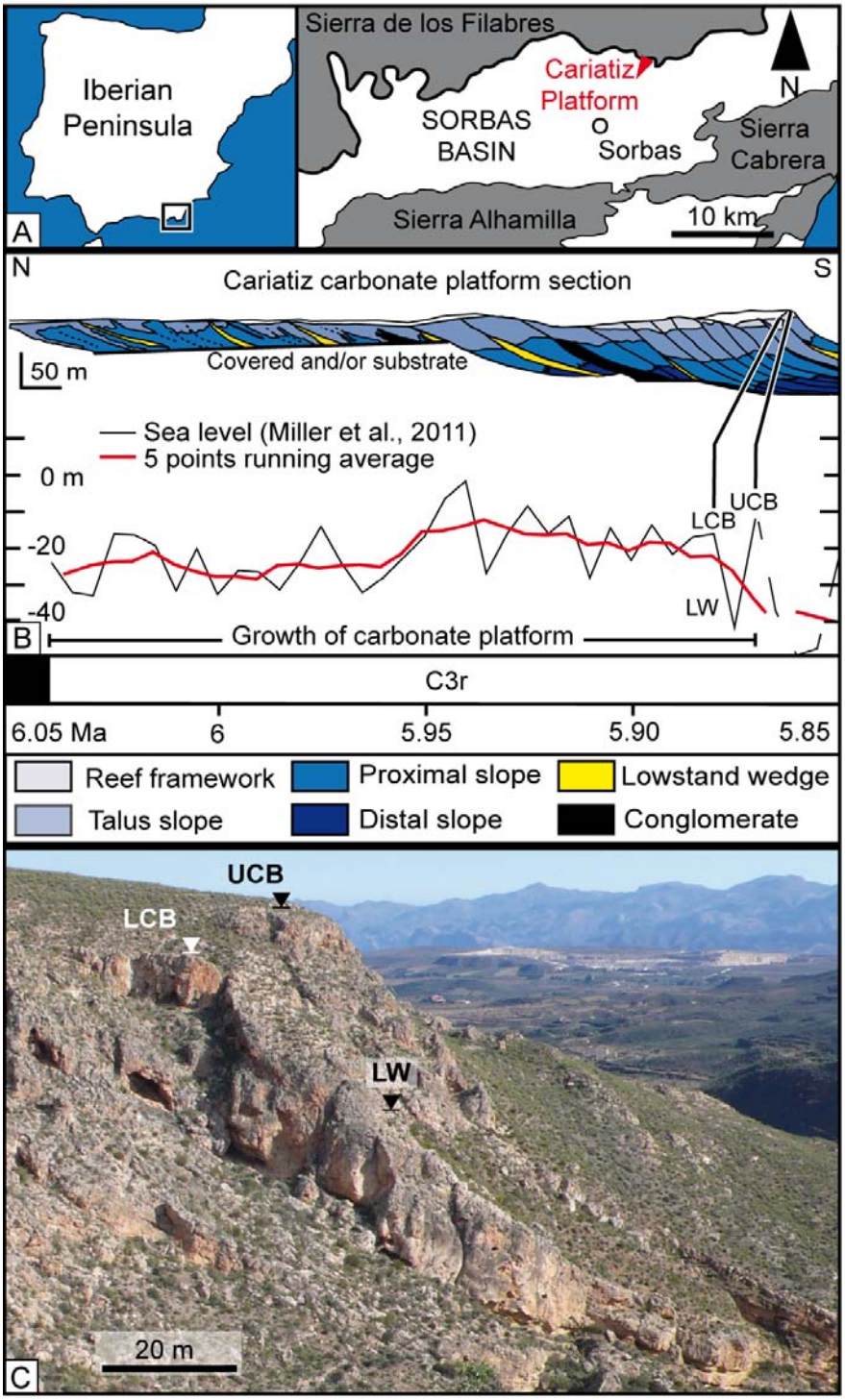

Fig. 3.1: A Location of the Cariatiz carbonate platform in the Sorbas Basin, SE Spain (red triangle). **B** Cariatiz carbonate platform section with facies according to Reolid et al. (2014), magnetostratigraphy according to Krijgsman et al. (1999), and global sea-level curve from Miller et al. (2011). **C** Field panorama of the clinoform bodies (LCB and UCB) and lowstand wedge (LW). Triangles indicate the position of highstands (LCB and UCB) and lowstand (LW). The top of the LCB is at 37° 8.809' N and 2° 6.181' W.

The last progradation stages of the Cariatiz carbonate platform comprise a series of facies belts consisting of lagoonal deposits and reef-crest, reef-framework, and reef-slope deposits (Braga and Martín, 1996; Reolid et al., 2014). The reef-framework and reef-slope facies are arranged into clinoform-delimited bodies, thinning downslope and basinwards. The reef-crest facies likely formed at or just below sea level (Riding et al., 1991; Braga and Martín, 1996), as in other late Miocene reefs of the Mediterranean region (Pomar and Ward, 1994; Goldstein and Franseen, 1995).

The stacking pattern, depositional geometries, and facies distribution throughout the section (Braga and Martín, 1996; Cuevas-Castell et al., 2007; Reolid et al., 2014), together with $\delta^{13}C$ and $\delta^{18}O$ values of planktonic and benthic foraminifera in distal slope deposits (Rodríguez-Tovar et al., 2013) indicate that the entire platform formed during four to five obliquity cycles of sea-level change with a superposition of seven to nine precessional cycles separated by basinward-thickening lowstand wedges. Within the sediment packages deposited during the precessional cycles, clinoform bodies reflect higher-frequency cyclicity in the sub-Milankovitch band. The total duration of platform growth estimated from the obliquity cycles is approximately 180 ky (Cuevas-Castell et al., 2007; Rodríguez-Tovar et al., 2013).

Magnetostratigraphic data indicate that the entire Cariatiz carbonate platform was deposited during the single period of reverse polarity of Chron C3r (Sánchez-Almazo et al., 2007), which has its lower boundary dated at 6.04 Ma (Krijgsman et al., 1999). Combined magneto- and cyclostratigraphic data reveal this platform interval was deposited between 5.89 and 5.87 Ma. During this period, the northern margin of the Sorbas Basin was tectonically stable and since then has uplifted at an average rate of 110 ± 5 m/Ma (Braga et al., 2003). The present tectonic tilt of this platform is less than 3 degrees (Braga and Martín, 1996).

3.3 Methods

The different facies and diagenetic zones were mapped at the outcrop and sampled with a hand drill, recovering plugs of 15x5 cm (Fig. 3.2). Polished slabs and 40 thin sections were analysed to identify microfacies and cements, and selected thin sections were analysed by cathodoluminescence microscopy (Lumic HC5-LM) and EDX spectroscopy (Zeiss LEO-1455VP) in the Institute of Geology, University of Hamburg. Representative cement samples were subsampled for $\delta^{13}C$ and $\delta^{18}O$ isotopic analyses at the Scientific Instruments Centre, University of Granada (Spain). The $\delta^{13}C$ and $\delta^{18}O$ values are reported relative to VPDB with and standard deviation of less than 0.05 ‰ respect to the NBS 19. Platform-

slope dimensions and the extension of diagenetic zones were extracted from LIDAR data with a spatial resolution of 5 cm, as presented in Reolid et al. (2014).

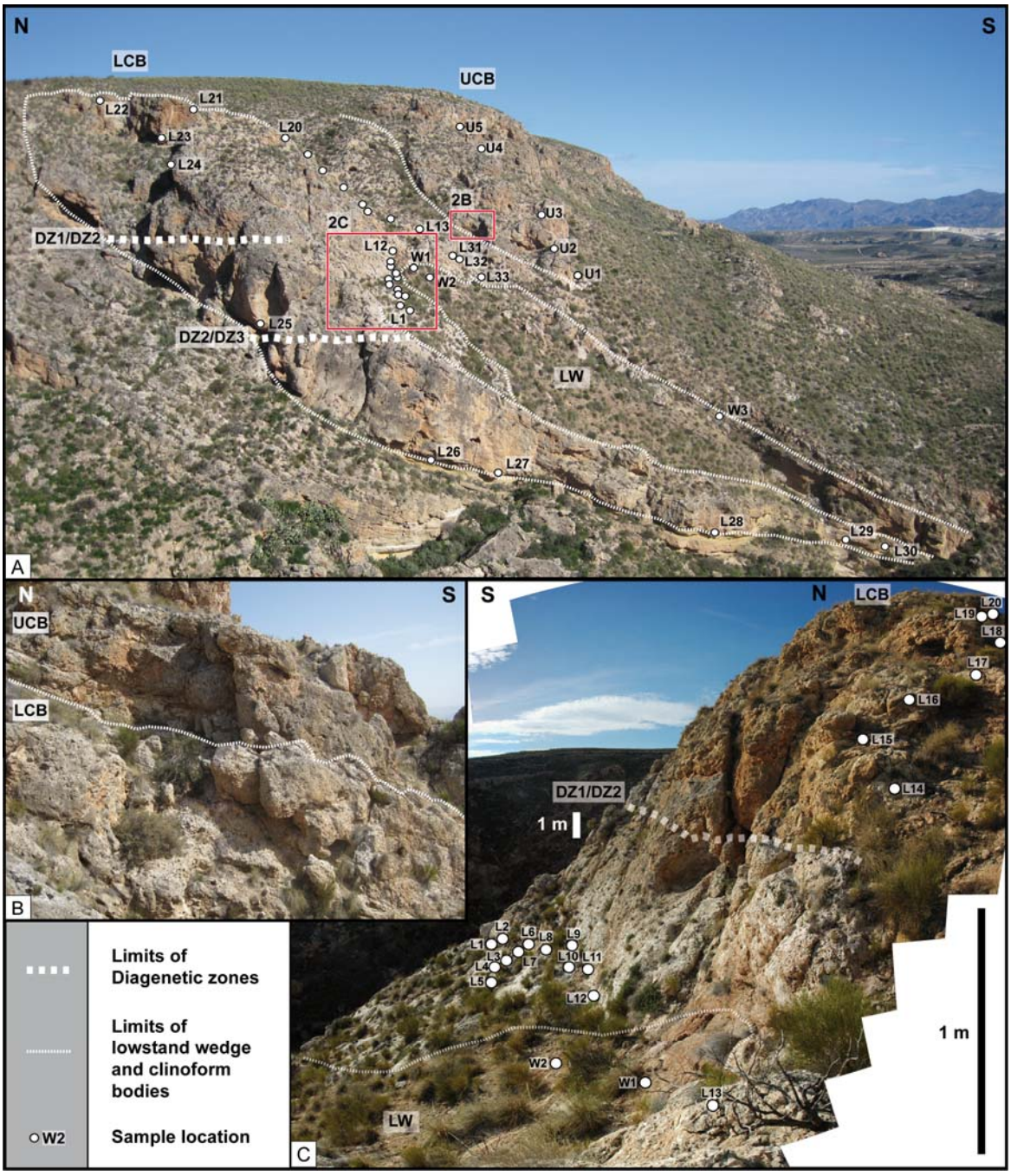

Fig. 3.2: A Panorama view of the Cariatiz carbonate platform slopes discussed in the text. White dots indicate the sample locations. Petrographical, sedimentary and diagenetic features of the samples are summarised in Tables 3.2 and 3.3. The thick white dashed lines mark the contacts between the different diagenetic zones which are discussed in the text. The vertical distance between both diagenetic boundaries is 15 m. Red frames mark the position of figures 2B and 2C. **B** Outcrop view of the contact between the cemented LCB and UCB with the dissolution features of DZ3. **C** Outcrop view of the contact between LCB and LW. The picture also shows the sharp contact between DZ1 and DZ2 in LCB.

.

3.4 Resutls

The section consists of two clinoform bodies (LCB, UCB) separated by a lowstand wedge (LW; Figs. 3.1, 3.2A). These are the last episodes of the Cariatiz carbonate platform development, which change here to the basinal sediments of the Sorbas Basin (Braga and Martín, 1996; Rodríguez-Tovar et al., 2013; Reolid et al., 2014).

3.4.1 Lower Clinoform Body

The top of the LCB consists of a reef framework of *Porites* coral that formed the reef crest at sea level (Riding et al., 1991). The corals are covered by coralline algal-foraminiferal and stromatolitic crusts. The framework front gradually changes into a breccia with decametre- to metre-scale reef-framework blocks. Among the blocks are sediment pockets with bioclastic rudstone to packstone. The distal slope deposits consist of bioclastic packstone with basinal silt and marl intercalations.

There are three main zones within this clinoform body with distinct porosities and cements in the pores (Table 3.1; Fig. 3.3). The upper part of the clinoform body (DZ1) extends down 23.5 m from the reef crest and is characterized by a high moldic porosity (Fig. 3.2; samples L14 to L24 in Table 3.2). Dissolved coral skeletons form a network of interconnected cavities (Fig. 3.4A).

Diagenetic Zone	Porosity	Cements	Occurrence
DZ1	10%	None.	LCB
DZ2	1-3%	(1) Granular calcite, (2) drusy calcite, and (3) radioaxial fibrous calcite.	LCB
DZ3	1-5%	Rare. Locally granular calcite.	LCB, LW, UCB

Table 3.1: Summary of the main features of the different diagenetic zones.

Downslope, below the lower boundary of DZ1, there is a 15 m thick interval (DZ2) characterized by the presence of calcitic cements partially to totally infilling the porosity and giving a white colour to the rock of this zone (Figs. 3.2, 3.3). This band is laterally limited by the base of the overlying clinoform body (UCB, Fig. 3.2B) and by the underlying conglomerate body, which is partially cemented. DZ2 has sharp upper and lower limits (Fig. 3.2C). The cements of DZ2 occur in bioclastic molds, including coral skeletons in reef-framework debris (Fig. 3.4B). The cement sequence in a pore starts with a granular calcite cement (Fig. 3.4C) and locally drusy cement (samples L1 to L13, L25 and L31 to L33 in Table 3.2). The last cementation phase consists of radiaxial fibrous calcite that, in some cases, can completely fill the remaining pore space (Fig. 3.4C). In

cathodoluminescence, all cements are non-luminescent. The iron content of the cements is too low to be determined with EDX analysis. The $\delta^{13}C$ and $\delta^{18}O$ values show an average of -7.38 ‰ for $\delta^{13}C$ and -7.77 ‰ for $\delta^{18}O$ (Fig. 3.5). Underlying the DZ2 interval, a third zone (DZ3) with low to moderate moldic porosity occurs. Rarely, granular calcite cements partially infill the dissolution pores (samples L26 to L30 in Table 3.2).

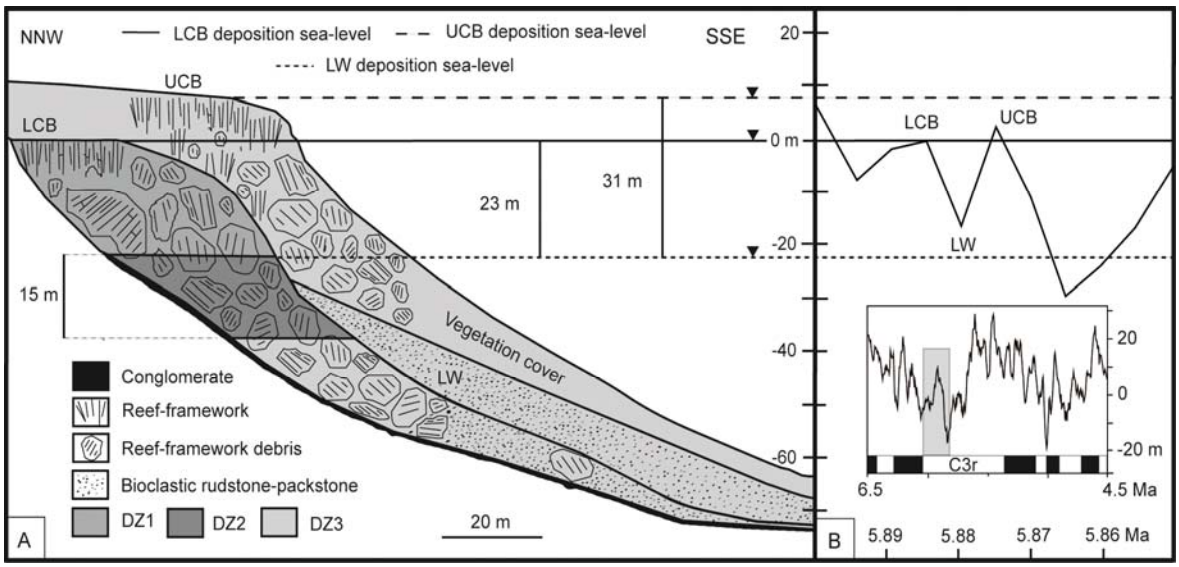

Fig. 3.3: A Study section including the lower (LCB) and upper clinoform body (UCB), the lowstand wedge (LW), and the LCB diagenetic zones (DZ1, DZ2, and DZ3 described in text and Table 3.1). Horizontal lines indicate sea-level position during the formation of the distinct sedimentary bodies. **B** Late Miocene sea-level changes according to Miller et al. (2011) compared to sea-level position pinning points in the Cariatiz carbonate platform. The gray rectangle in the inlay shows the time interval of the Cariatiz carbonate platform formation.

3.4.2 Lowstand Wedge

This sedimentary body, interpreted as lowstand deposits by Braga and Martín (1996), consists of bedded packstone to rudstone with bivalve fragments, bryozoans, red algae, and serpulids wedging out upslope 28 m below the reef crest of the LCB (Figs. 3.2C, 3.3A). The complete lowstand wedge shows the same characteristics as DZ3 with a low to moderate porosity with minor calcitic cement infills (samples W1 to W3 in Table 3.3).

3.4.3 Upper Clinoform Body

The UCB reef framework in its proximal part overlies the LCB reef framework, and its distal part covers the uppermost LCB slope (Figs. 3.2B, 3.3A). The UCB framework gradually changes basinwards into a breccia with metre-scale reef-framework blocks. Regarding the diagenetic characteristics, this body presents the same characteristics as in

DZ3 of the LCB and of the LW with low to moderate porosity with minor calcitic cement infills (samples U1 to U5 in Table 3.3).

Sample	Composition	Matrix	Pore type	Calcitic cement paragenesis	Body	Zone
L1	Coral- microbial framework, red algae, and serpulids.	Microbial micrite.	Moldic porosity after aragonitic bioclasts. Interparticle porosity.	Granular/drusy.	LCB	DZ2
L2 and L25	Coral- microbial framework.	Bioclastic microgranular and microbial micrite.	Moldic porosity after aragonitic bioclasts.	Granular.	LCB	DZ2
L3	Coral- microbial framework.	Microbial micrite.	Moldic porosity after aragonitic bioclasts.	Granular/drusy, radiaxial fibrous, and bladed.	LCB	DZ2
L4 and L5	Coral- microbial framework.	Microbial micrite.	Moldic porosity after aragonitic bioclasts.	Microcrystalline, granular, and radiaxial fibrous.	LCB	DZ2
L6	Coral- microbial framework and bivalve debris.	Microbial micrite	Moldic porosity after aragonitic bioclasts.	Microcrystalline, granular, and radiaxial fibrous.	LCB	DZ2
L7, L31, and L33	Coral- microbial framework.	Microbial micrite, locally brecciated.	Moldic porosity after aragonitic bioclasts.	Microcrystalline, granular, and radiaxial fibrous.	LCB	DZ2
L8	Coral- microbial framework.	Microbial micrite.	Moldic porosity after aragonitic bioclasts.	Microcrystalline, drusy, and radiaxial fibrous.	LCB	DZ2
L9	Coral- microbial framework.	Microbial micrite.	Moldic porosity after aragonitic bioclasts.	Microcrystalline, granular, blocky, and radiaxial fibrous.	LCB	DZ2
L10 and L32	Coral- microbial framework.	Microbial micrite.	Moldic porosity after aragonitic bioclasts.	Microcrystalline, granular, and radiaxial fibrous.	LCB	DZ2
L11	Coral- microbial framework and bivalve debris.	Microbial micrite.	Moldic porosity after aragonitic bioclasts.	Drusy, blocky, and radiaxial fibrous.	LCB	DZ2
L12	Serpulid cluster and bryozoans.	Bioclastic microgranular.	Inter- and intraparticle porosity. Moldic porosity after aragonitic bioclasts.	Granular and radiaxial fibrous.	LCB	DZ2
L13	Serpulid cluster.	Microbial micrite.	Inter- and intraparticle porosity. Moldic porosity after aragonitic bioclasts.	Microcrystalline, granular, blocky, and fibrous.	LCB	DZ2
L14, L15, L16, and L17	Coral- microbial framework.	Microbial micrite.	Moldic porosity after aragonitic bioclasts.	--	LCB	DZ1
L18	Coral- microbial framework, red algae, and serpulids.	Bioclastic microgranular and microbial micrite.	Moldic porosity after aragonitic bioclasts.	--	LCB	DZ1
L19, L21, L22, and L23	Coral- microbial framework.	Microbial micrite.	Moldic porosity after aragonitic bioclasts.	--	LCB	DZ1
L20 and LCB24	Coral- microbial framework, vermetids, and serpulids.	Microbial micrite.	Moldic porosity after aragonitic bioclasts.	--	LCB	DZ1
L26, L27, and L28	Coral- microbial framework.	Microbial micrite.	Moldic porosity after aragonitic bioclasts.	--	LCB	DZ3
L29 and L30	Bivalve fragments, bryozoans, gastropods, red algae, and serpulids.	Bioclastic microgranular and micrite.	Moldic porosity after partial dissolution of aragonitic bioclasts.	None. Minor granular cements in LCB 22.	LCB	DZ3

Table 3.2: Summary of the petrographical, sedimentary, and diagenetic characteristics of the samples in a transect across the different diagenetic zones.

Sample	Composition	Matrix	Pore type	Calcitic cement paragenesis	Body	Zone
W1, W2, and W3	Bivalve fragments, bryozoans, red algae, and serpulids.	Bioclastic microgranular.	Moldic after aragonitic bioclasts. Inter- and intraparticle porosity.	--	LW	DZ3
U1 and U2	Coral- microbial framework.	Bioclastic microgranular and microbial micrite.	Moldic porosity after aragonitic bioclasts.	--	UCB	DZ3
U3	Coral- microbial framework, red algae, and serpulids.	Microbial micrite and bioclastic microgranular.	Moldic porosity after aragonitic bioclasts.	--	UCB	DZ3
U4	Coral- microbial framework.	Microbial micrite, locally brecciated.	Moldic porosity after aragonitic bioclasts. Inter- and intraparticle porosity.	--	UCB	DZ3
U5	Coral- microbial framework.	Microbial micrite.	Moldic porosity after aragonitic bioclasts.	--	UCB	DZ3

Table 3.3: Summary of the petrographical, sedimentary, and diagenetic characteristics of the samples in the UCB and LW.

3.5 Interpretation and discussion

3.5.1 Diagenetic zones

The clinoform bodies and the lowstand wedge display a clear zonation of porosity and cements related to different diagenetic overprints (Table 3.1; Fig. 3.3A). The first diagenetic zone (DZ1) in the LCB has a high moldic porosity due to the extensive dissolution of aragonitic bioclasts and partial dissolution of calcitic bioclasts (Fig. 3.4A). The second diagenetic zone (DZ2) directly occurs below DZ1 and consists of a succession of calcitic cements infilling the pores (Fig. 3.4C). The third diagenetic zone (DZ3) affects the lower part of LCB as well as the complete LW and UCB (Fig. 3.3A). DZ3 also shows high moldic porosity due to the extensive dissolution of aragonitic bioclasts and partial dissolution of calcitic bioclasts with minor local precipitation of granular calcitic cements. The diagenetic overprint in the clinoform packages and the lowstand wedge is proposed to be linked to different positions of past sea-level stands and development of a meteoric karst in the Cariatiz carbonate platform.

3.5.2 Sea level and diagenesis

The first sea-level position in the succession corresponds to a high stand recorded by the reef-crest facies of the LCB. Falling sea level subaerially exposed the upper part of the LCB allowing its karstification by the action of meteoric waters and the dissolution of aragonite and high-Mg-calcite components as reported by Land (1970), Budd (1992), and Swart (2015) elsewhere. The dissolution of most of the components generated a network of connected cavities that developed to a coastal palaeoaquifer with two zones: (1) a

meteoric-vadose zone dominated by dissolution, corresponding to DZ1, and (2) a meteoric-phreatic zone dominated by calcite precipitation, corresponding to DZ2 (Figs. 3.2C, 3.3A). The sharp contact between both diagenetic zones represents the past position of the palaeowater table of the coastal palaeoaquifer (Fig. 3.2C).

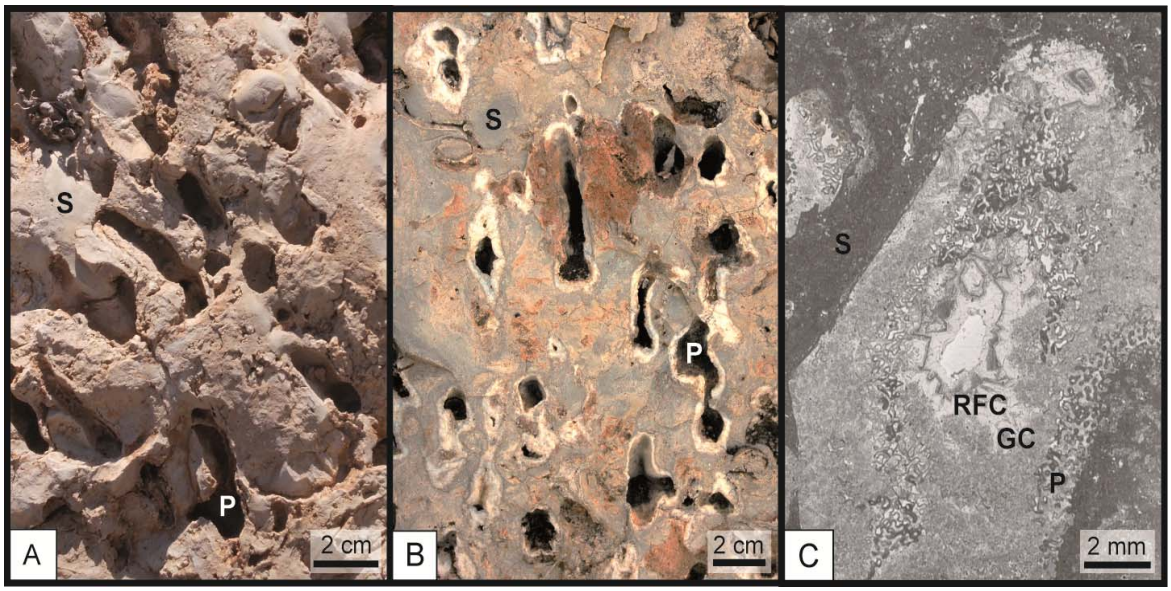

Fig. 3.4: A Outcrop view of the reef framework with *Porites* (P) molds and stromatolitic crusts (S) in DZ1. **B** Outcrop view of DZ2 with *Porites* molds partially infilled with calcitic cement. **C** Thin section view of cements in DZ2. Partially dissolved *Porites* is covered by granular (GC) and radiaxial fibrous cement (RFC).

The precipitation of granular and drusy cements in the moldic pores of DZ2 is congruent with the freshwater origin of the cements. Although radiaxial fibrous cements usually occur in phreatic-marine environments, they can also come about in the meteoric and meteoric-marine mixing zones as described by Richter et al. (2011). Unequivocal proof for the freshwater origin of these cements is provided by the $\delta^{13}C$ values of -7.38 ‰ and the $\delta^{18}O$ of -7.77 ‰ (Fig. 3.5; Hudson, 1977; Nelson and Smith, 1996). The non-luminescence of the calcitic cements also points towards a meteoric origin of the cements, although non-luminescence of calcitic cements may be also related to the relative abundance of Fe in the crystals (Hemming et al., 1989; Swart, 2015). The EDX analysis of the calcitic cements from DZ2 with Fe content below the EDX´s detection limit (around 1000 ppm), however, indicates that there is not enough Fe available to suppress the luminescence (Hemming et al., 1989).

During the sea-level fall that exposed LCB, freshwater mixed with marine water, changing the water chemistry of the palaeoaquifer promoting the dissolution of aragonitic and high-Mg-calcite components, and avoiding the precipitation of calcite in the meteoric phreatic

zone (Sanford and Konikow, 1989; Swart, 2015). It is therefore proposed that DZ2 cementation took place during the low sea-level stillstand while the lowstand wedge (LW) formed and the paleoaquifer was stable. The subsequent sea-level rise promoted again the mixture of fresh and marine water interrupting calcite precipitation (Sanford and Konikow, 1989; Swart, 2015).

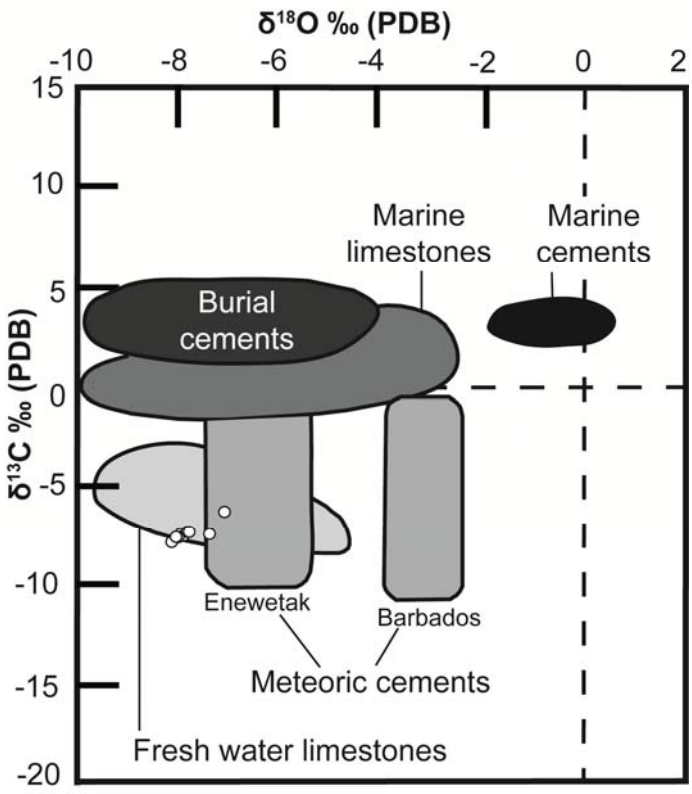

Fig. 3.5: Diagram showing the $\delta^{13}C$ and $\delta^{18}O$ isotopic values of nine cement samples. The isotopic values plotted within the diagnostic fields of fresh water limestones and meteoric cements as defined by Nelson and Smith (1996).

The ascending sea level flooded the exposed part of the LCB ending the karst development and allowing the development of the UCB reef framework (Fig. 3.2B) overlying the reef-crest deposits which earlier were exposed and karstified during the sea-level lowstand.

The dissolution which characterises DZ3 is thought to be related to the sea-level fall that ended the Cariatiz carbonate platform growth, because DZ3 diagenetic features are present in all the analysed sedimentary bodies including UCB (Fig. 3.3B). The diagenetic history (Fig. 3.3) and the stratal packaging therefore reflects a succession of events starting with a sea-level fall that triggered dissolution of LCB (DZ1), followed by a low sea-level stillstand that promoted the cement precipitation in LCB (DZ2). After this lowstand, a sea-level highstand allowed the UCB growth and a final sea-level fall and exposure affected the whole platform with dissolution (DZ3).

3.5.3 Amplitude of sea-level changes

As the Cariatiz carbonate platform developed during the 180 ka following the base of C3r, the selected clinoform bodies and lowstand wedge reflect a complete cycle of sea-level fall and rise between 5.89 and 5.87 Ma (Fig. 3.1B). In the global sea-level curve of Miller et al. (2011), this sea-level cycle is recorded as a 17 m sea-level fall followed by a sea-level rise of 20 m (Fig. 3.3B). The confidence for these amplitude values includes an error of approximately ± 10 m due to the uncertainties of the $\delta^{18}O$ proxy for sea-level reconstruction (Miller et al., 2012).

The studied cycle indicates a sea-level fall of 23 ± 1 m from the deposition of the LCB reef crest to the deposition of the LW, followed by a sea-level rise of 31 ± 1 m for the UCB reef-crest deposition (Fig. 3.3). These values rely on sedimentary and diagenetic pinning points. The two highstand pinning points in the succession are the LCB and UCB reef crests. The accuracy of the values includes an error of ± 1 m due to the uncertainty of the exact position of the *Porites* reef crest that should be no more than a metre below the sea surface for the Miocene reefs (Riding et al., 1991).

The sea-level lowstand position can be roughly derived from the highest onlap of the lowstand wedge (Braga and Martín, 1996; Cuevas-Castell et al., 2007). The position of the highest onlap of the LW is 25 m lower than the LCB reef crest. The relation of this level with respect to the sea surface, however, is poorly defined since the depth of base level for this depositional system is unknown. To overcome this uncertainty, it is proposed that the karst diagenetic zones, i.e. the contact between DZ1 and DZ2, are accurate pinning points to trace the sea-level lowstand position. Assuming that the thickness of DZ2 reflects the thickness of the meteoric-phreatic zone of a coastal palaeoaquifer it is possible to use a Dupuit-Ghyben-Herzberg analysis to determine the palaeoposition of the fresh to marine water interface. The Dupuit-Ghyben-Herzberg analysis, an empirical calculation based on the behaviour of present day coastal aquifers, calculates that the freshwater in the meteoric-phreatic zone reached a depth below sea level forty times greater than the elevation of the phreatic level above sea level (Vacher et al., 1990). In the studied outcrop, the fresh to marine palaeowater interface corresponds to the base of DZ2. Considering the 15-m thick cemented band, the top of the present day DZ2 would be approximately 35 cm above sea level. Therefore the sea-level position during the lowstand was 23 m lower than the LCB reef crest, which is 2 m above the onlap level of the lowstand wedge.

Previous studies of late Miocene sea-level changes in carbonate platforms indicated amplitudes of 20 m to more than 50 m for high-frequency sea-level variations (Goldstein et al., 1994; Braga and Martín, 1996; Cuevas-Castell et al., 2007). In contrast to these

earlier works, our analysis presents a very accurate reconstruction of high-frequency sea-level fluctuations in shallow water carbonate strata. Therefore, these data provide a unique opportunity for testing the validity of the amplitudes of global sea-level fluctuations as recorded in pelagic sequences. The outcrop-derived sea-level data are congruent with the values of the age-equivalent sea-level fluctuation identified by Miller et al. (2011) (Fig. 3.3B) but the proposed values have a narrower range of error, with a metre compared to a decametre scale. To our knowledge, this is the first outcrop example with reconstructable amplitude values of sea-level fluctuations related to precessional frequency during the Miocene. This approach can also be used in other examples of Neogene carbonate platforms which have good outcrop qualities.

3.6 Conclusions

The study of the diagenetic evolution together with classic pinning points of reef slopes has been proven to be an accurate tool to calibrate the amplitude of sea-level fluctuations recorded in a Neogene carbonate platform. Facies and diagenetic zones distribution reveals a complete high-frequency cycle of sea-level fall (23 ± 1 m) and rise (31 ± 1 m) between 5.89 and 5.87 Ma. These values for amplitudes of sea-level fluctuations are more accurate than those obtained by other approaches (i.e. the $\delta^{18}O$ analysis of benthic foraminifera in pelagic sequences).

This approach allows for first time the outcrop comparison and calibration of amplitudes of Miocene high-frequency sea-level fluctuations recorded in pelagic sequences. This approach can also be used in other examples of (Neogene) carbonate platforms with good outcrop qualities. This study provides a timely contribution with regard to the discussion on the occurrence of past high-frequency high-amplitude sea-level changes.

Chapter IV

Microbial binding: controlling factor of slope angles in post-Triassic carbonate slopes?

Abstract

The geometry and inclination of carbonate platform slopes are tipically described as the result of the sediment texture, components, and grain size occurring in the slope. Three carbonate slopes from the Holocene of the Tongue of the Ocean (Bahamas) and three slopes from an Upper Miocene carbonate platform in SE Spain were selected to identify the factors controlling dip angles. Although platforms differ in size and elevation with regard to the surrounding basin, both locations present slopes with linear profiles and steep angles over 35°. Petrographic analysis shows that the slope facies in both locations are similar with the matrix and some bioclasts presenting microfabrics indicative of the presence of microbial activity during deposition. These include (1) clotted micrite patches locally connecting bioclasts or infilling primary pores; (2) porostromate structures in the micrite; (3) dense micritic masses; (4) binding structures; (5) micritic envelopes; and (6) peloidal textures. The Holocene and Miocene depositional geometries and facies distribution are the response to different sedimentary processes including rockfalls, gravity flows, and in-situ carbonate production. The presence of an extensive microbial influence is proposed as a controlling factor of slope angles, a stabilizing factor of the steep slope as significant as in Palaeozoic and Triassic examples.

This chapter is based on **Reolid, J., Betzler, C., Eberli, G.P., and Grammer G.M.** (in prep.) Microbial binding: controlling factor of slope angles in post-Triassic carbonate slopes?

4.1 Introduction

Carbonate platform slopes form the transition between shallow-water shelf carbonates and deep-water basinal deposits, and one that is shaped by a series of different depositional and diagenetic processes. Factors controlling the slope geometry include the volume of sediment exported from the platform and the platform height (Schlager, 1981), the grain size (Kirkby, 1987), the erosion-deposition balance (Schlager and Camber, 1986), the response to shear strengths in fine-grained carbonate slope sediments (Kenter, 1990; Kenter et al., 2005; Schlager, 2005; Playton et al., 2010), early lithification (Grammer et al., 1993a; 1993b), and in-situ carbonate production and stabilization (Kenter, 1990; Della Porta et al., 2003; 2004; Kenter et al., 2005).

Carbonate slopes with angles steeper than 30°-45° in Palaeozoic and Triassic platforms are described as the result of stabilization by organic framebuilding, by microbial binding and by early lithification (Kenter, 1990; Adams and Kenter, 2014; Keim and Schlager, 2001; Della Porta et al., 2003; 2004; Kenter et al., 2005). In such platforms, organic framebuilding and early lithification are more significant than grain size in determining the slope geometry. In post-Triassic examples, Cretaceous of Mexico (Enos, 1977) and Miocene of the Gulf of Suez (Haddad et al., 1984), it was discussed if the steep angles of carbonate slopes are due to early submarine cementation or by sediment binding by various organisms. Microbial stabilization of the slope was recently described as playing a significant role in Neogene (Upper Miocene) carbonate platform slopes of the Mediterranean realm (Reolid et al., 2014). However, those results may be only conditionally accepted, as the platform studied was formed in a satellite basin of the Mediterranean where water circulation was becoming restricted as a prelude of the Messinian Salinity Crisis and the coral reefs grew with "aberrant" features (Esteban, 1980). These features include low reef-building species diversity, ample development of monospecific *Porites* reefs, and the presence and abundance of microbial related deposits, mainly forming stromatolites but also stabilizing *Halimeda* bioherms (Braga et al., 1996; Martín et al., 1997), and *Porites* reefs (Riding et al., 1991). While the presence of thick microbial deposits has been proved to be a common phenomenon in Holocene reef environments of normal marine conditions as the barrier reef of Tahiti (Camoin, 1999), and the Great Barrier Reef (Webb and Jell, 1997); the significance of microbial binding in slope deposits has not yet been determined. In order to test whether microbial stabilization of the slope is a frequent phenomenon in post-Triassic slope deposits, or if it is exclusively present in the especial Miocene Mediterranean outcrops, an example of steep slopes from well known carbonate platforms with normal marine conditions were studied.

Steep slope angles were described from the Tongue of the Ocean in the Bahamas carbonate platform (Grammer, 1991; Grammer and Ginsburg, 1992; Grammer et al., 1993a; 1993b). The origin of the steep angles was originally attributed to early cementation of the slope. Microfacies analysis, however, indicates many similarities to Upper Miocene Mediterranean slope facies, where microbial stabilization is significant. The aim of this study is thus to identify, characterise and quantify the presence of microbial binding in the Holocene slope from the Bahamas, to evaluate the microbial contribution to the slope architecture, and to compare both slope depositional systems, in the Bahamas and Mediterranean domain, for a better understanding of the microbial slope stabilization in post-Triassic deposits. Results indicate that microbial binding occurs throughout the slopes analysed.

4.2 Geological setting

Great Bahama Bank consists of a more than 104.000 km^2 of tropical shallow-water carbonate banks separated by deep troughs (Willian et al., 1989). One of these deep-water troughs is the Tongue of the Ocean (TOTO), which represents an extension of the Atlantic Ocean between the islands of New Providence and Andros (Fig. 4.1A). TOTO is a 1500 to 3600 m deep trough which is 160 km long and 32 to 64 km wide. The bottom of this embayment has a northward-deepening V-shaped profile between Andros and New Providence Islands changing into a U-shaped cul-de-sac in the south, where the studied slopes are located (Fig. 4.1A) (Andrews et al., 1970). These are located at the leeward (Privitt Place slope and Palmer Point slope) and windward flanks (Rock Range slope) of TOTO respectively (Fig. 4.1A). The sedimentary record in the cul-de-sac consists of gravity flow deposits composed of rubble and sand whose components vary according to the distribution of surface sediments on the surrounding platform (Grammer and Ginsburg, 1992). Grainy deposits are frequently intercalated with pelagic lime mud, especially in the lower portions of the slope (Schlager and James, 1978; William et al., 1989).

During the Messinian, the Sorbas Basin in southeast Spain (Fig. 4.1B) was rimmed by tropical carbonate platforms (Martín and Braga, 1994). The studied slopes represent three consecutive progradational stages of the Cariatiz carbonate platform. The present tectonic tilt of this platform is less than 3 degrees (Braga and Martín, 1996).

4.3 Methods

A total of 134 submersible dives with the two-person submersible *Delta* (Delta Oceanographics) were made during 3 cruises from 1988-1990 to characterize the different slopes of the TOTO (Grammer, 1991). Description and measurements of the different

features in the slope were documented by videotape and photography. Slope angles were obtained using a hand-held inclinometer from the inside of the submersible. A total of 90 samples from the three slopes were selected to define the facies and microfacies. Polished slabs and thin sections were made out of the lithified samples. The slope angles and general features presented herein were extracted from Grammer (1991). The petrographical data were obtained from Grammer (1991) and amended by new data from an analysis of the 90 original polished slabs and thin sections, as well as from 20 new thin sections out of Grammer´s samples.

Slope dimensions and slope angles in the Sorbas Basin outcrops based on Terrestrial Lidar data were presented in Reolid et al. (2014). The facies and microfacies based on the data presented in Reolid et al. (2014) are utilized, as well as the additional outcrop description and petrographic analysis of 30 thin sections.

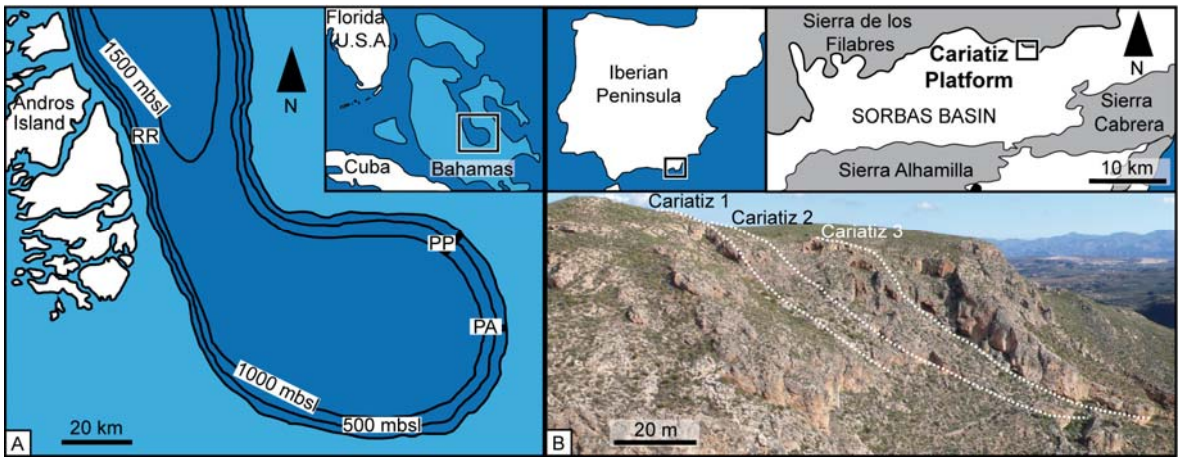

Fig. 4.1: A Location of the Tongue of the Ocean (Bahamas) with slope profiles discussed in the text (RR-Rock Range, PP-Privitt Place, and PA-Palmer Point). **B** Location of the Cariatiz carbonate platform in the Sorbas Basin (Spain). The photography shows the exact location of the outcrops analysed.

4.4 Results

The diverse facies, composition, sedimentary structures, and inclination of the different slopes are documented in Table 4.1.

4.4.1 Tongue of the Ocean slopes

4.4.1.1 Rock Range slope

This 150 m high slope is located along the windward margin of the TOTO. Basinwards, in N70E direction, it extends for nearly 260 m (Fig. 4.2A). The slope can be divided into two

segments with different angles. The upper segment has an inclination ranging from 50° to 60°, followed downslope by a nearly vertical cliff. The lower slope segment is 35° steep.

Slope	Composition	Fabric	Dominant slope facies	Matrix	Microbial features	Dip
Rock Range	US: Red algae, plate-like corals, sponges, and *Halimeda*. MS: *Halimeda*, corals, red algae, molluscs, equinoids, serpulids, bryozoans, and benthic foraminifera. Intraclasts.	US: Wall with cavities and vertical gullies. MS: Poorly bedded with small linear ridges (by submarine sliding).	*Halimeda* floatstone-rudstone.	Microbial micrite. Peloidal micritic matrix.	Microbial micrite including: (1) dense micrite and (2) clotted micrite. Micritic envelops. Trapping and binding structures.	US:50°-60° MS:35°
Privitt Place	US: *Halimeda*, red algae, and sponges. MS-LS: *Halimeda*, red algae, corals, molluscs, benthic foraminifera, and serpulids.	US: Wall with cavities and vertical gullies. MS: 20-30 cm beds. Abundant blocks from US. Slumps. Low relief ridges and swales (by submarine sliding). Cementation. LS: Blocks from US. High relief ridges and swales. Bioturbation.	*Halimeda* floatstone-rudstone (grainstone).	Microbial micrite. Peloidal micritic matrix.	Microbial micrite including: (1) dense micrite and (2) clotted micrite. Micritic envelops. Trapping and binding structures. Microbial domical structures.	US:60°-70° MS:55°-35° LS:32°-30°
Palmer Point	US: *Halimeda*, red algae, and sponges. MS-LS: Peloids. serpulids, corals, ooids, *Halimeda* and molluscs. Minor benthic foraminifera, and bryozoans.	US: Wall with cavities and vertical gullies. MS: 20-30 cm beds. Low relief ridges and swales (by submarine sliding). Cracks in the slope. Cementation. LS: Poorly bedded. Low and high relief ridges. Bioturbation.	Peloidal packstone-rudstone.	Peloidal micritic matrix. Microbial micrite.	Microbial micrite including: (1) dense micrite and (2) clotted micrite. Micritic envelops. Trapping and binding structures. Microbial domical structures.	US:70°-90° MS:45°-35° LS:30°
Cariatiz 1	US: *Porites* - stromatolite framework and framework blocks (up to 10 m in size). Bivalves, *Halimeda*, echinoids, red algae, brachiopods, and gastropods. Intraclasts.	US: In-situ *Porites* growths. Chaotic breccia. Reef-framework block size decrease basinward.	*Halimeda* breccia and *Halimeda* rudstone.	Microbial micrite. Peloidal micritic matrix.	Reef binding (thick laminated-domical crusts). Microbial micrite including:	US:60° MS:45°-30°
Cariatiz 2	MS: *Halimeda* plates. cm-dm reef-framework blocks. Bivalves (pectinids and oysters), gastropods, serpulids, red algae, echinoid spines, and benthic foraminifera. Intraclasts and minor siliciclastics.	MS: Chaotic. Poorly bedded (beds up to 40 cm thick). Local serpulid-red algal patches up to 1 m wide.	*Halimeda* breccia and *Halimeda* rudstone. Basinal sitls and marls.	Microbial micrite. Silts and marls. Peloidal micritic matrix.	(1) dense micrite and (2) clotted micrite, Micritic envelops binding bioclasts.	US:50°-60° MS:45°-30° LS: 15°-5°
Cariatiz 3	LS: Diatoms. Bivalves (pectinids), gastropods, serpulids, benthic foraminifera, red algae, and echinoid spines. Siliciclastic grains (7-10%).	LS: 5-30 cm thick beds, locally cross laminated. Alternation of slope sediment beds with basinal deposition sediment. Bioturbation.	*Halimeda* breccia and *Halimeda* rudstone. Basinal silts and marls.	Microbial micrite. Peloidal micritic matrix. Silts and marls.	Microbial features absent in LS.	US: 60° MS:40°-30° LS:15°-10°

Table 4.1: Summary of facies and microfacies, type of matrix, microbial features and slope angles at the different segment (upper-US, middel-MS, and lower-LS) of the studied carbonate platform slopes.

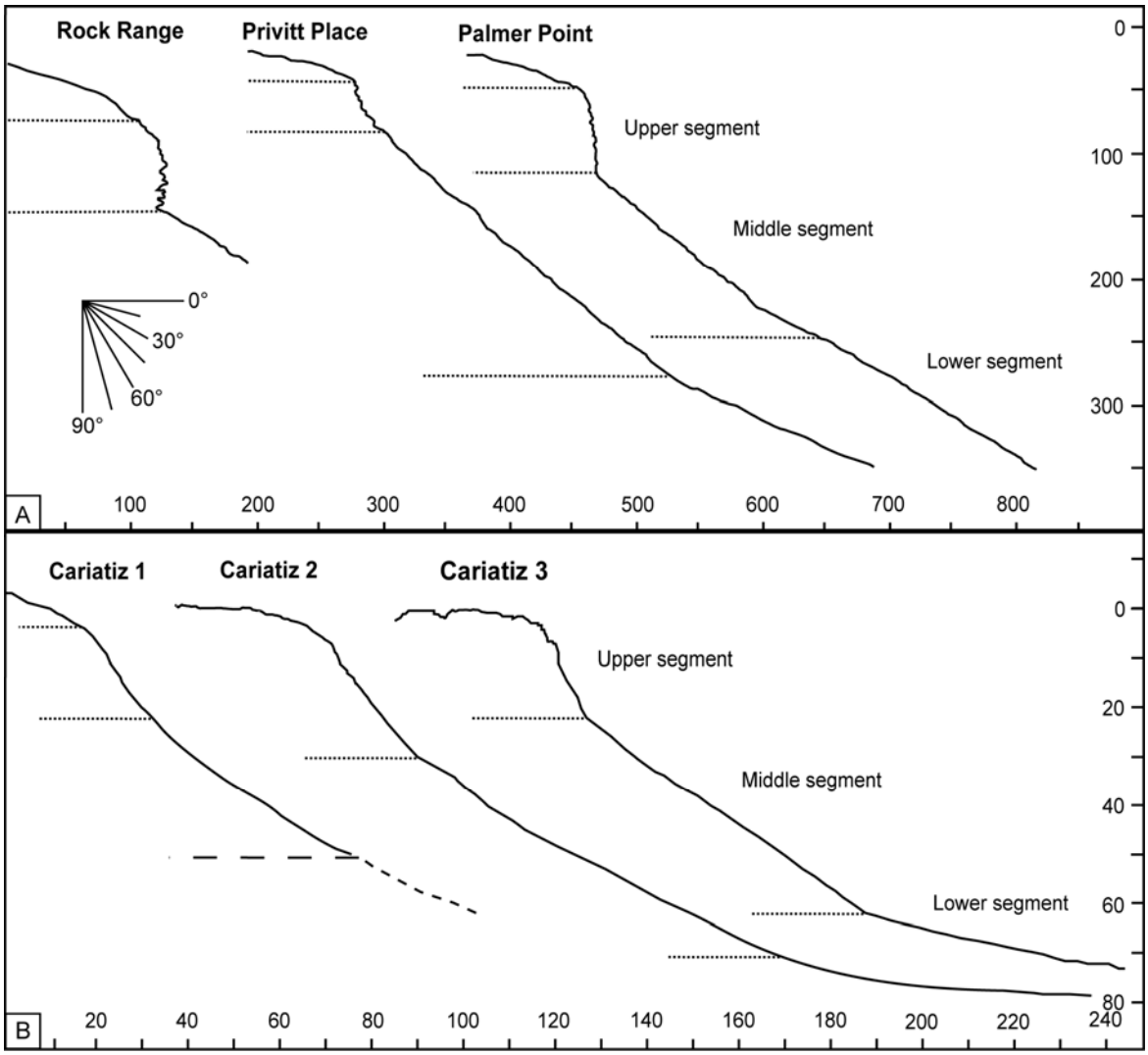

Fig. 4.2: A Tongue of the Ocean slope profiles with different segments (pointed line) with different angles. **B** Cariatiz carbonate platform slope profiles with segments with different angles. Note that the lower slope of Cariatiz 1 is covered. The dashed line indicates the estimated slope gradient.

The uppermost segment of the slope consists of plate-like corals, red algae, sponges, *Halimeda*, and sclerosponges along a ~80 m wall with abundant caves. The floors of these caves are locally covered by recent carbonate mud. The lower segment of the slope is made up of a *Halimeda* floatstone to rudstone with subordinate components such as coral debris, red algae, molluscs, benthic foraminifera, equinoids, serpulids, bryozoans, and intraclasts. Red algae mainly encrust large bioclasts, especially *Halimeda* grains, but also form small nodules. Bioclasts are usually observed floating in a micritic to microgranular matrix that may represent between 30 to 60% of the facies. Up to 85% of the matrix is made of dense to clotted micrite, with minor peloidal micrite. Locally the dense to clotted micrite is distributed in patches connecting bioclasts (Fig. 4.3A) The matrix may locally present a poorly developed layering consisting of an alternation of different packing densities by the binding of silt-sized components in the matrix (Fig. 4.3B). Bladed Mg-

calcite cement occurs lining interparticle and intraparticle voids and locally inside fractures within dense micritic patches (Fig. 4.3C). Botryoidal aragonite cements have a similar distribution in pore spaces but are present exclusively in the coarser grained areas.

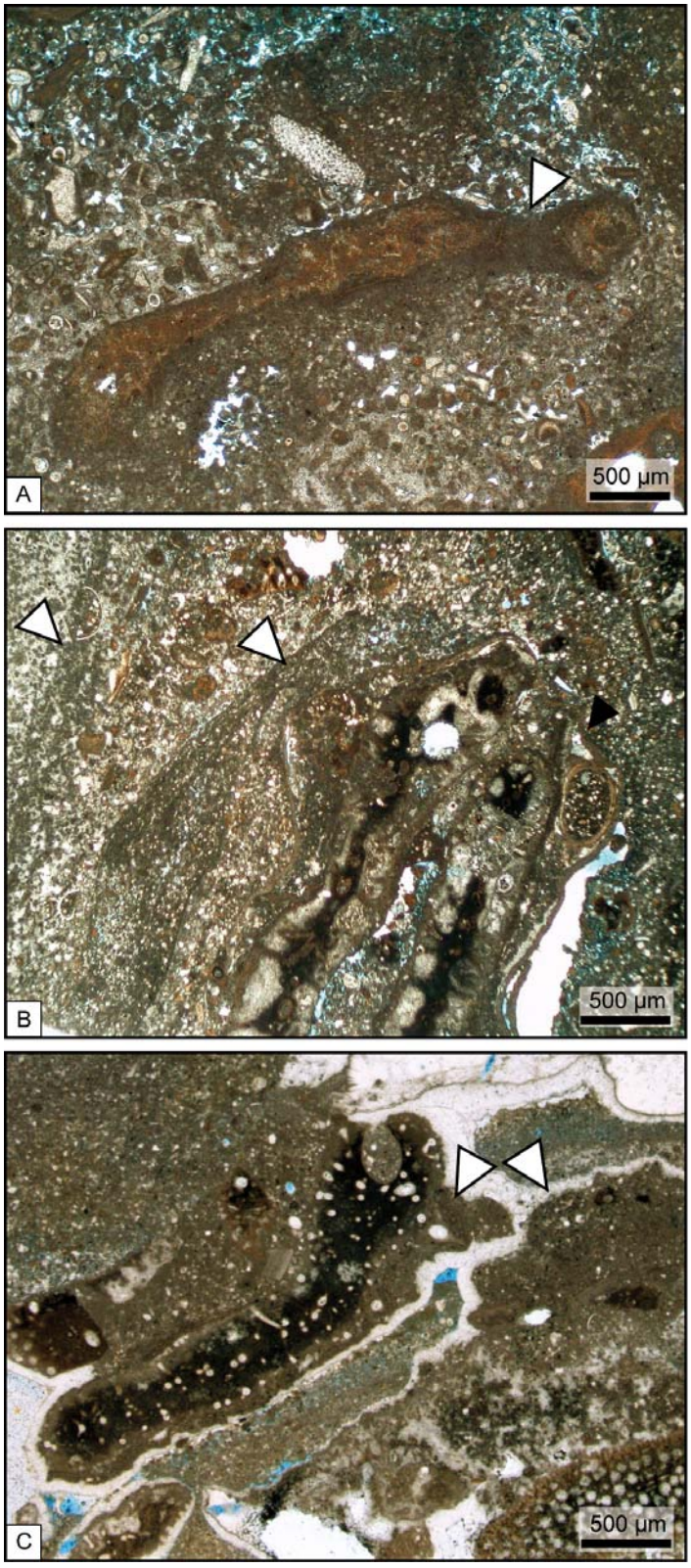

Fig. 4.3: Photomicrographs of the *Halimeda* floatstone from Rock Range slope (TOTO) showing: **A** dense micrite covering and connecting (white arrow) two *Halimeda* plates; **B** alternation of layers (white arrows) defined by different packing density by binding of silt-sized components in the matrix and over two *Halimeda* plates encrusted by red algae (black arrow); and **C** brecciated dense to clotted micrite with calcitic cement infilling the fractures.

4.4.1.2 Privitt Place slope

The 300 m high slope is located on the leeward side of TOTO. Basinwards, in N220E direction, it extends for nearly 540 m (Fig. 4.2A), and has a concave-upward linear profile (sensu Adams and Kenter, 2014), including three segments with different angles. The upper segment comprises angles from 60° to 70°. The middle segment ranges in inclination from 55° in the upper part, to 35° in the lower part. The lower segment has angles between 32° and 30°.

The uppermost segment of the slope consists of a 40 m sub-vertical slope with abundant *Halimeda* as well as red algae and sponges. The middle segment of the slope is characterized by the presence of different sedimentary structures including, from marginal to distal slope parts, large scale slumps and rounded domical structures (moguls), talus slope blocks, and low relief ridges and swales. The rounded domical structures are common around 120 m depth in the middle segment of the slope and are characterized by diameters of 1 to 0.5 m and heights of centimetres to decimetres over the surrounding slope deposits (Fig. 4.4A). These small mounds may exhibit a concentric lamination when broken, suggesting that they may have formed by successive episodes of sedimentation (Fig. 4.4B). The moguls are encrusted by red algae, and the topographic lows among the moguls are occupied by sediment. The sediment in this slope segment consists of *Halimeda* floatstone to rudstone with abundant red algae and coral debris, and minor molluscs, benthic foraminifera, and serpulids. *Halimeda* plates usually contain red algal and micritic crusts (Fig. 4.5A). These micritic crusts may extent over the matrix-binding silt-sized components (Fig. 4.5B). The matrix of this floatstone to rudstone, which comprises up to 60% of the facies, is made of micrite, which locally has a peloidal texture. Micritic peloids are of irregular shape and size. Clotted micrite, locally connecting bioclasts, is the most common texture of the matrix. In some samples the clotted micrite forms up to 80% of the matrix (Fig. 4.6). The clotted micrite eventually occurs partially or totally infilling the primary pores and the interior of some bioclasts. The clotted micrite may retain a porostromate structure (Fig. 4.6) consisting of a concentration of tubular pores. Locally, the micrite is dense and also distributed in patches connecting bioclasts (Fig. 4.7). The facies can be locally described as a grainstone with bladed Mg-calcite and botryoidal aragonite cements. The lower segment of the slope is characterized by the occurrence of high relief (decimetre to metre-scale) ridges and swales. The sediment is similar as in the previously described segment, but shows intense bioturbation with locally minor cementation.

4.4.1.3 Palmer Point slope

This leeward side slope is 290 m high. In N270E direction it extends for nearly 440 m (Fig. 4.2A). The slope has a concave-upward linear profile comprised of three segments

with different inclinations including (1) an upper segment with an inclination ranging from 70° to 90°, (2) a middle segment with angles from 45° in the upper part to 35° in the lower part, and (3) a lower segment with an inclination of 30°.

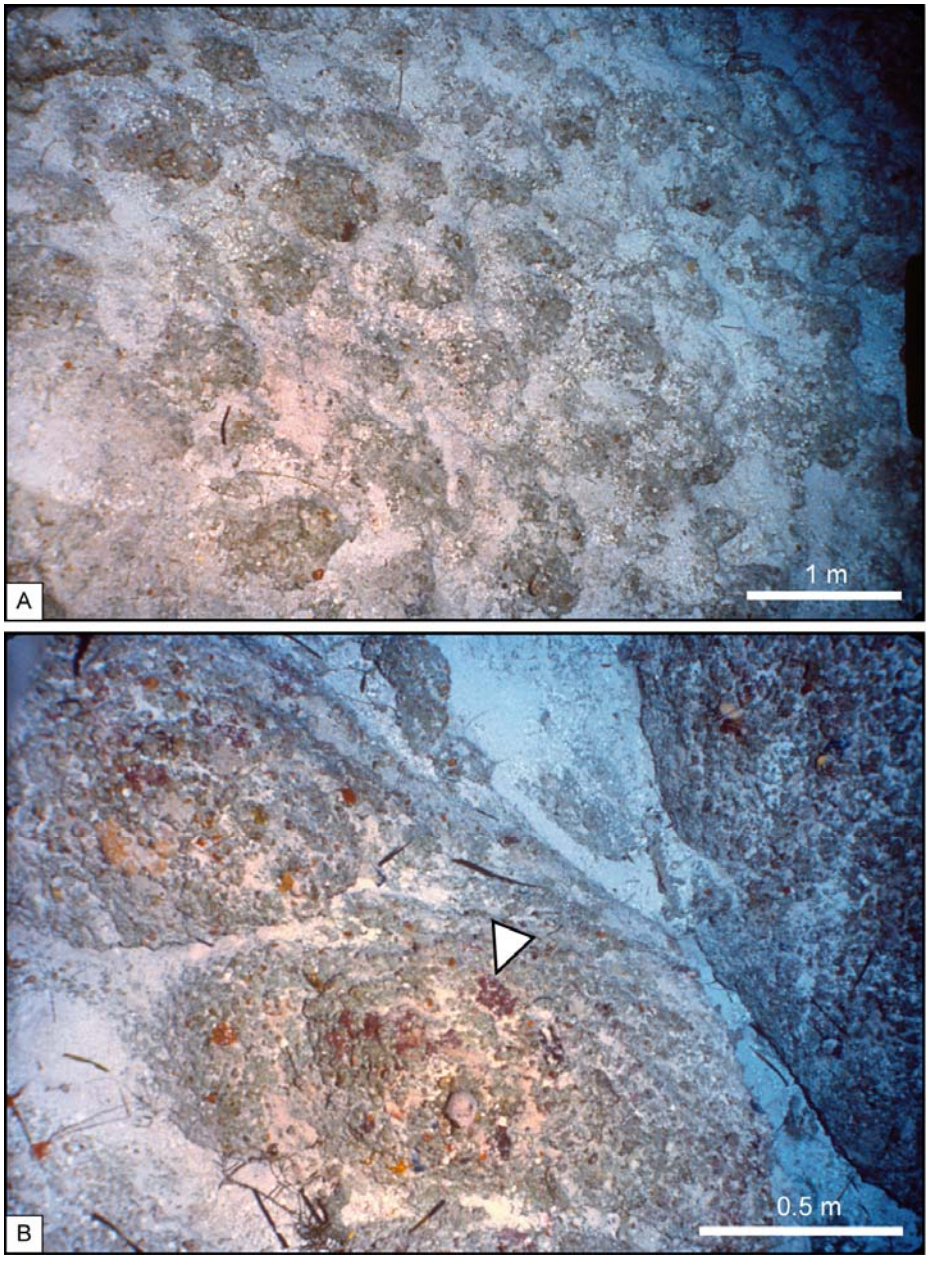

Fig. 4.4: A Photograph taken from the DELTA submersible showing a field of microbial domical structures (moguls) in Palmer Point slope at a water depth of 140 m. **B** Close-up photograph of the microbial domical structures. These structures seem to show an internal concentric lamination and present encrustation by different organism, mainly red algae (white arrow), in the surface.

The uppermost segment of the slope consists of a 70 m wall with caves and vertical gullies. *Halimeda*, red algae, and sponges are the main components in this interval. The middle segment presents moguls in the upper part, around 140 m depth, and some small

low-relief (decimetre scale) ridges that extend basinwards. The moguls, as in the other leeward slope of TOTO (Privitt Place), are a common feature in the uppermost part of the middle segment of the slope with diameters up to 1 m and a height of centimetres to decimetres over the surrounding slope deposits. Red algal crusts may cover the surface of the moguls. The sediment among the moguls consists of a peloidal packstone with abundant serpulids, coral fragments, ooids, *Halimeda* plates, and mollusc fragments. Benthic foraminifera and bryozoans occur as minor components. *Halimeda* plates usually have a micritic crust (Fig. 4.8). The matrix comprises up to a 40% of the facies and consists of micrite, which locally has a peloidal texture. Micritic peloids in the matrix are of irregular shape and size and usually arranged in bands with varying degrees of differential packing (Fig. 4.9). Clotted micrite may be locally present connecting some bioclasts. Bladed Mg-calcite and botryoidal aragonite cements may occur in interparticle and intraparticle voids as well as infilling fractures within dense micritic patches. The lower segment of the slope is characterized by the presence of talus blocks and large (centimetres to metres high and tens of metres long) low-relief ridges and swales. These facies are similar as in the previous segment but shows intense bioturbation and no cementation.

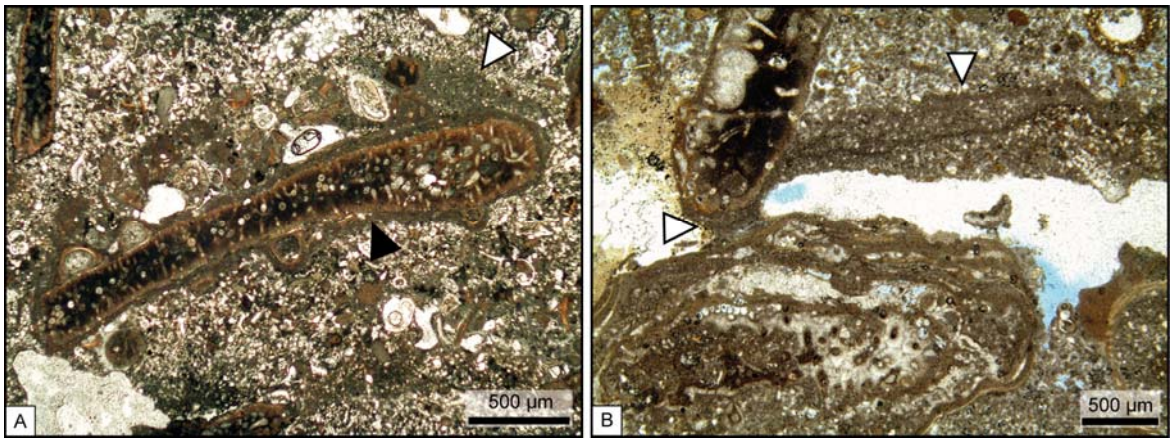

Fig. 4.5: Photomicrographs of *Halimeda* floatstone from Privitt Place slope (TOTO) showing: **A** *Halimeda* plate encrusted by small serpulids, red algae (black arrow) and dense micrite (white arrow); and **B** microbial binding (white arrows) changing into an envelope over a *Halimeda* plate.

4.4.2 Cariatiz slopes

4.4.2.1 Cariatiz slope 1

This clinoform body is 90 m high. The outcropping part of the slope extends for at least 100 m in the direction of progradation (N160E) (Figs. 4.1B, 4.2B). This body has a concave-upward linear to exponential profile, including two segments with different

angles: (1) an upper segment with an inclination of 60°, and (2) a middle segment with angles between 45° and 30°. The lower segment is poorly exposed in the outcrop.

The uppermost part of the body consists of a 7 m thick package of reef framework with *Porites* covered by thin coralline algal-foraminiferal crusts overgrown by thick stromatolitic crusts. A bioclastic matrix fills in the remaining spaces. Downslope there is a 13 m interval characterized by reef-framework blocks. The middle segment consists of a slope breccia comprised of abundant *Halimeda* plates that gradually changes into a bedded *Halimeda* rudstone. Molluscs, serpulids, and rarely red algae occur as minor components. Most of the bioclasts present micritic envelopes locally connecting them (Fig. 4.10A). The matrix represents up to a 60% of the facies and consists of dense micrite, locally with a clotted texture. Micritic peloids are locally common.

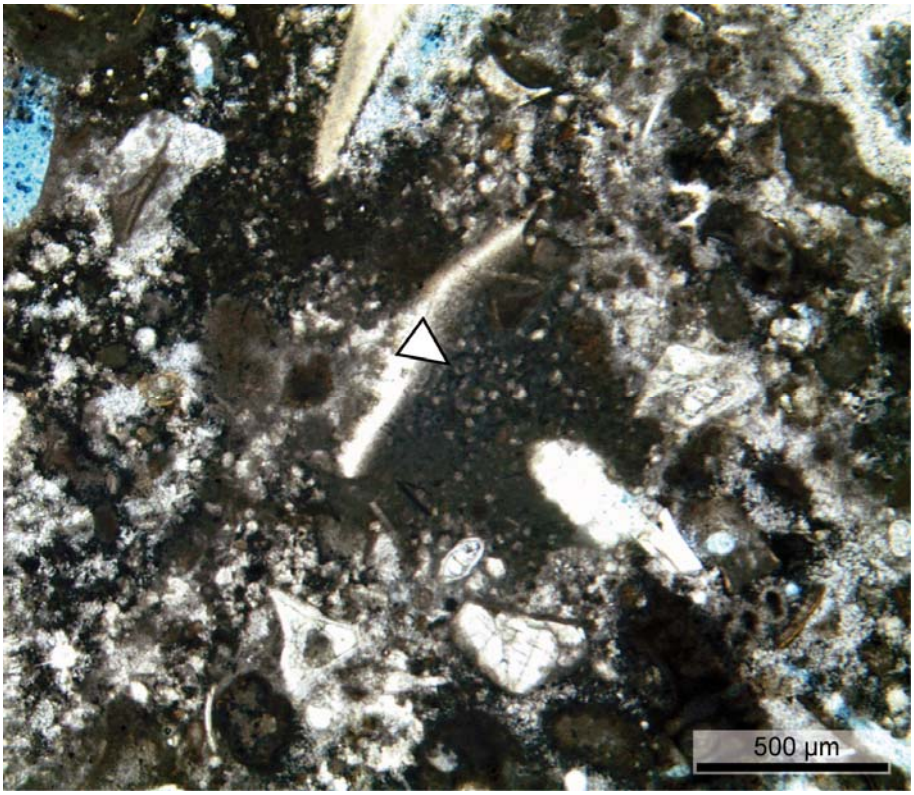

Fig. 4.6: Photomicrograph of a sample from Privitt Place slope (TOTO) showing the occurrence of dense and clotted micrite among fine grained bioclasts. The center of the picture (white arrow) displays a concentration of tubular micropores, porostromate structure, separating the micritic clots.

4.4.2.2 Cariatiz slope 2

This clinoform body is 80 m high. In the direction of progradation, it extends for nearly 200 m (Figs. 4.1B, 4.2B). This body has a concave-upward linear profile comprising three segments with different angles. The upper segment has an inclination of 60° to 50°, the

middle segment between 45° and 30°, and the lower segment has angles between 15° and 5°.

The uppermost part of the slope consists of a 15 m thick package of *Porites*-stromatolite reef framework as in the previous slope. Basinward, there is a 25 m interval dominated by reef-framework blocks. The middle segment consists of a slope breccia with *Halimeda*. This facies gradually changes into a bedded *Halimeda* rudstone with molluscs, serpulids, and red algae. Most of the bioclasts present micritic envelopes which locally connect these components. The matrix makes up to 40% of this facies and consists of a dense to layered micrite, which rarely exhibits a peloidal texture. The dense micrite is distributed in patches connecting bioclasts (Fig. 4.7). A poorly developed layering occurs in numerous samples. It consists of an alternation of layers defined by different packing densities of small components and peloids in the matrix (Fig. 4.9). The layering in the matrix can spread over the bioclasts as binding. The lower segment is defined by a change in the degree of lithification, which parallels the basinward decrease in abundance of encrusting organisms. The *Halimeda* rudstones gradually change into bioturbated basinal silts and marls.

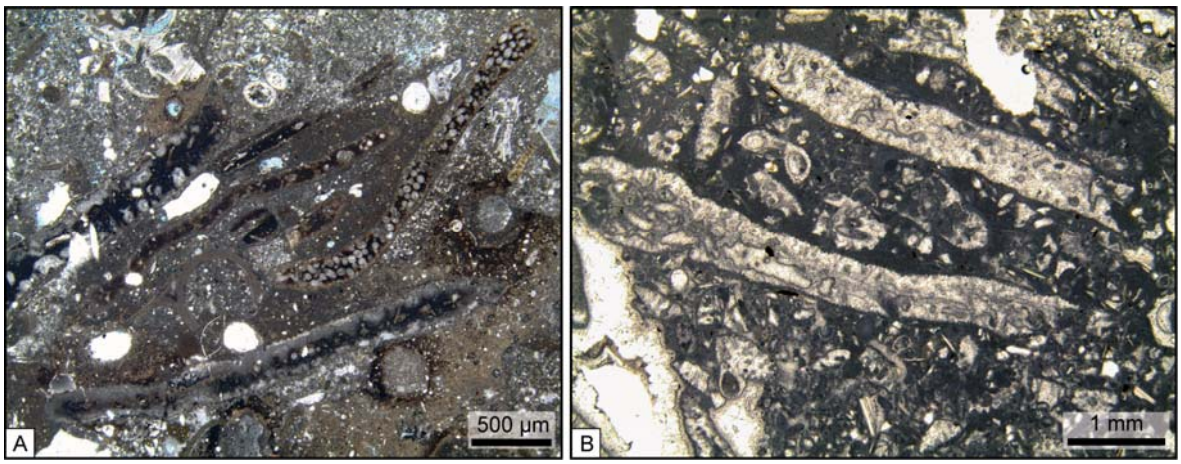

Fig. 4.7: A Photomicrograph of *Halimeda* floatstone to rudstone from Privitt Place (Holocene, TOTO) where dense micrite matrix connects the different *Halimeda* plates. **B** Photomicrograph of *Halimeda* rudstone from Cariatiz slope 1 (Upper Miocene, SE Spain) with dense micrite connecting the different bioclasts. The dense micrite is better developed in the upper part of the bioclasts.

4.4.2.3 Cariatiz slope 3

This clinoform body has a concave-upward linear profile that is 80 m high and extends nearly 200 m in the direction of progradation (CB1 in Reolid et al., 2014) (Figs. 4.1B, 4.2B). The slope has three segments: (1) the upper segment with an inclination of 60°, (2) the middle segment with angles between 40° and 30°, and (3) the lower segment with angles between 15° and 10°.

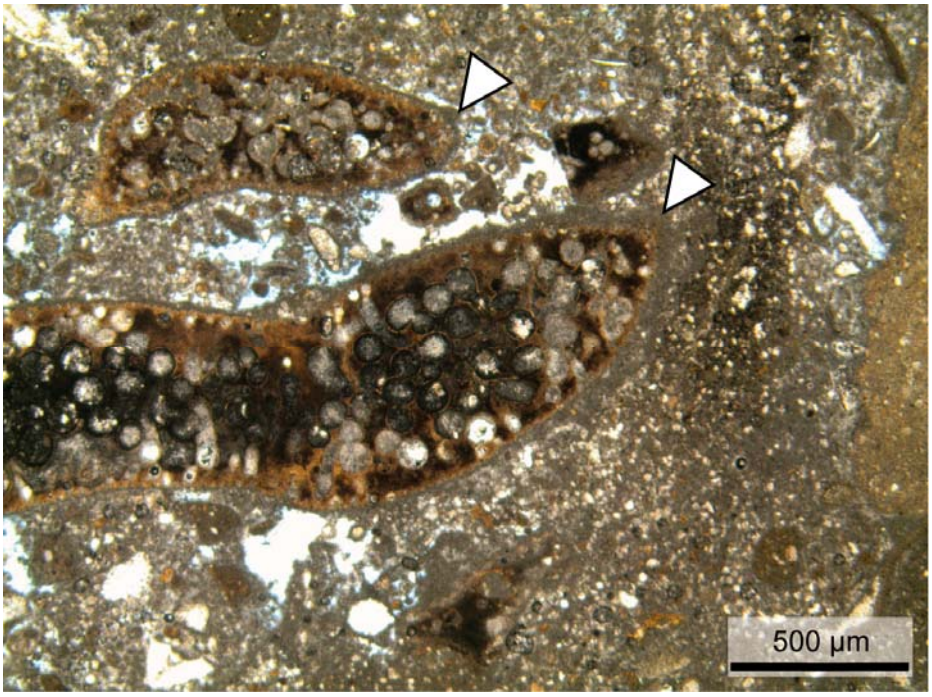

Fig. 4.8: Photomicrograph of micritic envelopes (white arrows) over *Halimeda* plates from Palmer Point slope (TOTO). The micritic envelopes show different thickness in different sides of the *Halimeda* plates.

The uppermost part of the body consists of a 10 m thick package of *Porites*-stromatolite reef framework. Downslope there is a 22 m interval characterized by reef-framework blocks. The middle segment facies are the breccia with *Halimeda* and the *Halimeda* rudstone. Within the *Halimeda* breccia, some patches of serpulid-tube clusters and red algae occur. Micritic envelopes on the bioclasts are abundant, usually connecting components. The matrix makes up to 50% of the facies and consists of clotted and dense to layered micrite, locally with peloidal texture. Clotted and dense micrite patches, locally connecting bioclasts, are the most common micritic texture in the matrix (Fig. 4.10B). The clotted micrite rarely presents porostromate structure. A poorly developed layering occurs in numerous samples by different packing densities of peloids. Micritic peloids of different sizes are locally abundant. A change in the degree of lithification with decreasing amount of encrusting organisms characterizes the lower segment. The *Halimeda* rudstone gradually changes into bioturbated basinal silts and marls.

4.5 Discussion

4.5.1 Origin of steep slopes

The depositional geometries and the facies distribution in the TOTO slopes, as well as in the Cariatiz carbonate platform slopes, are the response to different sedimentary processes in a fluctuating sea-level context (Grammer and Ginsburg, 1992; Reolid et al., 2014).

Rockfalls, gravity flows and in-situ carbonate production were the main processes controlling facies distribution in the upper and middle segments of the studied profiles, while gravity flows and hemipelagic rain, especially at the Cariatiz slopes, were the dominating processes in the lower segments (Grammer and Ginsburg, 1992; Reolid et al., 2014). Grammer et al's. (1993a) observations at the TOTO slopes indicate that windward and leeward slopes present different patterns of Holocene sediment accumulation. The leeward slopes, Privitt Place and Palmer Point, show a significantly better development of the third lower segment of the slope in comparison to the windward slope of Rock Range as a result of greater amounts of sediment being winnowed from the shallow bank top along the open leeward platform (Grammer and Ginsburg, 1992; Grammer et al., 1993a). Schlager (1981) pointed out that the volume of sediment must increase with the platform height to keep the same geometry of the slope, such is the case in the studied outcrops where TOTO slopes are significantly higher than the slopes from Cariatiz according to the greater amount of sediment available in Great Bahama Bank respect to the Cariatiz carbonate platform. However, the slope geometries of both locations are comparable as the volume of sediment in both cases is proportional to the slope size.

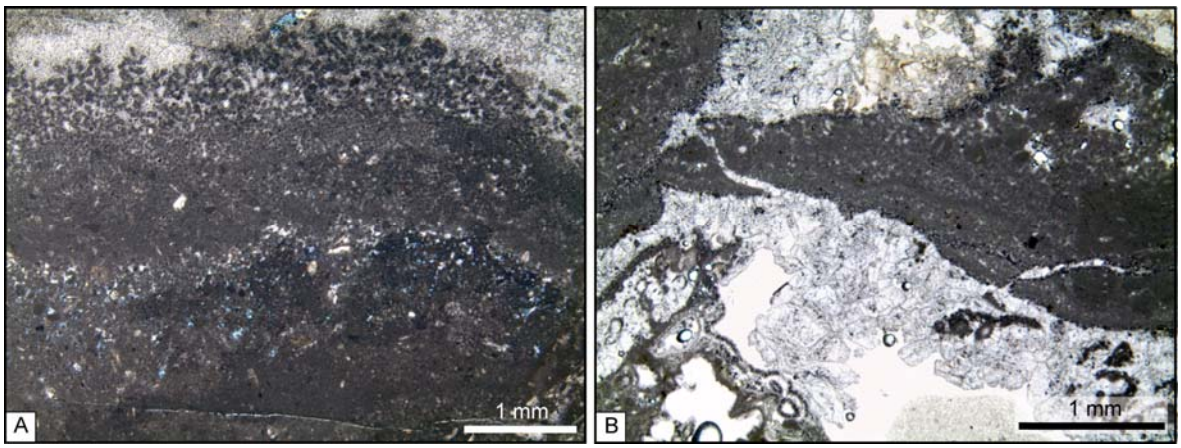

Fig. 4.9: A Photomicrograph of a peloidal micrite showing a differential packing probably related to microbial trapping/binding in Palmer Point (Holocene, TOTO). **B** Photomicrograph of peloidal micrite with microbial binding from Cariatiz slope 2 (Upper Miocene, SE Spain).

The sedimentary processes controlling the facies distribution also shaped the slope profiles. In the upper segment of TOTO profiles, the angles of 60°-90° are interpreted as an erosional cliff developed during the last lowstand (Grammer and Ginsburg, 1992). In the Cariatiz slopes, the imbrication of reef-framework debris at the base of the reef framework allowed the formation of the high angle of 60° in the upper segment (Reolid et al., 2014). The slope angles of 50°-30° in the middle and lower segment of the TOTO slopes and the angles of 45°-30° in the middle segment of the Cariatiz slopes correspond to the maximum angles of repose of sand and gravel (Kirkby, 1987). Although these high

angles of repose are present in these two examples, many other field and seismic examples exhibit lower slope-angles than those described in this work (Fig. 4.11) (Kirkby, 1987; Kenter, 1990; Adams and Schlager, 2000). Together with the grain size, the sediment fabric also exerts a control over the steepness of the slope (Kenter, 1990), however, the slopes studied in both locations are characterized by higher angles than expected for a grain-supported facies (Fig. 4.11).

Steep carbonate slopes, with angles of over 30°-45° (Fig. 4.11), as in the studied profiles, are traditionally described as the result of stabilization by organic framebuilding or early lithification (Kenter, 1990). Processes of early lithification and cementation of the slope sediments, and in-situ carbonate production and stabilization are widely known and reported from Palaeozoic and Triassic examples (Kenter, 1990; Della Porta et al., 2003, 2004; Kenter et al., 2005), but also documented in Neogene slopes from the Gulf of Suez (James et al., 1988), and recently in south Spain (Reolid et al., 2014). In those outcrops, the microbial binding exerts a significant control over the slope geometry favoring the sediment accumulation in high, over 35º, angles of repose (Adams and Kenter, 2014).

In the case of TOTO slopes, Grammer et al. (1993a; 1993b) proposed the rapid growth rate of pore-filling cements as the stabilizing factor of the steep slope angles. According to Grammer et al. (1993a; 1993b) the occurrence of cements in the middle segment of TOTO slopes includes bladed Mg-calcite (infilling approximately up to 31% of the primary porosity), fibrous aragonite (up to a 13%), and botryoidal aragonite (between a 12% and 20%) without any consistent paragenetic trend. Textural evidence suggested that pore-filling botryoidal aragonite cements were one of the last cements to precipitate and AMS radiocarbon dating of botryoidal cements indicate that the cements grew at an average rate of 8-10 mm/100 yr with maximum rates of 25 mm/100 yr (Grammer et al., 1993a). These growth rates and the similarity of radiocarbon ages between some botryoidal cements and coexisting skeletal grains suggest that the majority of cementation took place probably within several tens to a few hundreds of years after deposition of the components (Grammer et al., 1993a).

According to Allen (1985), granular materials first build up to their angle of initial yield, and then undergo shear failure that results in the sediment being left at the more stable angle of repose. Rapid growth rates of pore-filling cements were reported by Grammer et al. (1993a) to favour an extremely rapid cementation and "freezing" of the deposits at their angle of initial yield. However, some of the cements are located in fractures of a previously consolidated, or at least partially consolidated, sediment. This implies that an earlier stage of stabilization preceded cement growth.

4.5.2 Microbial influence on the steep slopes

The presence of an extensive microbial influence in TOTO slopes is proposed as an additional stabilizing factor of the steep slope angles. The microbial coating and binding of the slope sediment would prevent the shear failure of the steep slope deposits and allow the conservation of the original angles of repose for these materials in an early stage (Kenter, 1990; Adams and Kenter, 2014).

A preliminary comparison of TOTO and Cariatiz slopes evidences the similarities in slope geometries and angles, as well as in facies components and microfabrics. In the TOTO slopes, there are distinctive micritic textures considered by some authors as indicative of microbial activity during sediment formation including (1) clotted micrite (Fig. 4.6; Camoin, 1999; Riding, 2000; Reid et al., 2003) with porostromate structures (Fig. 4.6; Andrews, 1986; Lehrmann, 1999; Castagner et al., 2014), (2) dense micrite (Figs. 4.3A, 4.7A; Riding, 2000), and (3) binding structures (Figs. 4.3B, 4.9A; Riding, 2000).

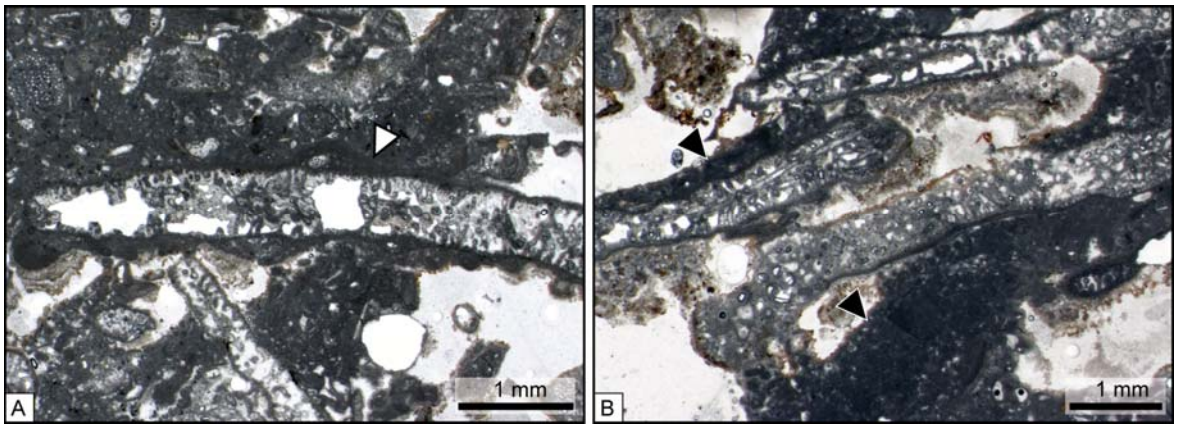

Fig. 4.10: Photomicrographs of the *Halimeda* floatstone to rudstone from the middle segment of the Cariatiz slopes showing: **A** *Halimeda* plate with a micritic envelope that locally preserves the porostromate structure (white arrow); and **B** clotted to dense micrite patches (black arrows) connecting the *Halimeda* plates and preserving the primary interparticle porosity.

The clotted micrite texture (Fig. 4.6), locally connecting bioclasts and partially or totally infilling the primary pores and the interior of some bioclasts, is typically reported as representing microbial agglutination of particles as documented in stromatolites (Reid et al., 2003). The porostromate structure (Fig. 4.6) consisting of a concentration of tubular micropores separating the micritic clots, represents the original morphology of cyanobacteria that mediated the agglutination/precipitation of micrite (Andrews, 1986; Lehrmann, 1999; Castagner et al., 2014). The dense micritic matrix in patches connecting bioclasts (Figs. 4.3A, 4.7A) is also reported as the result of microbial activity by calcification of bacterial cells or biofilms (Riding, 2000).

The interpretation of the dense micrite as calcified biofilms is congruent with the presence of micritic envelopes in some grains, especially on *Halimeda* plates (Figs. 4.3, 4.8). Examples of *Halimeda* accumulations stabilized by organic binding similar to those recorded in TOTO slopes were reported from the Miocene of SE Spain (Braga et al., 1996; Martín et al., 1997). This microbial binding can also be linked to the lamination locally observed in the matrix (Fig. 4.3B) and in banded peloidal aggregates (Fig. 4.9A). Micritic peloids of irregular shape and size, the main component of the facies in Palmer Point slope (Fig. 4.9A), can be also interpreted as calcified microbial aggregates (Riding, 2000).

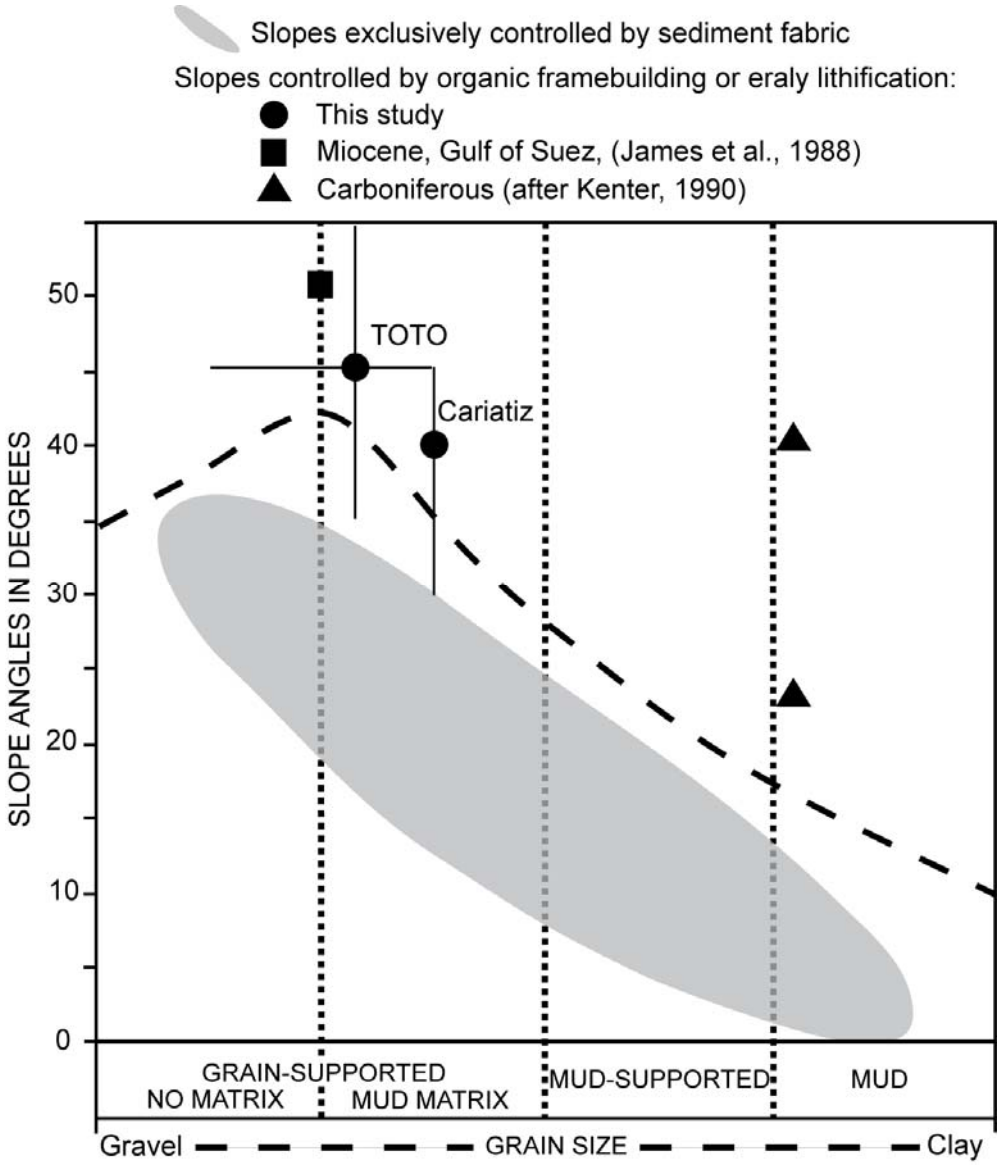

Fig. 4.11: Plot of slope angle vs. dominant sediment fabric (after Kenter, 1990) and vs. grain size (after Kirkby, 1987). The gray field represents the general trend reported from slopes without organic frame building or early cementation. The dashed line represents the maximal angle of repose of sediment ranging in size from gravel to clay. For the slopes presented in this work, the range in slope angle and fabric is indicated by bars.

The moguls in the upper middle segment of the leeward TOTO slopes are another feature of possible microbial origin. Structures similar to the moguls, with diameter of up to 20 cm and diffuse to clear internal lamination, were interpreted as deep water stromatolites formed along foreslopes at depths between 50-100 m below the level of the platform edge in the Gulf of Suez (James, 1988). The microbial stabilization together with the contemporary and later cementation proposed by Grammer et al. (1993a), appear as one process which fosters the preservation of steep slopes in TOTO.

In the Neogene slopes of Cariatiz there are also features reminiscent of microbial activity in distinct facies (Reolid et al., 2014), such as (1) dense micrite among the bioclasts (Fig. 4.7B), (2) micritic envelopes binding the bioclasts (Fig. 10A), (3) clotted micrite connecting the allochems (Fig. 4.10B), and (4) fine peloidal micritic matrix (Fig. 4.9B). The *Halimeda* breccia and *Halimeda* rudstone in the upper and middle segment present the most extensive development of microbial binding, which decreases basinwards as the sediment supply decays and basinal deposition dominates (Reolid et al., 2014).

4.6 Conclusions

This work compares Holocene and Miocene carbonate platform slopes and proposes an explanation for the steep angles of these slopes. The carbonate slopes from the Holocene of the Tongue of the Ocean in the Bahamas and the slopes from an Upper Miocene carbonate platform in SE Spain present slopes with linear profiles and angles in excess of 35°, as well as similar grain sizes, textures and bioclastic components with *Halimeda* plates as a major constituent. The most significant feature of the slope facies is that in the matrix and enveloping bioclasts there are distinctive microfabrics indicative of microbial activity during deposition, such as: (1) clotted micrite patches, locally connecting bioclasts or infilling primary pores, which can present (2) porostromate structure; (3) dense micritic masses; (4) trapping/binding structures; (5) micritic envelopes; and (6) peloidal texture.

The presence of an extensive microbial influence in the studied slopes is proposed as an early-stage slope stabilizing factor, as is the case in Palaeozoic and Triassic carbonate platforms. The occurrence of microbial binding prevented the slope failure in an early stage (several tens of years) and preserved the steep angles of repose of the slope. The occurrence of microbial binding in the Holocene slopes from the Tongue of the Ocean proves that the microbial stabilization in carbonates slopes is significant in normal-marine conditions and not exclusively related to any special conditions such as those of the Mediterranean Sea during the Upper Miocene. This work proves that microbial binding is a previously underestimated factor of slope stabilization in Neogene and Holocene carbonate platform slopes.

Chapter V

Facies variability in mixed carbonate-siliciclastic platform slopes

Abstract

Miocene tropical carbonate platform slopes show classical reef-slope facies distribution but also an unexpected abundance of serpulid-red algal facies, locally forming build-ups. Two sections from the Miocene Sorbas and Níjar basins in SE Spain were mapped and petrographically analysed in order to determine the factors controlling their facies variability. Reef-slope facies intercalate with serpulid-rich facies and siliciclastic bodies. The extensive occurrence of the serpulid-red algal rich facies seems to be related to the presence of high amounts of siliciclastics in the system. A comparison of these slopes with other examples from the Miocene carbonate platform slopes of SE Spain shows that slopes affected by siliciclastics display higher facies variability than pure carbonate systems. Neither deterministic models like facies belts nor stochastic models like facies mosaics can accurately or suffiently explain the facies distribution in the Miocene tropical carbonate platform slopes of SE Spain. Our observations add a valuable element to the ongoing discussion about the validity of the concept of facies belts versus the concept of facies mosaics.

This chapter is based on **Reolid, J., Betzler, C., Singler, V., Stange, C., and Linhorst, S.** (submitted) Facies variability in mixed carbonate-siliciclastic platform slopes (Miocene).

5.1 Introduction

Carbonate platform slope facies are reported to have a zonation into depth-dependent facies belts (Wilson, 1975; McIlreath and James, 1978; Schlager, 2005). The belts are the product of the combination of several intrinsic factors such as initial bathymetry, biological and sedimentary processes (Wright and Burgess, 2005). This concept of facies belts alone, however, cannot explain the complex facies variability observed in outcrops, as carbonate slopes are not uniform factories. Potential production areas may occur in patchworks or mosaics and alongslope processes may be localized (Wright and Burgess, 2005). Many of these mosaic elements are not depth-dependent and can change through time as a consequence of subtle extrinsic factors, i.e. siliciclastic input in the carbonate factory (Wright and Burgess, 2005).

Miocene tropical carbonate platform slopes are well exposed in the Neogene basins of the Betic Cordillera in SE Spain and have been the subject of numerous studies (Esteban, 1980; Dabrio et al., 1981; 1985; Riding et al., 1991; Martín and Braga, 1994; Braga and Martín, 1996; Esteban, 1996; Franseen and Goldstein, 1996; Cuevas-Castell et al., 2007). In cross-section, both the Cariatiz carbonate platform in the Sorbas Basin and the Polopos carbonate platform in the Níjar Basin display a progradational pattern with well-developed clinoform bodies. These clinoform bodies show a downslope facies zonation, from reef-framework blocks and breccia to fine-grained packstone. This facies distribution is not static, it differs in distinct growth packages depending on available accommodation (Reolid et al., 2014).

Mapping of facies distribution and microfacies analysis reveal that selected carbonate platform slopes in cross-section exhibit a high facies variability, which is mostly determined by the presence of abundant serpulids and siliciclastics. The extensive occurrence of the serpulid-red algal rich facies seems to be linked to the presence of high amounts of siliciclastics in the depositional system.

This study addresses these points and seek to clarify the causes and significance of the factors controlling the facies distribution in carbonate platform slope clinoform bodies, thus contributing to the better general understanding of carbonate slope facies distribution.

5.2 Geological setting

Carbonate platform slope facies are well exposed in the intramontane Neogene basins of southeast Spain (Fig. 5.1). Two sections from the Cariatiz carbonate platform at the northern margin of the Sorbas Basin and two sections from the Polopos and Níjar

carbonate platforms at the northern margin of the Níjar Basin were analysed (Fig. 5.1). The Sorbas Basin is an E-W elongated depression bounded by metamorphic rocks from the Internal Betic Zone cropping out in the Sierra de los Filabres to the north and in the Sierra Alhamilla and Sierra Cabrera to the south. There, a Messinian carbonate platform with coral reefs (Fringing Reef Unit, Riding et al., 1991; Braga and Martín, 1996) and related basinal silty marls, marls and diatomites from the Upper Abad Member (Martín and Braga, 1994) is dissected by several ravines which provide insight into platform-internal and slope facies architecture (Fig. 5.2A). The NE-SW elongated Níjar basin is bounded by Sierra Alhamilla to the North and by Neogene volcanic complex of Cabo de Gata to the southeast. Attached to the northern margin of the basin, there is a Messinian carbonate platform with coral reefs and associated basinal silty marls from the Upper Abad Member (Fig. 5.2B; Drabrio et al., 1981).

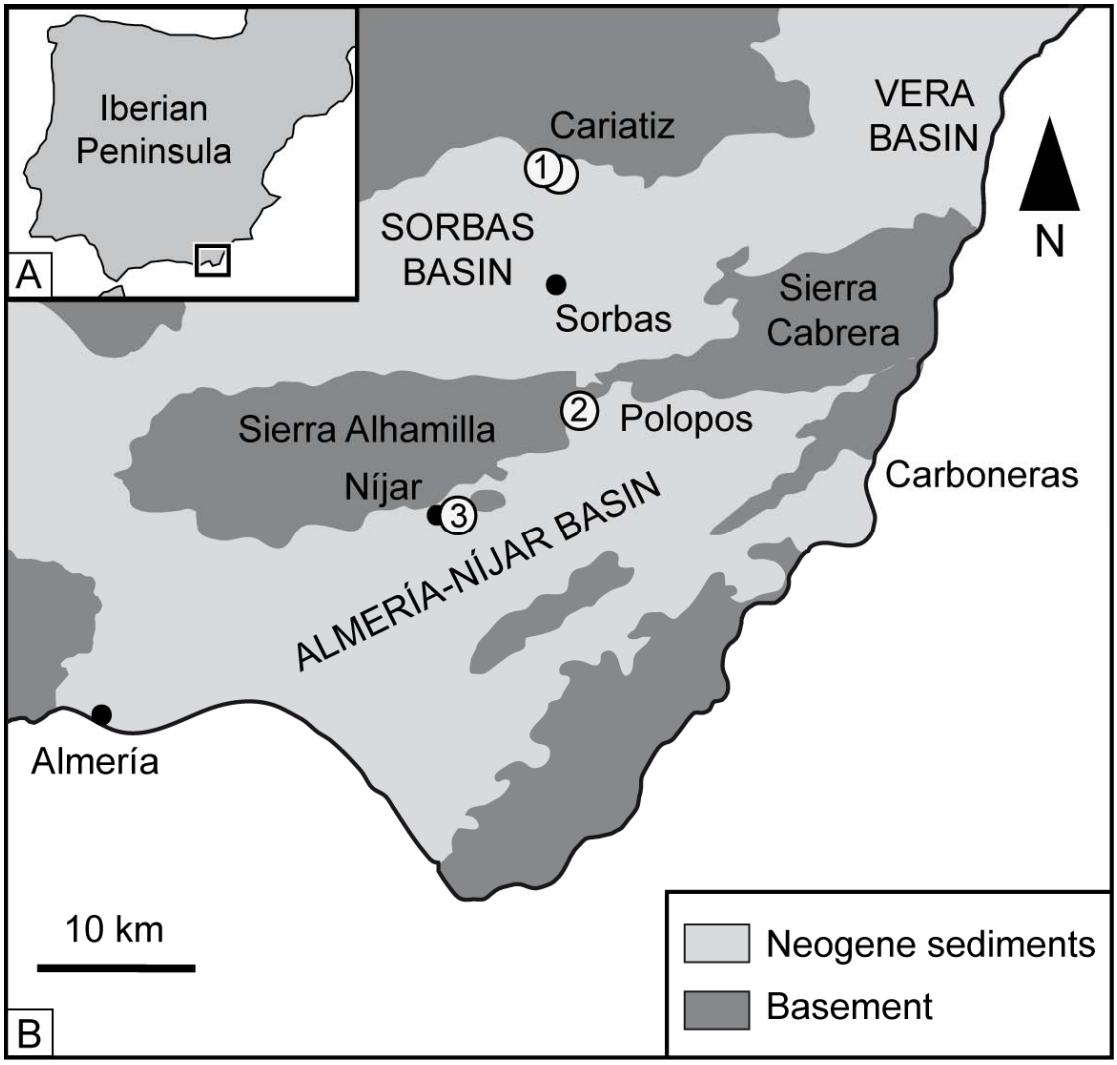

Fig. 5.1: A Location map of the study area in SE Spain. **B** Regional setting of the Neogene basins of SE Spain showing the carbonate platform discussed in this study: Cariatiz (northern and southern section), Polopos and Níjar.

5.3 Methods

Carbonate platform slope facies were mapped using panoramic photomosaics of the best-exposed successions. Two hundred samples from the different facies were petrographically analysed to identify microfacies and components. Polished slabs were additionally used to analyse large bioclasts, sedimentary fabrics and structures. Where accessible, the slopes of the Cariatiz carbonate platform were scanned with an Optech Laser Imaging ILRIS 3D terrestrial LIDAR of the Institute of Geology of Hamburg University. LIDAR data were digitally processed using 3D-Reconstructor (Gexcel).

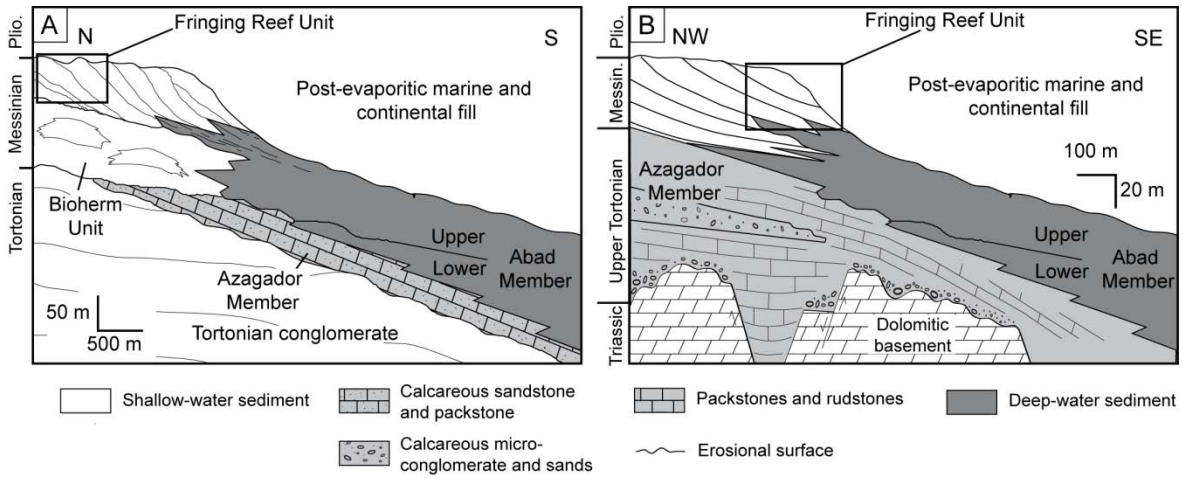

Fig. 5.2: A Neogene lithostratigraphy of the Sorbas Basin. The rectangle indicates the interval of the succession shown in detail in Fig. 5.3 (Modified from Reolid et al., 2014). **B** Neogene lithostratigraphy of the Polopos section. The rectangle indicates the interval of the succession shown in detail in Fig. 5.7.

5.4 Results

5.4.1 Carbonate slope facies

The characteristics of the main slope facies of the Messinian fringing reef slopes are summarised in Tables 5.1 and 5.2. Fourteen different slope facies are defined based on their components, grain-size, sedimentary structures, and position in the slope. The reef-talus slope facies are characterised by breccia deposits consisting of reef-framework debris floating in a rudstone matrix (i.e siliciclastic-coral breccia and *Halimeda* breccia). The proximal slope facies are bioclastic rudstones to floatstones with abundant bivalves, gastropods, red algae and equinoid remains, or with abundant serpulids and red algae. Distal slope facies contain fine grained deposits with some large bioclasts, mostly molluscs, locally floating in the matrix as in the bioclastic wackestone to floatstone. Locally, there are facies containing up to a 50%, siliciclastics (Tables 5.1, 5.2); individual slope bedsets may even consist entirely of siliciclastic.

Facies	Components	Matrix	Fabric	Coatings	Position	Dip
Breccia	5 cm to 300 cm reef-framework blocks. Coralline algae, bivalves, gastropods, echinoid spines, bryozoans, serpulids, benthic foraminifera (mainly miliolids), and rare *Halimeda* plates. Intraclasts and siliciclastics (quartz and mica).	Microgranullar matrix (wackestone-packstone of unidentifiable bioclasts).	Chaotic. Massive.	Red algae (especially on serpulids and bivalves).	Talus slope.	35°-25°
Bioclastic floatstone	Up to 4 cm large bioclasts including echinoid spines, bivalve fragments, benthic foraminifera (usually miliolids), and red algae, and minor coral fragments, gastropods, serpulids, and bryozoans. Locally 3 mm to 11 mm *Halimeda* plates rudstones (up to 80% of the rock). Siliciclastics (quartz and mica).	Microgranullar matrix (wackestone of silt-sized bioclasts).	30 to 70 cm beds. Shells are locally in contact in grain supported patches with similar proportions of concave- and convex-up orientation. 60 to 100 cm thick and 3 to 4 m wide *Halimeda* mound.	Red algal coatings.	Proximal slope.	25°-15°
Bioclastic wackestone to floatstone	Bivalves (pectinidae, glycymeridae, veneridae, mytilidae and ostreidae), solitary corals, bryozoans, red algae, benthic and planctonic foraminifera, and minor serpulids and *Halimeda* plates. Siliciclastic up to 15% of the facies.	Marls.	30 to 40 cm thick beds. Shells are randomly oriented to bedding with similar proportions of convex- and concave-up orientation.	Red algae, serpulids bryozoans.	Distal slope.	15°-10°
Serpulid boundstone	Clusters and up to 2 mm fragments of serpulids (about the 85 to 90% of the rock). Red algae, oysters, and bryozoans siliciclastic grains (up to 10%), mostly phylosilicates, and scarce intraclasts.	Microgranullar matrix (wackestone-packstone of silt-sized bioclasts).	Patches of articulated oysters in life position.	Red algae, serpulids bryozoans.	Talus to proximal slope.	30°-20°
Serpulid-red algal rudstone to floatstone	Up to 20 cm serpulid-red algal nodules. Bryozoans, bivalves, gastropods, echinoids, and rarely coral fragments. Intraclasts.	Marls, locally microgranullar carbonate matrix.	10 to 30 cm thick beds. Locally parallel lamination and subparalel orientation of bivalves. Alternance of thin limes and marls beds and thick nodule-accumulation beds.	Red algae, serpulids bryozoans.	Distal slope.	20°-5°
Bioclastic floatstone (lowstand wedges)	Up to 4 cm red algal nodules. Bryozoans, serpulids, bivalves, echionoid spines, and benthic foraminifera.	Microgranular matrix.	30 to 60 cm thick thining-upward beds.	Red algae and bryozoans.	Proximal to distal slope.	30°-15°
Siliciclastics	Up to 10 cm quartz, schist, marble and serpentinite clasts. Serpulids, benthic foraminifera, echinoid spines, bryozoans, and red algae.	Mixture of sand and microgranullar carbonate matrix.	Poorly bedded.	Bryozoans and red algae.	Talus to distal slope.	30°-15°

Table 5.1: Reef-slope facies of northern section of the Cariatiz carbonate platform.

Facies	Components	Matrix	Fabric	Coatings	Position	Dip
Siliciclastic-coral breccia	Fragments of reef-framework debris (cm to m scale), red algae, bryozoans, serpulids, bivalves, benthic foraminifera, echinoid spines, and solitary corals. Siliciclastics (pebble to cobble-size) between to 25-30% (locally up to 50%).	Microgranular to dense/clotted/ peloidal micrite.	Chaotic. Locally centimetric to decimetric siliciclastic beds.	Red algae and locally stromatolites.	Talus slope.	35°-20°
Halimeda breccia	*Halimeda* plates, framework blocks (m to cm), gastropods, bivalves, red algae (locally as rhodoliths), foraminifera, fragments of solitary corals, bryozoans, echinoid spines, serpulids, and barnacles. Sand to pebble siliciclastic content up to 7%.	Dense micrite (locally microgranular).	Massive to poorly bedded. Locally patches formed by red algal crusts and serpulid tubes among a microbial to micritic matrix.	Red algae, serpulids and barnacles.	Talus slope.	25°-20°
Siliciclastic-coral floatstone	Up to 2 cm fragments of corals, bivalves, red algae, bryozoans, gastropods, echinoid spines, and miliolids. Sand to pebble siliciclastic content up to 10%.	silt- to sand-sized siliciclastic grains in a micritic matrix.	Massive to poorly bedded.	Red algae.	Proximal slope.	20°-15°
Siliciclastic-red algal-serpulid rudstone	Sand to pebble sized fragments of serpulids, red algae, bivalves, bryozoans, miliolids, gastropods, and echinoid spines. Up to 15 cm siliciclastics between 5 to 15% of the facies.	Microgranular (rarely micritic).	Alternating bedding of centimetric to decimetric rudstone and floatstone beds.	Serpulids and red algae (preferentially on large siliciclastics). Bryozoans.	Proximal slope.	20°-15°
Serpulid rudstone	Up to 2 cm large bioclasts including serpulids, bivalves, red algae, miliolids and rarely echinoid spines, bryozoan, gastropods, barnacles, and coral fragments. Up to 4 cm large siliciclastics are the 5% of the facies.	Micritic to microgranular.	20 cm thick and 15 to 40 cm wide patches of in-situ encrustation of serpulids. 10 to 50 cm thick beds alternating coarser and finer rudstones. Beds with locally wavy bottoms. Decimetric siliciclastic-rich beds are intercalated.	Serpulids and red algae.	Proximal slope.	20°-15°
Red algal-bivalve packstone to floatstone	Sand sized bioclasts (locally up to 15 cm) including red algae, bivalves (pectinids and oysters), corals, bryozoans, gastropods, serpulids, benthic foraminifera, echinoid spines, and rarely planktonic foraminifera. Sand to pebble siliciclastics up to 10%.	Micrite.	Alternation of 20 to 100 cm greyish bioturbated floatstone intervals and reddish stratified packstone beds.	Micritic envelopes.	Proximal to distal slope.	15-10°
Siliciclastic-rich packstone to rudstone	Red algae, bivalves, serpulids, corals, gastropods, echinoid spines, and barnacle fragments. The amount of siliciclastics can be up to 35%. (up to 5 cm)	Micritic to locally microgranular.	Aternation of decimetric packstone and rudstone beds.	Red algae.	Proximal to distal slope.	15-10°
Siliciclastics	Up to 5 cm quartz, schist, marble and serpentinite clasts. Serpulids, benthic foraminifera, echinoid spines, bryozoans, and red algae.	Mixture of sand and microgranullar carbonate matrix.	Poorly bedded.	Bryozoans, serpulids and red algae.	Talus to distal slope.	25°-15°

Table 5.2: Reef-slope facies of northern section of the Polopos carbonate platform.

5.4.2 Cariatiz carbonate platform: slope facies distribution

The more than 190 m long Rambla de la Mora section at the northern Cariatiz carbonate platform contains several packages of carbonate platform progradation (Fig. 5.3). The slope facies, which are described in Table 5.1, occur in fourteen sedimentary bodies, including reefal clinoform bodies (CB), serpulid bioherms, lowstand wedges, and siliciclastic-rich bodies (Fig. 5.3).

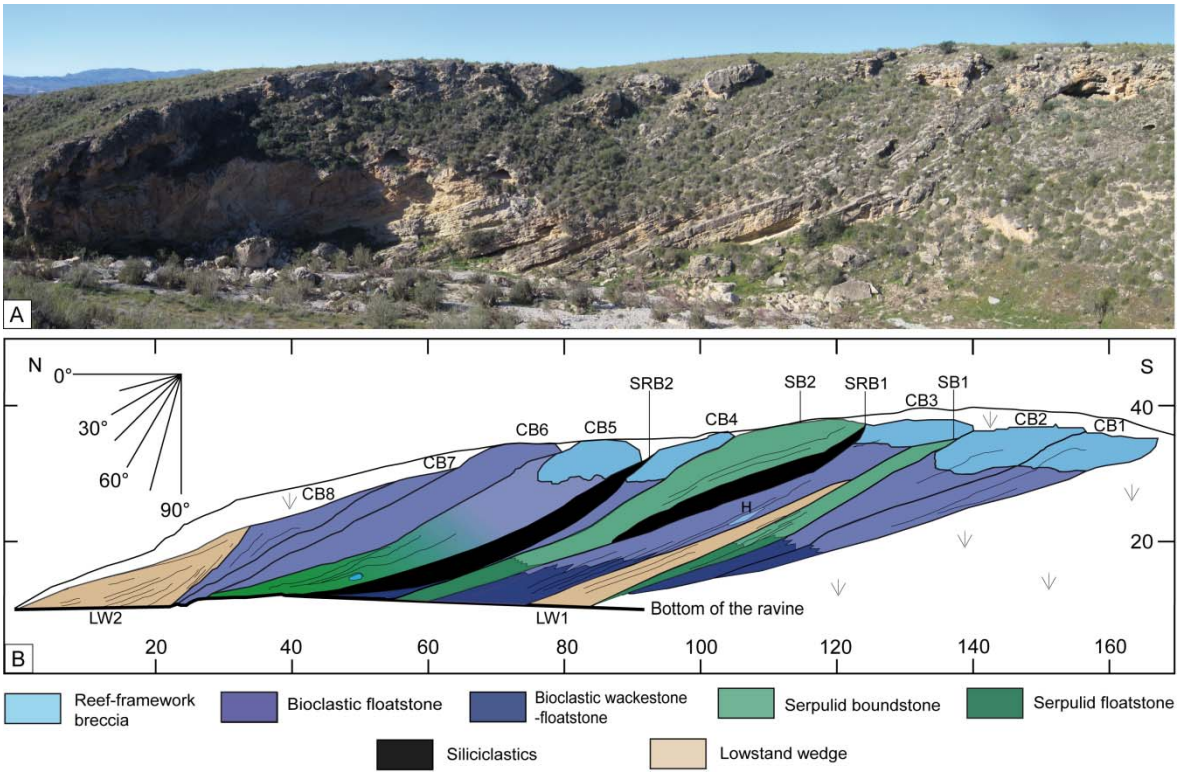

Fig. 5.3: A Outcrop panorama of the northern section of the Cariatiz carbonate platform. **B** 2D projection of main surfaces traced onto a plane oriented paralel to progradation direction (N170E) derived from the LIDAR data. The slope facies form fourteen sedimentary bodies, including reefal clinoform bodies (CB) with a *Halimeda* mound (H), serpulid bioherms (SB), lowstand wedges (LW), and siliciclastic-rich bodies (SRB).

5.4.2.1 Clinoform bodies

There are seven clinoform bodies in the Rambla de la Mora section. The maximum height of these bodies is 30 m, and the maximum extension in the direction of progradation (approximately N170E) is 80 m. The slope angles vary from up to 35° at the reef talus to 25° at the proximal slope, and to 15° at the distal slope. The facies distribution follows the model presented by Riding et al. (1991). The uppermost facies in these clinoform bodies is the breccia facies (Fig. 5.4A). The average thickness of this facies is up to 5 m. Stick-like *Porites* occur in the reef-framework blocks. Reef-framework debris size and amount

decrease basinward and the lithology gradually changes into a bioclastic floatstone in the proximal slope.

In the proximal reef-slope it is possible to identify a small mound consisting of an accumulation of *Halimeda* plates within one of the clinoform bodies (CB3 in Fig. 5.3). This mound is approximately 60 to 100 cm thick and 3 to 4 m wide. The *Halimeda* plates range in size from 2 to 10 mm and make up a rudstone with minor micritic matrix in the remaining pore spaces (Fig. 5.4B).

The gradual transition from the proximal to the distal slope deposits corresponds to a well-bedded bioclastic wackestone to floatstone facies fining downslope (Fig. 5.4C). Where present, bioturbation is at the finest intervals. In some beds there are patches rich in bivalves, mainly from the families veneridae, glycymeridae, and pectinidae.

5.4.2.2 Serpulids bioherms

These bodies are up to 28 m high and up to 70 m wide in the direction of progradation. Their uppermost part consists of serpulid boundstone (Fig. 5.5A-B), downslope there is a change towards accumulations of fragmented serpulid debris (Fig. 5.5C-D). The serpulid-rich bodies are faintly bedded. Bedding is better developed downslope, where other bioclasts, especially red algae and bivalves, are common. In these parts, deposits are marls.

Clinoform Body 5 (Fig. 5.3) contains a mixture of serpulid bioherm and coral reef facies, and is topped by a breccia with some large reef-framework blocks. The proximal slope is covered by vegetation and it is not possible to identify the facies, but the distal slope consists of an accumulation of serpulid-red algal nodules arranged in 20 to 30 cm thick beds locally deformed by the load of large reef-framework blocks. The nodules range in size from 5 to 20 cm and consist of clusters of red algae, serpulids, and rarely bryozoans (Fig. 5.5E). It is possible to recognise an alternance of thin fine-grained beds and thick nodule-accumulation beds (Fig. 5.5F). The fine-grained beds are made up of marls alternating with sand-grade carbonate bioclasts.

5.4.2.3 Siliciclastic bodies

Two siliciclastic intervals, each up to 5 m thick, are intercalated into the carbonate platform slope succession (Fig. 5.3). The older body consists of a conglomerate with up to 5 cm clasts in a sand-sized matrix which is a mixture of siliciclastic and carbonate grains. Most of the siliciclastics pebbles are coated by different generations of encrusters starting with bryozoans and followed by serpulids and red algae (Fig. 5.6). The younger body consists of a mixed carbonate-siliciclastic sand with unidentifiable sand-sized bioclasts.

5.4.2.4 Lowstand wedges

The platform slope succession also contains two packages of well-bedded bioclastic floatstone, which are up to 10 m thick and have an extension of 40 m (Fig. 5.3). The bodies thin out upslope.

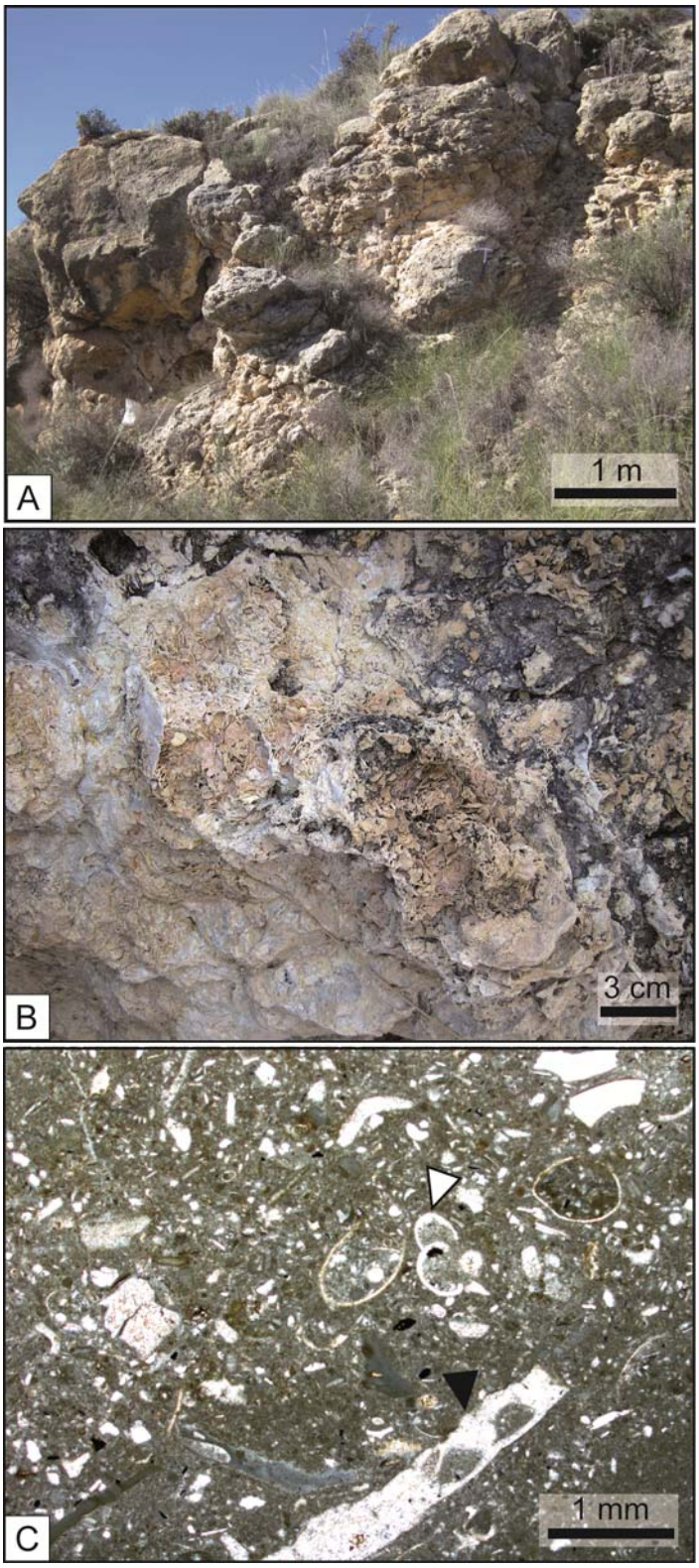

Fig. 5.4: Clinoform body facies in the northern Cariatiz section. **A** Breccia facies in the talus slope with large *Porites*-framework blocks. **B** Close-up of the *Halimeda* mound in the proximal slope of CB3 (Fig. 5.3). **C** Photomicrograph of the distal-slope bioclastic wackestone with bryozoan fragments (black arrow) and planctonic foraminifera (white arrow) in a silt-sized bioclastic matrix with minor siliciclastics.

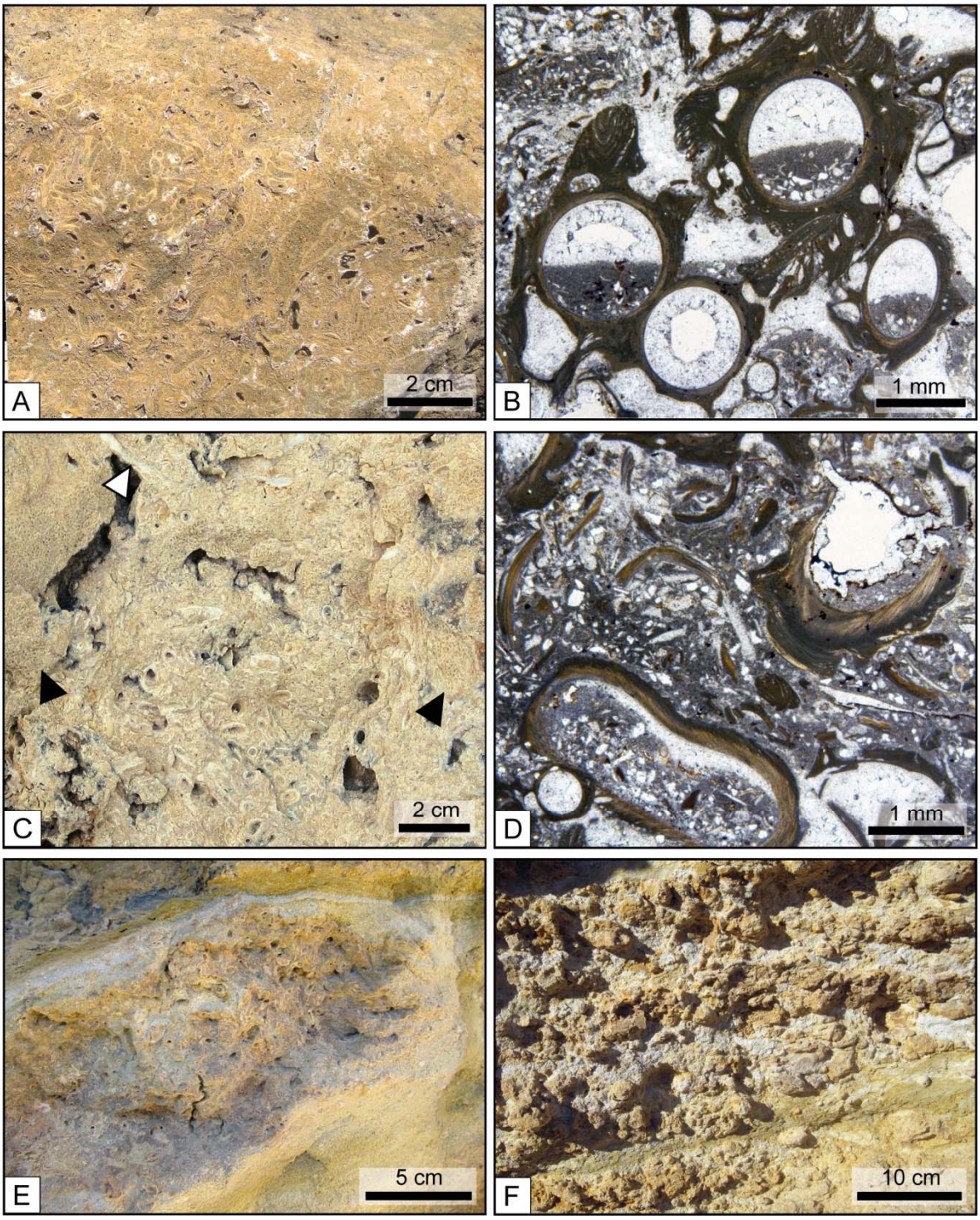

Fig. 5.5: Serpulid-rich facies in the northern Cariatiz section. **A** Close-up of the surface of the serpulid boundstone facies of SB2 (Fig. 5.3). **B** Photomicrograph of the serpulid boundstone. **C** Close-up of the serpulid rudstone facies of SB1 with oyster debris (white arrow) and abundant bryozoan coatings (black arrows). **D** Photomicrograph of the serpulid rudstone with commom fragmentation of the serpulid tubes. **E** Close-up of a serpulid-red algal nodule floating in a marl matrix from the distal slope of CB5. **F** Outcrop picture of the distal slope of CB5 with an alternance of thin marl beds and thick nodule-accumulation beds.

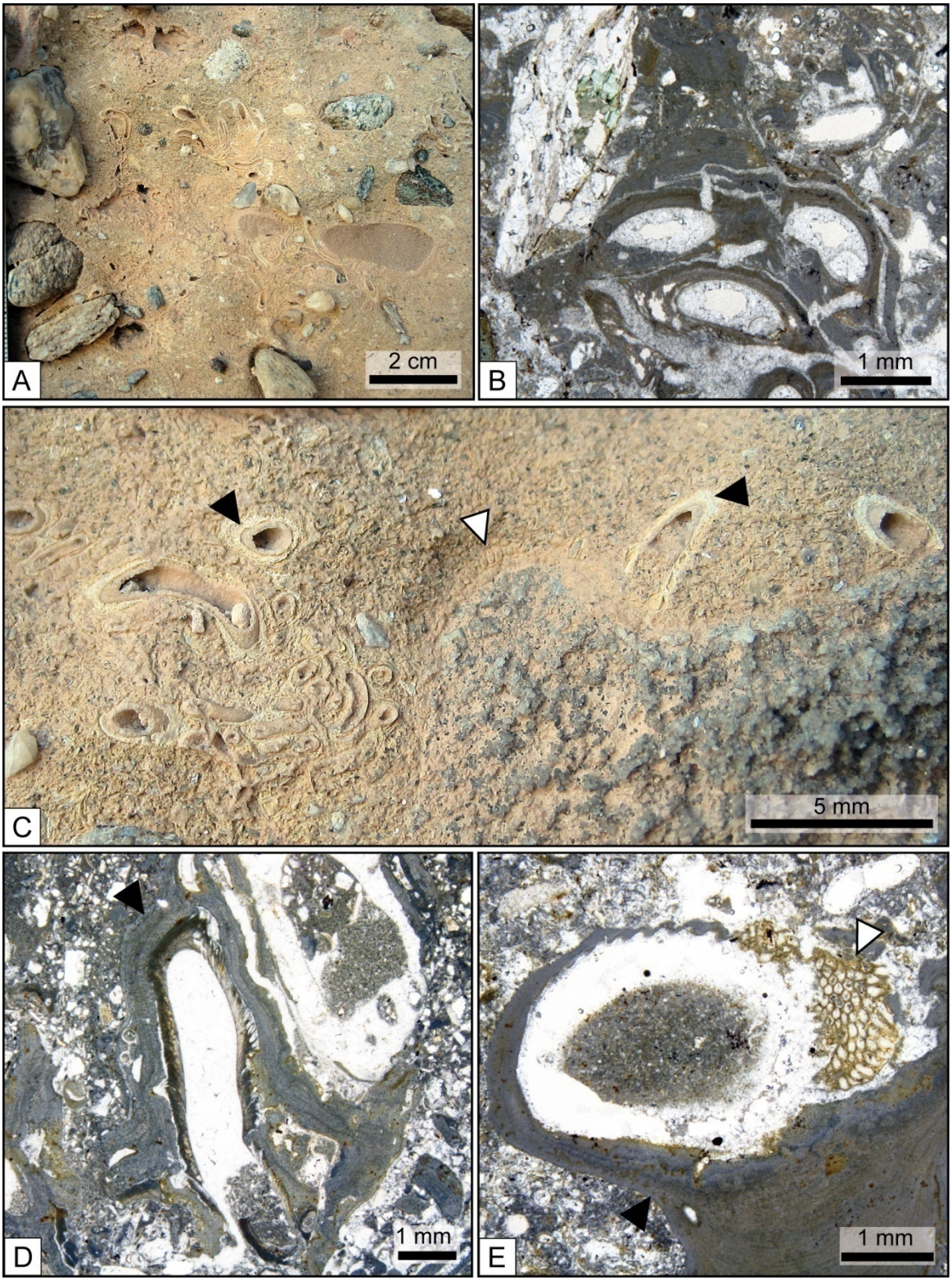

Fig. 5.6: Siliciclastic-rich facies and encrusters of the Cariatiz section. **A** Close-up of the siliciclastic-rich facies with abundant serpulids. **B** Photomicrograph of the siliciclastic-rich facies with serpulids from SRB1 (Fig. 5.3). **C** Close-up of a coarse grain from the siliciclastic-rich facies encrusted by bryozoans (white arrow) and serpulids. Serpulids are encrusted by red algae (black arrow). **D** Photomicrograph of a bioclastic floatstone with common siliciclastic and serpulids encrusted by red algae (black arrow). **E** Photomicrograph of a bioclastic floatstone with common siliciclastic showing a large bioclast encrusted by bryozoans (white arrow) and by red algae (black arrow).

5.4.3 Polopos carbonate platform: slope facies distribution

A succession of seven SE-prograding clinoform bodies extending over 300 m gives a good overview of the slope facies arrangement of this carbonate platform (Fig. 5.7). The slope facies are described in Table 5.2 and are distributed into seven sedimentary bodies, including reefal clinoform bodies (CB) with intercalated siliciclastic bodies.

The clinoform bodies comprise in their uppermost part the reef-framework facies with stick-like colonies of *Porites* with thick stromatolitic crusts. The coral colonies form sub-vertical cliffs with an inclination of 80° to 60° (Fig. 5.8A). The thickness of the reef-framework facies commonly varies from 10 m to 15 m with a maximum thickness of 15 m. The extension of the reef framework in the direction of progradation ranges from 15 m to 25 m. The reef-framework facies may contain up to a 15% of siliciclastics ranging from sand-sized (Fig. 5.8B) to pebble-sized (Fig. 5.8C). Locally, lagoonal facies overlie the reef framework (Fig. 5.7).

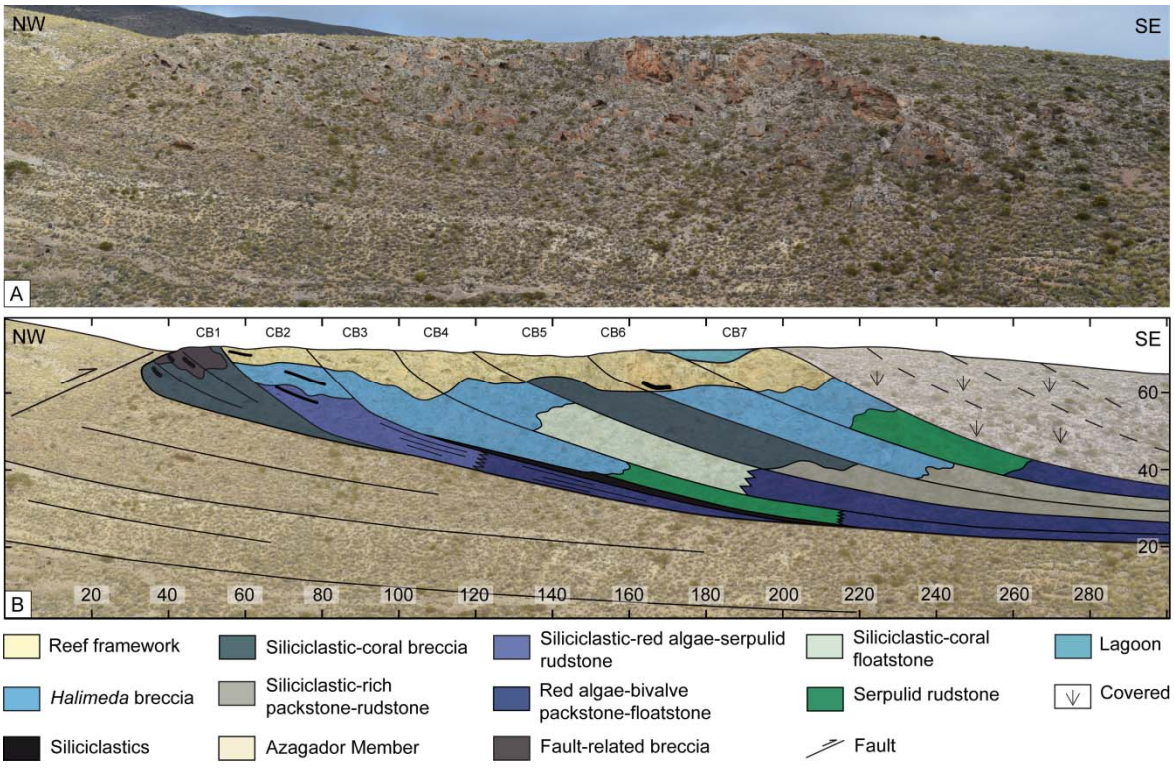

Fig. 5.7: A Outcrop panorama of the Polopos carbonate platform section. **B** Interpretation of the main clinoform bodies (CB), bedding and facies.

The reef-talus slope has an inclination of 25° and is dominated by *Halimeda* breccia with large reef-framework debris (Fig. 5.9). The *Halimeda* breccia packages are 5 to 20 m thick and extend between 10 and 70 m in the direction of progradation. In the case of CB1 and CB5 (Fig. 5.7), the talus-slope facies is a siliciclastic-coral breccia with a maximum

thickness of 15 m and a lateral extension in the direction of progradation of 70 m. Sandstone to conglomerate beds locally cut across the siliciclastic-coral breccia and the *Halimeda* breccia (Fig. 5.9).

The proximal slopes in the Polopos carbonate platform display angles of 20° to 15° and considerable facies variability. The facies may consist of (1) a siliciclastic-red algal-serpulid rudstone, locally displaying an alternation of floatstone intervals with *Halimeda* rudstone beds in the contact with the *Halimeda* breccia (Fig. 5.10A-B); (2) a serpulid rudstone (CB3 and CB7 in Figs. 5.7, 5.10C-D); and (3) a siliciclastic-coral rudstone.

The distal slope has an inclination of between 15° and 10° and consists of red algal-bivalve packstone to floatstone that may interfinger with the proximal slope facies in its upper part. The thickness of the red algal-bivalve packstone to floatstone facies decreases downslope from 10 m to 5 m. Where the siliciclastic content is high, the red algal-bivalve facies occurs as a siliciclastic-rich packstone to rudstone (CB5 and CB6 in Fig. 5.7).

In general, the reef-slope facies are rich in siliciclastics. The thickest siliciclastic body is a two-metre-thick greyish conglomeratic sandstone between CB2 and CB3 (Figs. 5.7, 5.9).

5.5 Discussion

5.5.1 Miocene carbonate platform slopes from SE Spain

The carbonate platform slopes presented in this work show a higher facies variability than other Miocene carbonate platform slopes from SE Spain (Fig. 5.11). Slope facies composition and distribution result of the interaction of several factors including coral growth, in-situ slope carbonate production, rockfalls and sediment gravity flows, hemipelagic rain, reworking of reef-slope facies, as well as siliciclastic input (Reolid et al., 2014). Changes in accommodation related to sea-level fluctuations controlled the relative impact of these factors (Reolid et al., 2014).

Most of the recorded Miocene tropical carbonate platform slopes are rimmed in their uppermost part by a *Porites*-stromatolite reef framework (Fig. 5.11). Stromatolites encrusted the *Porites* colonies, producing an early lithification (Riding et al., 1991). The breakage of the *Porites*-stromatolite framework at the reef front subsequently produced rock and debris falls (Martinsen, 1994; Drzewiecki and Simó, 2002; Reolid et al., 2014). This process resulted in the accumulation of blocks and debris on the reef-talus slope (Figs. 5.4, 5.9, 5.11). Rockfalls and debris falls triggered sediment flows spreading basinward to the distal reef-slope with decreasing transport capacity (Adams et al., 1998, Reolid et al.,

2014). Under conditions of low accommodation these rockfalls may export large reef-framework blocks to more distal settings than during conditions of high accommodation, as recorded in the southern Cariatiz carbonate platform (Fig. 5.11; Reolid et al., 2014). During lowstand periods, the erosion of the platform increased and the gravity-driven processes intensified, resulting in the accumulation of bioclastic sands in fan-like bodies which form the lowstand wedges of the Cariatiz carbonate platform (Fig. 5.11; Schlager, 1989; Braga and Martín, 1996; Cuevas-Castell et al., 2007).

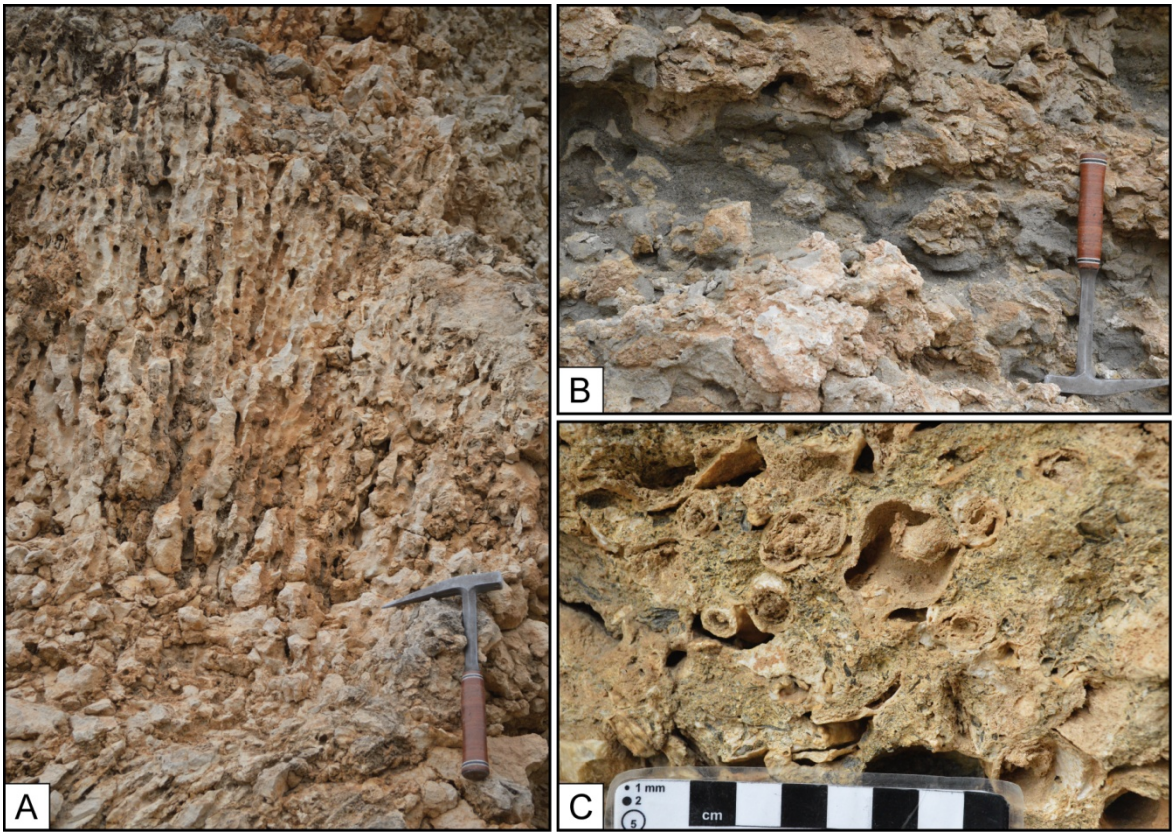

Fig. 5.8: A Outcrop picture of the reef-framework facies with vertical *Porites* tubes and thick stromatolitic crusts from CB3 (Fig. 5.7). **B** Outcrop example of fine grained siliciclastic in the gaps among stromatolitic crusts at the base of the reef framework. **C** Outcrop example of coarse siliciclastic grains among horizontal *Porites* tubes in the transition from the reef framework to the siliciclastic-coral breccia.

Miocene carbonate platform slope facies in the area studied are dominated by *Halimeda* plates as documented by (Mankiewicz, 1988; Martín and Braga, 1989; Riding et al., 1991; Braga and Martín, 1996; and Reolid et al., 2014). *Halimeda* plates either accumulated in-situ as small mound-like structures (Fig. 5.4B) or were exported downslope by sediment flows, forming parautochtonous to allochtonous accumulations along the slope (Fig. 5.10). Mankiewicz (1988) described similar *Halimeda*-rich facies and related them to upwelling conditions. Reolid et al. (2014) proposed that upwelling of nutrient-rich waters during sea-level rise and highstand stages promoted the flourishing of *Halimeda* in the Cariatiz

carbonate platform. These upwelling conditions persisted during the early stages of a sea-level fall as evinced by the presence of *Halimeda* rudstone facies (Fig. 5.11). The decreasing accommodation with continued sea-level fall finally promoted the mixture of water masses and consequently the interruption of upwelling (Reolid et al., 2014). The end of upwelling conditions most likely explains the absence of *Halimeda* algae in clinoform bodies formed under conditions of low accommodation (Fig. 5.11). When the conditions were not suitable for the extensive development of *Halimeda* algae, bioclastic packstone to rudstone formed with common bivalves, gastropods, equinoids, red algae, serpulids, and benthic foraminifera (Fig. 5.11).

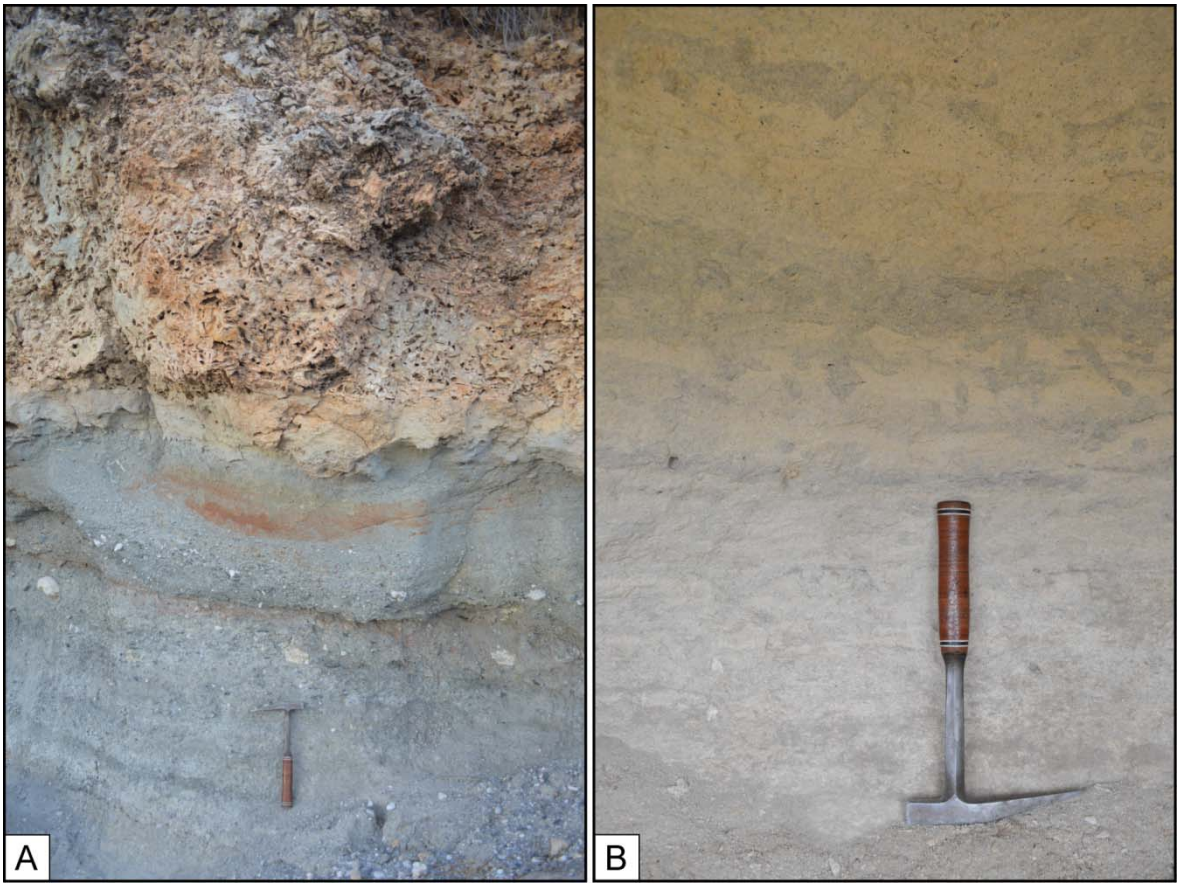

Fig. 5.9: A Outcrop picture of large framework blocks from the *Halimeda* breccia facies of CB3 overlying a thick siliciclastic body (Fig. 5.7). **B** Outcrop picture of the bioturbated red algal-bivalve packstone facies that are mixed with siliciclastics in the distal slope of CB3.

Together with the *Halimeda* algae, serpulids and red algae are the main components in the Miocene carbonate platforms analysed, especially in the bioherms intercalated with the reef-slope facies (Figs. 5.5, 5.11). In the Polopos section, red algae and serpulid patches are in-situ build-ups in the *Halimeda* breccia (Fig. 5.10; Riding et al., 1991; Braga et al., 1996, Reolid et al., 2014). Similar build-ups in reef slopes also occur in other Messinian carbonate platforms in the region (Reolid et al., 2014; Sola et al., 2013).

The presence of silts and marls in the distal reef-slope (Fig. 5.11) is interpreted as deposition from suspension under relatively quiet-water conditions (Drzewiecki and Simó, 2002). The distal slope facies may be significantly reduced in sea-level fall and lowstand clinoform bodies (Fig. 5.11).

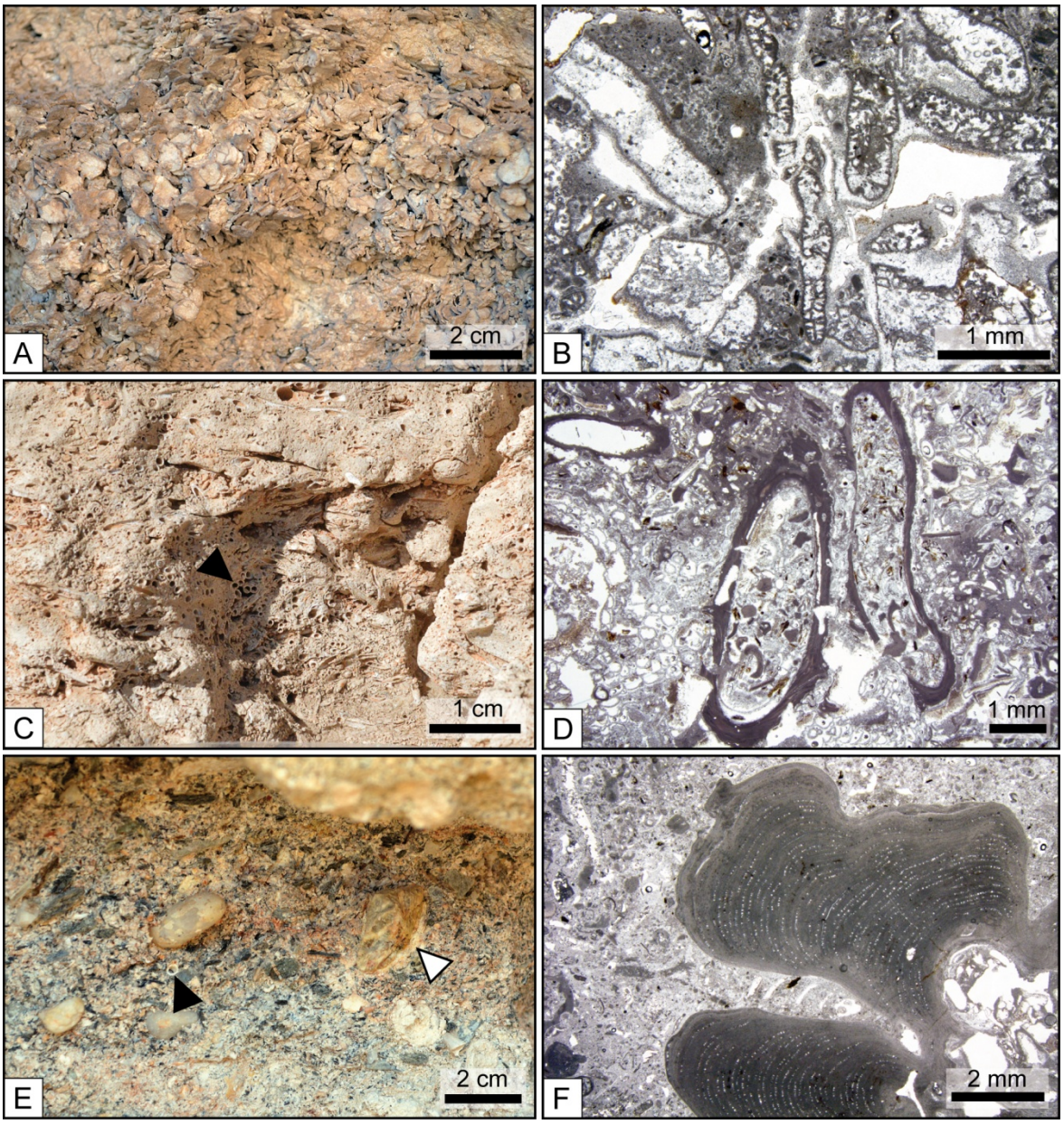

Fig. 5.10: Main carbonate producers in the slope facies. **A** Close-up of a talus-slope accumulation of *Halimeda* plates. **B** Photomicrograph of a *Halimeda* rudstone interval within the *Halimeda* breccia facies. **C** Outcrop picture of a serpulid patch in the siliciclastic-red algal-serpulid rudstone. **D** Photomicrograph of the siliciclastic-red algal-serpulid rudstone facies showing two serpulid tubes infilled with siliciclastic grains. **E** Close-up of a conglomeratic interval within the siliciclastic-red algal-serpulid rudstone with serpulid tubes (black arrows) and red algal crust (white arrow). **F** Photomicrograph of a rhodolith, red algal encrustation arround a bioclasts, in the *Halimeda* breccia facies.

5.5.2 Siliciclastic input and facies variability

The Miocene tropical carbonate platforms analysed were subjected to temporary siliciclastic input (Fig. 5.11). The presence of siliciclastics is especially significant in the northern part of the Cariatiz platform and in the Polopos carbonate platform and is proposed to be the cause of the highest facies variability in these platform slopes (Fig. 5.11).

Slope facies with abundant serpulids have higher siliciclastic contents than the rest of the slope facies, especially those dominated by *Halimeda* algae (Tables 5.1, 5.2; Figs. 5.3, 5.7, 5.11). During the Messinian, the Polopos carbonate platform and part of the Cariatiz carbonate platform developed in an environment with occasional sedimentation of coarse grained sands and conglomerates (Braga et al., 1996). Both carbonate platforms represent reef systems associated with fan-delta deposits common in the Upper Miocene in the Neogene basins of SE Spain (Martín et al., 1989; Braga et al., 1990). The shedding of fan delta systems started during the early Messinian and is related to the uplift of the Sierra de los Filabres and Sierra Alhamilla (Braga et al., 2003). In the Polopos area, the synsedimentary activity of the dextral-reverse Polopos fault, which limits the carbonate platform to the northwest, triggered the siliciclastic input in the area (Pedrera et al., 2012; Giaconia et al., 2012). The intermittence of the tectonic activity and the intensification of weathering has been forwarded to control the fluctuations of siliciclastic input. These fluctuations are independent of sea-level changes (Braga and Martín, 1996).

The abundance of serpulids and red algae in the slope facies appears to be linked to the amount of siliciclastics. Pebbles represented ideal hard substrates to be encrusted by serpulids, red algae, and bryozoans (Fig. 5.6; Halfar and Mutti, 2005). Silicilastic influx promoted nutrient-rich and reduced-light conditions that favoured the abundance of these encrusters, especially red algae (Carannante et al., 1988). Serpulids and red algae are more tolerant (Navarro et al., 2008) than *Porites* or *Halimeda* (Mankiewicz, 1988) under environmental stress conditions (i.e. high turbidity by siliciclastic input).

Under such conditions serpulids rapidly developed and formed large sedimentary bodies (Fig. 5.3), because the average energy of the streams providing the siliciclastics was moderate and allowed the development of bioherms as described for other cases (Navarro et al., 2008). Similar to bioherms from the Jurassic of the Betic Cordillera, the dense packing of the serpulid build-ups is proposed to enhance the resistance against high-energy events but also to prevent the colony from being overgrown by other sessile organisms (Navarro et al., 2008). Serpulids, which lived outside of the bioherms, are commonly encrusted by red algae (Fig. 5.6). Once the water conditions were suitable the *Porites* reef

developed again and *Halimeda* dominated the slope deposits with serpulids and red algae being restricted to small patches.

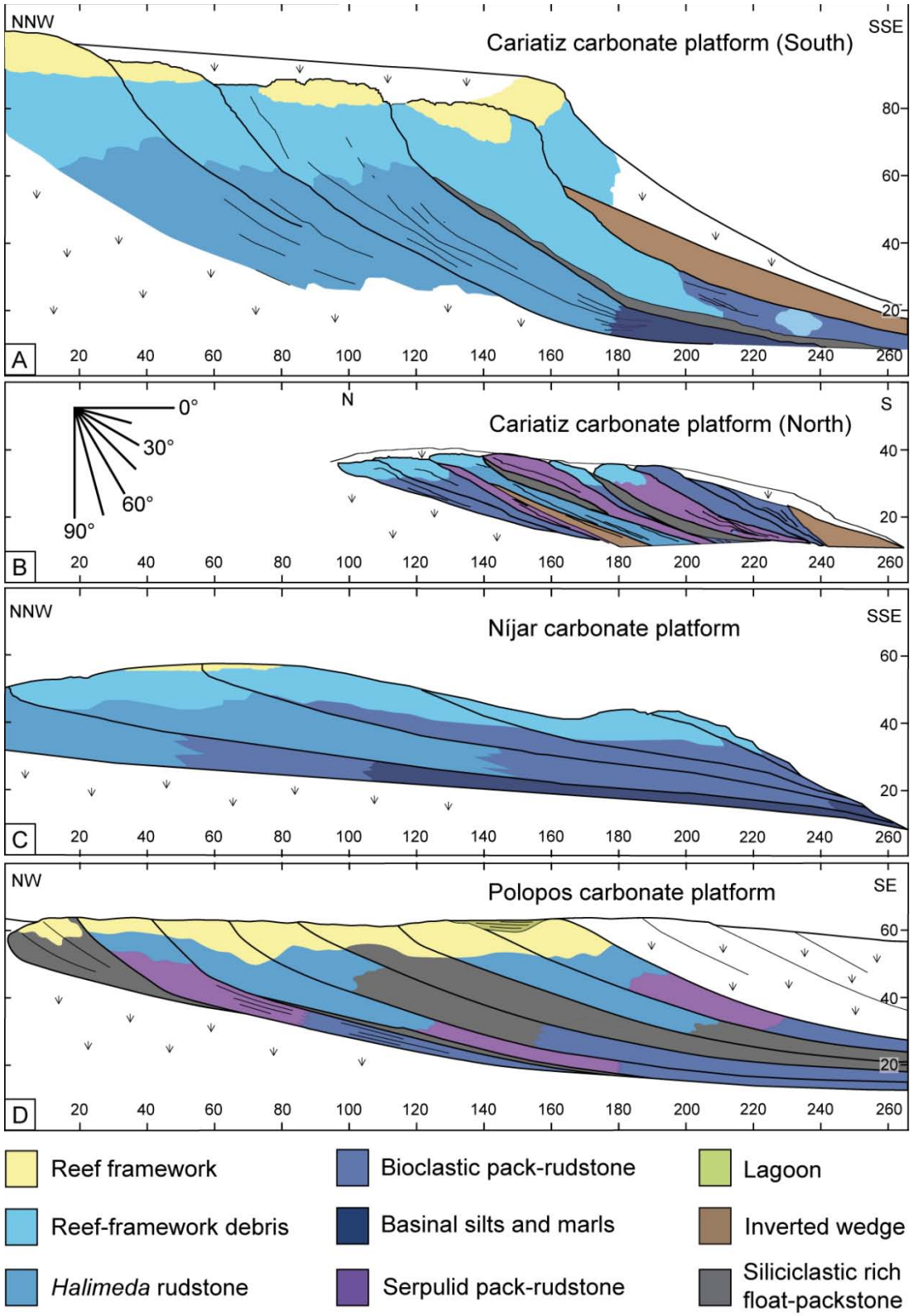

Fig. 5.11: Comparison of Miocene tropical platform slopes from SE Spain including: **A** southern and **B** northern Cariatiz carbonate platform slopes; **C** Níjar carbonate platform slopes; and **D** Polopos carbonate platform slopes.

In summary, the fluctuating amount of siliciclastics affected the slope facies in different ways by:
(1) *Introducing components which served as a growth substrate.*
(2) *Interrupting the development of the reef-framework facies*: Coarse-grained gravel of the fan deltas may provide an ideal substrate for coral colonization (Hayward, 1982), and *Porites* is one the most resistant corals to terrigenous influence (Esteban, 1980). An excessive siliciclastic influx, however, results in erosion of coral larvae and juvenile corals that die due to abrasion by sand as described by Rogers (1990) (Fig. 5.9). The turbidity of the water further suppresses the colonization by light-dependent zooxantelate corals (Buddemeier and Hopley, 1988; MacIntyre et al., 1992; Hopley, 1995). River discharge finally causes nutrient-rich conditions that limit reef growth (Hallock and Schlager, 1986).
(3) *Interrupting or avoiding the development of the Halimeda-rich facies*: High-nutrient conditions after river discharge might be suitable for *Halimeda* development as they preferentially developed in high-nutrient environments (Mankiewicz, 1988), but the turbidity associated with this discharge restricted the development of the light-dependent algae.
(4) *Favouring the growth of serpulid and red algae*: Serpulid and red algae were able to extensively develop as their main competitors for substrate and nutrients were absent due to the high turbidity. The pebbles provided a firm substrate where these encrusting organisms could grow.

5.5.3 Facies belts or facies mosaics?

Previous studies on western Mediterranean Miocene reefs (Esteban, 1996) used the scheme of facies belts to describe the facies distribution in reef slopes from Mallorca (Pomar, 1991; Pomar and Ward, 1994) and Almería, especially in the Níjar and Sorbas Basin (Dabrio et al., 1981; Franseen and Mankiewicz, 1991; Riding et al., 1991; Braga and Martín, 1996; Cuevas-Castell et al., 2007). Facies belts result from the combination of controlling factors such as the initial bathymetry as well as biological and sedimentary processes (Wright and Burgess, 2005). The Miocene tropical carbonate platform slopes of Almería show a downslope facies zonation, i.e. facies belts, by the basinward decrease in grain size, from reef-framework blocks and breccia to fine-grained packstone (Fig. 5.11).

The facies distribution of the Miocene platform slope was assumed to be static when performing architectural and stratigraphical analyses (Braga and Martín, 1996; Cuevas-Castell et al., 2007). Reolid et al. (2014), however, showed that slope facies arrays are not static, because changes in accommodation controlled the relative impact of processes affecting the slope (i.e. carbonate production and gravity flows) as well as their intensity,

and, in this respect the extension and occurrence of facies belts (Fig. 5.11; Reolid et al., 2014).

The model of facies belts alone, however, does not explain the facies variability of the Polopos and Cariatiz carbonate platform slopes (Fig. 5.11). Successive clinoform bodies display an apparently random facies distribution that cannot be predicted by Walther´s Law. Wright and Burgess (2005), drawing on Wilkinson et al. (1999), proposed the concept of facies mosaics to define slopes with an arrangement of lithological elements lacking significant linear trends but showing some statistically significant relationship between element size and frequency. According to Wright and Burgess (2005), rates of facies change typically exceed rates of accommodation space creation leading to the superimposing and mixing of sediments from different environments. Walther´s Law cannot predict the facies arrangement of these superimposing environments. According to Wright and Burgess (2005) the processes determining the facies distribution in a mosaic could be derived for each patch of sediment, but collecting such information is difficult to impossible, and most likely so complex that the resulting model lacks simple patterns.

In the case of the discussed Miocene tropical platform slopes it is proposed that the main causes of facies change are related to several factors including variations in the intensity of gravity-driven processes along the slope margin, and variation of the siliciclastic input (Fig. 5.12). The gravity-driven processes are usually triggered by collapse of the reef front (Riding at al., 1991; Reolid et al., 2014), and it is logical to assume that these collapses are not uniform, varying in occurrence and intensity along the platform edge (Fig. 5.12; Playton et al., 2010). The variability associated with gravity-driven processes may result in the reduction or obliteration of some facies belts (Fig. 5.12). Together with the lateral variability of the gravity-driven processes, the occurrence of siliciclastic influx into the systems leads to a local change in the water quality that changes the dominant facies assemblage. Serpulids and red algae are especially ubiquituous in areas with high amounts of siliciclastics, but their abundance may decrease with increasing distance from the siliciclastic influx (Fig. 5.12). Finally, sea-level fluctuations may also affect the facies variability (Reolid et al., 2014).

The apparently random facies association of the Miocene tropical carbonate slopes (Fig. 5.11), resulted from the patchy distribution of reef-framework debris, *Halimeda* accumulations, serpulids bioherms, and alluvial fans along the platform slope (Fig. 5.12). Here it is proposed that although the occurrence of siliciclastic input in the carbonate platform slopes seems to be random, the facies association related to the input is predictable (Fig. 5.12). Therefore a new model is needed, a more accurate one than the

static facies belts or the stochastic facies mosaic, that takes into account the facies variability related to intrinsic and extrinsic factors (i.e. siliciclastic input) (Fig. 5.12).

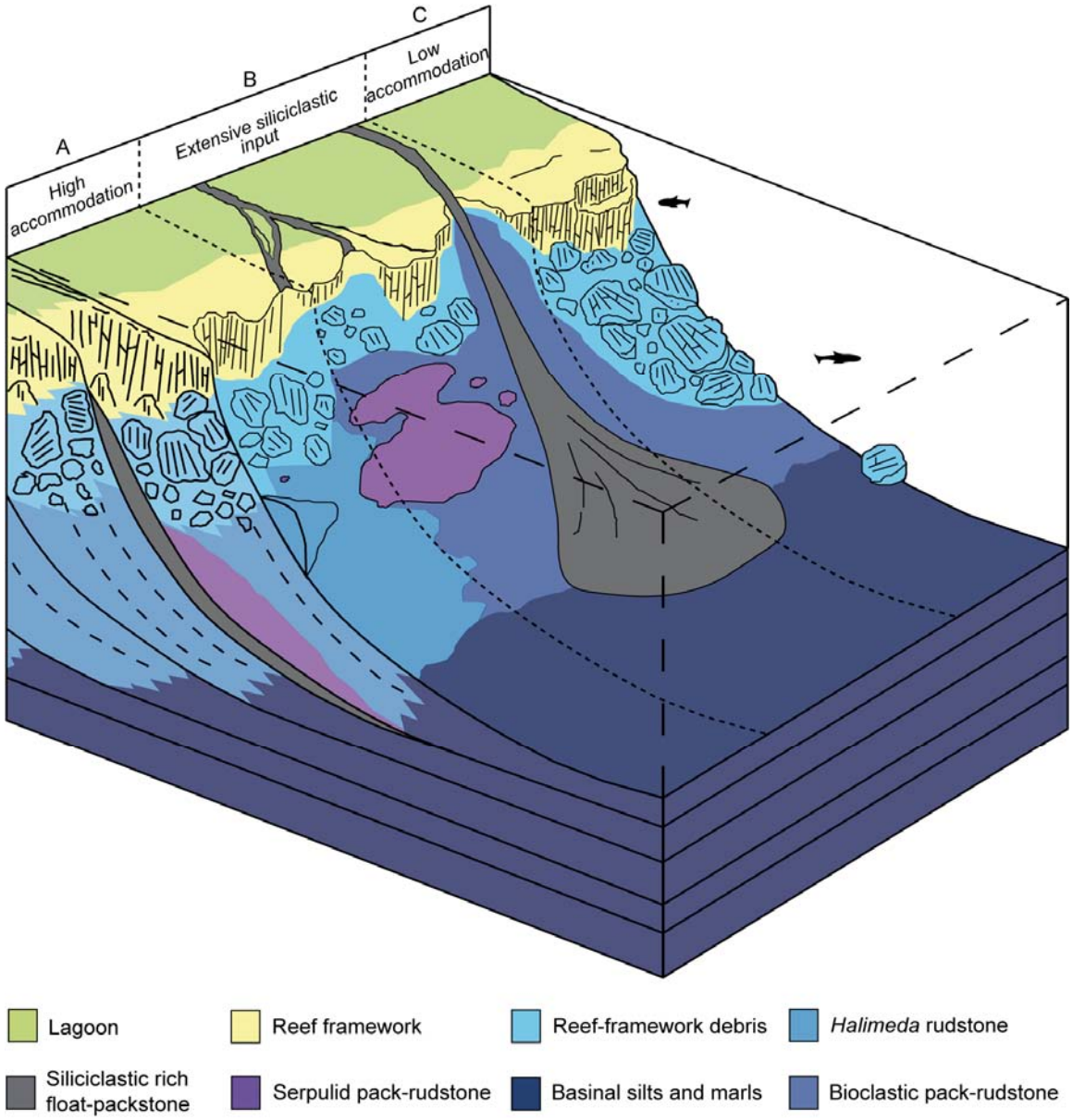

Fig. 5.12: Model showing the facies variability in the Miocene tropical carbonate platform slopes from SE Spain (Fig. 5.11). **A** Slope facies distribution under conditions of increased accommodation space. Facies display a downslope decrease of grain size, from reef-framework blocks and breccia to fine-grained sediments at the distal slope, and an extensive development of *Halimeda* algae related to the occurrence of upwelling. Such conditions are typical of highstand conditions (Reolid et al., 2014). **B** Facies distribution along a slope with episodic siliciclastic input. The abundance of siliciclastic causes a poor development or absence of reef framework and extensive *Halimeda* growths. Siliciclastics trigger the growth of large serpulid build-ups. **C** Facies distribution in slopes forming under conditions of decreased accommodation space affected by intensive rock falls and gravity flows. Some facies belts may be reduced or supressed by the extensive distribution of reef-framework debris.

5.6 Conclusions

Miocene tropical carbonate platform slopes show classical reef-slope facies distribution but also an unexpected abundance of serpulid-red algal facies, locally forming build-ups. It is proposed that the extensive occurrence of the serpulid-red algal rich facies is related to the presence of high amounts of siliciclastics, due to intermittent tectonic activity or weathering. Platform slopes affected by siliciclastics display higher facies variability than those exclusively dominated by carbonates. A new model, more accurate than the static facies belts or the stochastic facies mosaic, that considers the facies variability related to intrinsic and extrinsic factors is introduced. Accordingly, this study also adds an important element to the discussion concerning the validity of the concept of facies belts versus the concept of facies mosaics.

Chapter VI

Conclusions

This study aims to contribute to the better understanding of the factors controlling facies composition and distribution, geometries, as well as diagenesis of tropical carbonate platform slopes. For this purpose, Miocene tropical carbonate platform slopes from Almería (SE Spain) were mapped, sampled, and digitalized with LIDAR. Field observations were backed up by microfacies analysis, cathodoluminescence, SEM, EDX, and isotopic analysis. In addition, samples from the slopes of the Tongue of the Ocean (Bahamas) were petrographically analysed for a comparison of Neogene and Holocene depositional systems.

The following results were obtained:

(1) Tropical carbonate platform slope facies distribution and composition are the result of the interaction of several factors including coral growth, *in-situ* slope carbonate production, rockfalls and sediment gravity flows, hemipelagic rain, reworking of reef-slope facies, and siliciclastic input.

(2) Changes in accommodation space, ultimately related to sea-level fluctuations, control the intensity and relative impact of the factors affecting slope deposition, and, in this respect, the type of sediment that is finally accumulated along the platform slopes.

(3) Sea-level fluctuations change the hydrographical conditions of the basin eliminating water stratification and consequently the upwelling that promotes the abundance of *Halimeda* algae in the studied slopes.

(4) Serpulids and red algae are the main carbonate producers in platform slopes with high siliciclastic content. Serpulids can develop decametric bioherms that intercalate with the reef-slope facies.

(5) Slopes affected by siliciclastics display higher facies variability than those exclusively dominate by carbonates.

(6) Sea-level fluctuations related to precessional frequency between 5.89 and 5.87 Ma display a complete cycle of sea-level fall (23 ± 1 m) and rise (31 ± 1 m), as recorded by the occurrence of a palaeokarst in the Cariatiz carbonate platform (SE Spain).

(7) Miocene Cariatiz carbonate platform slopes from SE Spain and Holocene slopes from the Tongue of the Ocean in Bahamas present slopes with linear profiles and slope angles in excess of 35°. The deposits have similar grain sizes, textures, bioclastic components with

Halimeda plates as a major constituent and a micritic matrix with distinctive microfabrics indicative of microbial activity during deposition.

These results allow making further general conclusions that can be applied to other Neogene carbonate platform slopes elsewhere. It is proposed that slope facies changes are dynamic and which amend the models with static facies arrays. The patchy distribution of reef-framework debris, *Halimeda* accumulations, serpulids build-ups, and alluvial fans favours a new model which is more accurate than the classical and static facies belts or the stochastic facies mosaics to understand the facies distribution in such carbonate platform slopes.

Regarding the geometry of carbonate platform slopes, this study has shown that the steep angles observed in the tropical carbonate platform slopes of SE Spain resulted from extensive microbial binding of the slope sediment as in Palaeozoic and Triassic settings. It is therefore proposed that microbial binding is a previously underestimated factor of slope stabilization in Neogene and Holocene carbonate platform slopes.

Finally, the study of the diagenetic evolution together with classic pinning points of reef slopes has proven to be an accurate tool to calibrate the amplitude of sea-level fluctuations on Neogene carbonate platform slopes. For the first time this approach has allowed the outcrop comparison and calibration of amplitudes of Miocene high-frequency sea-level fluctuations which were previously reconstructed from proxies in pelagic sequences.

References

Adams, E.W., and Kenter, J.A.M. (2014) So different, yet so similar: comparing and contrasting siliciclastic and carbonate slopes. In: *Deposits, Architecture and Controls of Carbonate Margin, Slope and Basinal Settings* (Eds. Verwer, K., Playton, T.E., and Harris, P.M.). *SEPM Special Publication*, 105, 14–25.

Adams, E.W., and Schlager, W. (2000) Basic types of submarine slope curvature. *Journal of Sedimentary Research*, 70, 814–828.

Adams, E.W., Schlager, W., and Wattel, E. (1998) Submarine slopes with an exponential curvature. *Sedimentary Geology*, 117, 135–141.

Adams, E.W., Morsilli, M., Schlager, W., Keim, L., and Van Hoek, T. (2002) Quantifying the geometry and sediment fabric of linear slopes: examples from the Tertiary of Italy (Southern Alps and Gargano Promontory). *Sedimentary Geology*, 154, 11–30.

Adams, E.W., Schröder, S., Grotzinger, J.P., and McCormick, D.S. (2004) Digital reconstruction and stratigraphic evolution of a microbial-dominated, isolated carbonate platform (Terminal Proterozoic, Nama group, Namibia). *Journal of Sedimentary Research*, 74, 479–497.

Allen, J.R.L. (1985) Principles of Physical Sedimentology. George Allen and Unwin, London, 272 pp.

Andrews, J.E. (1986) Microfacies and geochemistry of Middle Jurassic algal limestones from Scotland. *Sedimentology*, 33, 499–520.

Andrews, J.E., Shepard, F.P., and Hurley, R.J. (1970) Great Bahama Canyon. *Bulletin of the Geological Society of America*, 81, 1061–1078.

Betzler, C., Lindhorst, S., Lüdmann, T., Weiss, B., Wunsch, M., and Braga, J.C. (2015) The leaking bucket of a Maldives atoll: Implications for the understanding of carbonate platform drowning. *Marine Geology*, 366, 16–33.

Berra, F. (2007) Sedimentation in shallow to deep water carbonate environments across a sequence boundary: effects of a fall in sea-level on the evolution of a carbonate system (Ladinian-Carnian, eastern Lombardy, Italy). *Sedimentology*, 54, 721–735.

Bosellini, A. (1984) Progradation geometries of carbonate platforms: examples from the Triassic of the Dolomites, northern Italy. *Sedimentology*, 31, l–24.

Braga, J.C., and Martín, J.M. (1996) Geometries of reef advance in response to relative sea-level changes in a Messinian (uppermost Miocene) fringing reef (Cariatiz Reef, Sorbas Basin, SE Spain). *Sedimentary Geology*, 107, 61–81.

Braga, J.C., Martín, J.M., and Alcalá, B. (1990) Coral reefs in coarse-terrigenous sedimentary environments (Upper Tortonian, Granada Basin, southern Spain). *Sedimentary Geology*, 66, 135–150.

Braga, J.C., Martín, J.M., and Riding, R. (1996) Internal structure of segment reefs: *Halimeda* algal mounds in the Mediterranean Miocene. *Geology*, 24, 35–38.

Braga, J.C., Martín, J.M., and Quesada, C. (2003) Patterns and average rates of late Neogene-Recent uplift of the Betic Cordillera, SE Spain. *Geomorphology*, 50, 3–26.

Budd, D.A. (1992) Dissolution of high-Mg calcite fossils and the formation of biomolds during mineralogical stabilization. *Carbonates and evaporites*, 7, 74–81.

Buddemeier, R.W., and Hopley, D. (1988) Turn-ons and turn-offs: causes and mechanisms of the initiation and termination of coral reef growth. *Proceedings of the Sixth International Coral Reef Congress, Townsville*, 1, 253–261.

Camoin, G.F., Gautret, P., Montaggioni, L.F., and Cabioch, G. (1999) Nature and environmental significance of microbialites in Quaternary reefs: the Tahiti paradox. *Sedimentary Geolology*, 126, 271–304.

Carannante, G., Esteban, M., Milliman, J.D., and Simone, L. (1988) Carbonate lithofacies as paleolatitude indicators: Problems and limitations. *Sedimentary Geology*, 60, 333–346.

Castagner, A., Jarochowskab, E., Munneckeb, A., and Desrochersa, A. (2014) Ultrastructures of porostromate microproblematica from a Mulde Event (Homerian, Silurian) bioherm in Podolia, Western Ukraine. *Estonian Journal of Earth Sciences*, 64, 24–30.

Cornée, J.J., Saint Martin, J.P., Conesa, G., Münch, P., André, J.P., Saint Martin, S., and Roger, S. (2004) Correlations and sequence stratigraphic model for Messinian carbonate platforms of the Western and central Mediterranean. *International Journal of Earth Sciences*, 93, 621–633.

Cuevas-Castell, J.M., Betzler, C., Rössler, J., Hüssner, H., and Peinl, M. (2007) Integrating outcrop data and forward computer modelling to unravel the development of a Messinian carbonate platform in SE Spain (Sorbas Basin). *Sedimentology*, 54, 423–441.

Dabrio, C.J., Esteban, M., and Martín, J.M. (1981) The coral reef of Níjar, Messinian (uppermost Miocene), Almería Province, S.E. Spain. *Journal of Sedimentary Petrology*, 51, 521–539.

Dabrio, C.J., Martín, J.M., and Megías, A.G. (1985) The tectosedimentary evolution of Mio-Pliocene reefs in the province of Almería (SE Spain). In: *Sixth European Regional Meeting of the International Association of Sedimentologists* (Eds. Milá, M.D., and Rosell, J.). *Excursion guidebook*, 269–305.

Della Porta, **G., Kenter, J.A.M., Bahamonde, J.R., Immenhauser, A., and Villa, E.** (2003) Microbial boundstone dominated carbonate slope (Upper Carboniferous, N Spain): microfacies, lithofacies distribution and stratal geometry. *Facies*, 49, 175–208.

Della Porta, G., Kenter, J.A.M., and Bahamonde, J.R. (2004) Depositional facies and stratal geometry of an Upper Carboniferous prograding and aggrading high-relief carbonate platform (Cantabrian Mountains, N Spain). *Sedimentology*, 51, 267–295.

Drew, E.A., and Abel, K.M. (1983) Growth of *Halimeda* in reefal and inter-reefal environments. In: *Great Barrier Reef Conference* (Eds. Baker, J.T., Carter, R.M., Sammarco, P.W., and Stark, K.P.). *Proceedings*, 299 –304.

Drzewiecki, P.A., and Simó, J.A. (2002) Depositional processes, triggering mechanisms and sediment composition of carbonate gravity flow deposits: examples from the Late Cretaceous of the south-central Pyrenees, Spain. *Sedimentary Geology*, 146, 155–189.

Eberli, G.P., and Ginsburg, R.N. (1989) Cenozoic progradation of northwestern Great Bahama Bank, record of lateral platform growth and sea-level fluctuations. In: *Controls on Carbonate Platform and Basin Development* (Eds. Crevello, P.D., Wilson, J.L., Sarg, J.F., and Read, J.F.). *SEPM Special Publication*, 44, 339 –354.

Enos, P. (1977) Tamabra Limestone of the Poza Rica Trend, Cretaceous, Mexico. In: *Deep-water Carbonate Environments* (Eds. Cook, H.E., and Enos. P). *SEPM Special Publication*, 25, 273–314.

Esteban, M. (1980) Significance of the Upper Miocene coral reefs of the Western Mediterranean. *Palaeogeography, Palaeoclimatology, Palaeoecology*, 29, 169–188.

Esteban, M. (1996) An overview of Miocene reefs from Mediterranean areas: general trends and facies models. In: *Models for Carbonate Stratigraphy from Miocene Reef Complexes of Mediterranean Regions* (Eds. Franseen, E.K., Esteban, M., Ward, W.C., and Rouchy, J.M.). *SEPM Concepts in Sedimentology and Paleontology*, 5, 3–53.

Franseen, E.K., and Goldstein, R.H. (1996) Paleoslope, sea-level and climate controls on upper Miocene platform evolution, Las Negras area, Southeastern Spain. In: *Models for Carbonate Stratigraphy from Miocene Reef Complexes of Mediterranean Regions* (Eds. Franseen, E.K., Esteban, M., Ward, W.C., and Rouchy, J.M.). *SEPM Concepts in Sedimentology and Paleontology*, 5, 159–176.

Franseen, E.K., and Mankiewicz, C. (1991) Depositional sequences and correlation of middle (?) to late Miocene carbonate complexes, Las Negras and Níjar areas, southeastern Spain. *Sedimentology*, 38, 871–898.

Franseen, E.K., Esteban, M., Ward, W.C., and Rouchy, J.M. (1996) Models for Carbonate Stratigraphy from Miocene Reef Complexes of Mediterranean Regions: Introduction. In: *Models for Carbonate Stratigraphy from Miocene Reef Complexes of Mediterranean Regions* (Eds. Franseen, E.K., Esteban, M., Ward, W.C., and Rouchy, J.M.). *SEPM Concepts in Sedimentology and Paleontology*, 5, v–ix.

Giaconia, F., Booth-Rea, G., Martínez-Martínez, J.M., Azañón, J.V., Pérez-Peña, M., Pérez-Romero, J., and Villegas, I. (2012) Geomorphic evidence of active tectonics in the Sierra Alhamilla (eastern Betics, SE Spain). *Geomorphology*, 145-146, 90–106.

Gill, A.E., and Clarke, A.J. (1974) Wind-induced upwelling, coastal currents, and sea level changes. *Deep-Sea Research*, 21, 325–345.

Ginsburg, R.N. (2001) The Bahamas drilling project: Background and acquisition of cores and logs. In: *Subsurface Geology of a Prograding Carbonate Platform Margin Great Bahama Bank* (Ed. Ginsburg, R.N.). *SEPM Special Publications*, 70, 3–13.

Goldstein, R.H., and Franseen, E.K. (1995) Pinning points: a method of providing quantitative constraints on relative sea-level history. *Sedimentary Geolology*, 95, l–10.

Goldstein, R.H., Franseen, E.K., and Mills, M.S. (1994) Diagenesis associated with subaerial exposure of Miocene strata, southeastern Spain: Implications for sea-level change and preservation of low-temperature fluid inclusions in calcite cement. *Geochimica et Cosmochimica Acta*, 54, 699–704.

Grammer, G.M. (1991) Formation and evolution of Quaternary carbonate foreslopes, Tongue of the Ocean, Bahamas (unpublished Ph.D. thesis): University of Miami, Rosenstiel School of Marine and Atmospheric Sciences, Miami, 375 pp.

Grammer, G.M., and Ginsburg, R.N. (1992) Highstand vs. lowstand deposition on carbonate platform margins: Insight from Quaternary foreslopes in the Bahamas. *Marine Geology*, 103, 125–136.

Grammer, G.M., Ginsburg, R.N., Swart, P.K., McNeil, D.F., Jull, A.J.T., and Prezbindowski, D.R. (1993a) Rapid growth rates of syndepositional marine aragonite cements in steep marginal slope deposits, Bahamas and Belize. *Journal of Sedimentary Petrology*, 63, 983–989.

Grammer, G.M., Ginsburg, R.N., and Harris, P.M. (1993b) Timing of deposition and failure of steep carbonate slopes in response to a high-amplitude/high-frequency fluctuation in sea level, Tongue of the Ocean, Bahamas. In: *Recent advances and applications of carbonate sequence stratigraphy* (Eds. Loucks, R., and Sarg, R.). *AAPG Memoir*, 57, 107–131.

Haddad, A., Aissaoui, M.D., and Soliman, M.A. (1984) Mixed carbonate-silicic1astic sedimentation on a Miocene fault-block, Gulf of Suez. *Sedimentary Geology*, 37, 182–202.

Halfar, J., and Mutti, M. (2005) Global dominance of coralline red-algal facies: a response to Miocene oceanographic events. *Geology*, 33, 481–484.

Hallock, P., and Schlager, W. (1986) Nutrient excess and the demise of coral reefs and carbonate platforms. *Palaios*, 1, 389–398.

Haq, B.U., Hardenbol, J., and Vail, P.R. (1987) Chronology of fluctuating sea levels since the Triassic (250 million years ago to present). *Science*, 235, 156–167.

Hayward, A.B. (1982) Coral Reefs in a Clastic Sedimentary Environment: Fossil (Miocene, S.W. Turkey) and Modern (Recent, Red Sea). *Coral reefs*, 1, 109–114.

Hemming, N.G., Meyers, W.J., and Grams, J.C. (1989) Cathodoluminescence in diagenetic calcites: the roles of Fe and Mn as deduced from electron probe and spectrophotometric measurements. *Journal of Sedimentary Petrology*, 59, 404–411.

Hine, A.C., Locker, S.D., Tedesco, L.P., Mullins, H.T., Hallock, P., Belknap, D.F., Gonzales, J.L., Neumann, A.C., and Snyder, S.W. (1992) Megabreccia shedding from modern, low relief carbonate platforms, Nicaraguan Rise. *Geological Society of America Bulletin*, 104, 928–943.

Hopley, D. (1995) Continental shelf reef systems. In: *Coastal Evolution: Late Quaternary Shoreline Morphodynamics* (Eds. Carter, R.W.G., and Woodroffe, C.D.). Cambridge University Press, Cambridge, 517 pp.

Hudson, J.D. (1977) Stable isotopes and limestone lithification. *Journal of the Geological Society of London*, 133, 637–660.

James, N.P., Coniglio, M., Aissaoui, D.M., and Purser, G.H. (1988) Facies and geologic history of an exposed Miocene rift-margin carbonate platform: Gulf of Suez, Egypt. *The American Association of Petroleum Geologists Bulletin*, 72, 555–572.

Jiménez, A.P., and Braga, J.C. (1993) Occurrence and taphonomy of bivalves from the Níjar reef (Messinian, Late Miocene, SE Spain). *Palaeogeography, Palaeoclimatology, Palaeoecology*, 102, 239–251.

Kendall, C.G.S.C., and Schlager, W. (1981) Carbonates and relative changes in sea-level. *Marine Geology*, 44, 181–212.

Kenter, J.A.M. (1990) Carbonate platform flanks: Slope angle and sediment fabric. *Sedimentology*, 72, 777–794.

Kenter, J.A.M., Harris, P.M., and Della Porta, G. (2005) Steep microbial boundstone-dominated platform margins - examples and implications. *Sedimentary Geology*, 178, 5–30.

Keim, L., and Schlager, W. (2001) Quantitative compositional analysis of a Triassic carbonate platform (Southern Alps, Italy). *Sedimentary Geology*, 139, 261–283.

Kirkby, M.J. (1987) General models of long-term slope evolution through mass movement. In: *Slope Stability, Geotechnical Engineering and Geomorphology* (Eds. Anderson, M.G., and Richards, K.S.). Jon Wiley and Sons, London, 648 pp.

Kleverlaan, K. (1989) Three distinctive feeder-lobe systems within one time slice of the Tortonian Tabernas fan, SE Spain. *Sedimentology*, 36, 25–45.

Krijgsman, W., Hilgen, F.J., Raffi, I., Sierro, F.J., and Wilson, D.S. (1999) Chronology, causes and progression of the Messinian salinity crisis. *Nature*, 400, 652–655.

Land, L.S. (1970) Phreatic versus vadose meteoric diagenesis of limestones: evidences from a fossil water table. *Sedimentology*, 14, 175–185.

Lehrmann, D.J. (1999) Early Triassic calcimicrobial mounds and biostromes of the Nanpanjiang Basin, South China. *Geology*, 27, 357–362.

Li, Z., Goldstein, R.H., and Franseen, E.K. (2014) Climate, duration, and mineralogy controls on meteoric diagenesis, La Molata, Southeast Spain. *Interpretation*, 2, SF111–SF123.

MacIntyre, I.G., Glynn, P.W., and Cortes, J. (1992) Holocene reef history in the eastern Pacific: mainland Costa Rica, Cano Island, Cocos Island and Galapagos Islands. *Proceedings of the Seventh International Coral Reef Symposium Guam*, 2, 1174–1184.

McIlreath, I.A., and James, N.P. (1978) Facies models 13, Carbonate slopes. *Geoscience Canada*, 5, 189–199.

Mankiewicz, C. (1988) Occurrence and paleocologic significance of *Halimeda* in late Miocene reefs, Southeastern Spain. *Coral Reefs*, 6, 271–279.

Martín, J.M., and Braga, J.C. (1989) Arrecifes Messinienses de Almería. Tipologías de crecimiento, posición estratigráfica y relación con las evaporitas. *Geogaceta*, 7, 66–68.

Martín, J.M., and Braga, J.C. (1994) Messinian events in the Sorbas Basin in the Southeastern Spain and their implications in the recent history of the Mediterranean. *Sedimentary Geology*, 90, 257–268.

Martín, J.M., Braga, J.C., and Rivas, P. (1989) Coral successions in Upper Tortonian reefs in SE Spain. *Lethaia*, 22, 271–286.

Martín, J.M., Braga, J.C., and Riding, R. (1997) Late Miocene *Halimeda* alga-microbial segments reefs in the marginal Mediterranean Sorbas Basin, Spain. *Sedimentology*, 44, 441–456.

Martinsen, O. (1994) Mass movements. In: *The Geological Deformation of Sediments* (Ed. Maltman, A.). Chapman & Hall, London, 127–165.

Meyers, W. (1978) Carbonate cements: Their regional distribution and interpretation in Mississippian limestones of southwestern New Mexico. *Sedimentolology*, 25, 371–400.

Miller, K.G., Kominz, M.A., Browning, J.V., Wright, J.D., Mountain, G.S., Katz, M.E., Sugarman, P.J., Cramer, B.S., Christie-Blick, N., and Pekar, S.F. (2005) The Phanerozoic record of global sea-level change. *Science*, 310, 1293–1298.

Miller, K.G., Mountain, G.S., Wright, J.D., and Browning, J.V. (2011) A 180-million-year record of sea level and ice volume variations from continental margin and deep-sea isotopic records. *Oceanography*, 24, 40–53.

Miller, K.G., Wright, J.D., Browning, J.V., Kulpecz, A., Kominz, M., Naish, T.R., Cramer, B.S., Rosenthal, Y., Peltier, W.R., and Sosdian, S. (2012) High tide of the warm Pliocene: Implications of global sea level for Antarctic deglaciation. *Geology*, 40, 407–410.

Mutti, M., Piller, W., and Betzler, C. (2010) Miocene carbonate systems: an introduction. In: *Carbonate Systems During the Oligocene-Miocene Climatic Transition* (Eds. Mutti, M., Piller, W., and Betzler, C.). *IAS Special Publication*, 42, vii–xii.

Navarro, V., Reolid, M., Molina, J.M., and Ruiz-Ortiz, P.A. (2008) Slope breccias colonized by bivalves and serpulids during the Middle Jurassic (Subbetic, SE Spain). *Facies*, 54, 403–415.

Nelson, C.S., and Smith, A.M. (1996) Stable oxygen and carbon isotope compositional fields for skeletal and diagenetic components in New Zealand Cenozoic nontropical carbonate sediments and limestones: a synthesis and review. *New Zealand Journal of Geology and Geophysics*, 39, 93–107.

Pedrera, A., Galindo-Zaldívar, J., Marín-Lechado, C., García-Tortosa, F.J., Ruano, P., Garrido, A.L., and Giaconia, F. (2012) Recent and active faults and folds in the central-eastern Internal Zones of the Betic Cordillera. *Journal of Iberian Geology*, 38, 191–208.

Playton, T.E., Janson, X., and Kerans, C. (2010) Carbonate slopes. In: *Facies Models 4*, *GEOtext 6: Geological Association of Canada* (Eds. James, N.P., and Dalrymple, R.W.). St John's, Newfoundland, 449–476.

Pomar, L. (1991) Reef geometries, erosion surfaces and high-frequency sea-level changes, upper Miocene Reef Complex, Mallorca, Spain. *Sedimentology*, 38, 243–269.

Pomar, L., and Ward, W.C. (1994) Response of late Miocene Mediterranean reef platform to high-frequency eustasy. *Geology*, 22, 131–134.

Principaud, M., Mulder, T., Gillet, H., and Borgomano, J. (2015) Large-scale carbonate submarine mass-wasting along the northwestern slope of the Great Bahama Bank (Bahamas): Morphology, architecture, and mechanisms. *Sedimentary Geology*, 317, 27–42.

Reid, R.P., Dupraz, C., Visscher, P.T., Decho, A.W., and Sumner, D.Y. (2003) Microbial processes forming modern marine stromatolites: microbe-mineral interactions with a three billion-year rock record. In: *Fossil and Recent Biofilms - a Natural History of Life on Earth* (Eds. Krumbein, W., Paterson, D.M., and Zavarzin, G.A.). *Kluwer Academic Publishers*, 103–118.

Reolid, J., Betzler, C., Braga, J.C., Martín, J.M., Lindhorst, S., and Reijmer, J.J.G. (2014) Reef Slope Geometries and Facies Distribution: Controlling Factors (Messinian, SE Spain). *Facies*, 60, 737–753. (Chapter II of this thesis).

Richter, D.K., Neuser, R.D., Schreuer, J., Gies, H., and Immenhauser, A. (2011) Radiaxial-fibrous calcites: A new look at an old problem. *Sedimentary Geology*, 239, 23–36.

Riding, R. (2000) Microbial carbonates: the geological record of calcified bacterial-algal mats and biofilms. *Sedimentology*, 47, 179–214.

Riding, R., Martín, J.M., and Braga, J.C. (1991) Coral stromatolite reef framework, Upper Miocene, Almería, Spain. *Sedimentology*, 38, 799–818.

Riding, R., Braga, J.C., and Martín, J.M. (1999) Late Miocene Mediterranean desiccation: topography and significance of the 'Salinity Crisis' erosion surface on-land in Southeast Spain. *Sedimentary Geology*, 123, 1–7.

Rodríguez-Tovar, F.J., Sánchez-Almazo, I., Pardo-Igúzquiza, E., Braga, J.C., and Martín, J.M. (2013) Incidence of obliquity and precession-forced Milankovitch cycles in the western Mediterranean: early Messinian sedimentation in the Sorbas Basin (Almería, Southern Spain). *International Journal of Earth Sciences (Geologische Rundschau)*, 102, 1735–1755.

Rogers, C.S. (1990) Responses of coral reefs and reef organisms to sedimentation. *Marine Ecology Progress Series*, 62, 185–202.

Ruegg, G.J.H. (1964) Geologische onderzoekingen in het bekken van Sorbas, S.E. Spanje. Geological Institute, University of Amsterdam, Amsterdam, 64 pp.

Saint Martin, J.P., Pestrea, S., and Conesa, G. (2001) Messinian diatom assemblages of infra-gypsum diatomites in the Sorbas basin (SE Spain). *Cryptogamie Algology*, 22, 127–149.

Sánchez-Almazo, I.M., Braga, J.C., Dinarès-Turell, J., Martín, J.M., and Spiro, B. (2007) Palaeoceanographic controls on reef deposition: the Messinian Cariatiz reef (Sorbas Basin, Almería, SE Spain). *Sedimentolology*, 54, 637–660.

Sanford, W.E., and Konikow, L.F. (1989) Porosity development in coastal carbonate aquifers. *Geology*, 17, 249–252.

Schlager, W. (1981) The paradox of drowned reefs and carbonate platforms. *Geological Society of America*, 92, 197–211.

Schlager, W. (1989) Drowning unconformities on carbonate platforms. In: *Controls on Carbonate Platform and Basin Development* (Eds. Crevello, P.D., Wilson, J.L., Sarg, J.F., and Read, J.F.). *SEPM Special Publications*, 44, 15–26.

Schlager, W. (2005) Carbonate sedimentology and sequence stratigraphy. In: *Concepts in Sedimentology and Paleontology 8*. SEPM, Tulsa, 200 pp.

Schlager, W., and Adams, E.W. (2001) Model for the sigmoidal curvature of submarine slopes. *Geology*, 29, 883–886.

Schlager, W., and Camber, O. (1986) Submarine slope angles, drowning unconformities, and self-erosion of limestone escarpments. *Geology*, 14, 762–765.

Schlager, W., and James, N.P. (1978) Low-magnesian calcite limestones forming at the deep-sea floor Tongue of the Ocean, Bahamas. *Sedimentology*, 25, 675–702.

Schlager, W., and Reijmer, J.J.G. (2009) Carbonate platform slopes of the Alpine Triassic and the Neogene - a comparison. *Austrian Journal of Earth Sciences*, 102, 4–14.

Sierro, F.J., Flores, J.A., Civis, J., González-Delgado, J.A., and Francés, G. (1993) Late Miocene globorotaliid event-stratigraphy and biogeography in the NE-Atlantic and Mediterranean. *Marine Micropaleontology*, 21, 143–168.

Sola, F., Braga, J.C., and Aguirre, J. (2013) Hooked and tubular coralline algae indicate seagrass beds associated to Mediterranean Messinian reefs (Poniente Basin, Almería, SE Spain). *Palaeogeography, Palaeclimatology, Palaeoecology*, 374, 218–229.

Swart, P.K. (2015) The geochemistry of carbonate diagenesis: The past, present and future. *Sedimentology*, 62, 1233–1304.

Vacher, H.L., Bengstsson, T.O., and Plummer, L.N. (1990) Hydrology of meteoric diagenesis: Residence time of meteoric ground water in island fresh-water lenses with application to aragonite-calcite stabilization rate in Bermuda. *Geological Society of America Bulletin*, 102, 223–232.

Van Hengstum, P.J., Scott, D.B., Gröcke, D.R., and Charette, M.A. (2011) Sea level controls sedimentation and environments in coastal caves and sinkholes. *Marine Geology*, 286, 35–50.

Völk, H.R., and Rondeel, H.E. (1964) Zur Gliederung des Jungtertiärs im Becken von Vera, Südost-Spanien. *Geologie en Mijnbouw*, 43, 310–315.

Warrlich, G., Bosence, D., and Waltham, D. (2005) 3D and 4D controls on carbonate depositional systems: sedimentological and sequence stratigraphic analysis of an attached carbonate platform and atoll (Miocene, Níjar Basin, SE Spain). *Sedimentology*, 52, 363–389.

Webb, G.E., and Jell, J.S. (1997) Cryptic microbialite in subtidal reef framework and intertidal solution cavities in beachrock, Heron Reef, Great Barrier Reef, Australia: Preliminary observations. In: *Biosedimentology of microbial buildups, International Geological Correlation Programme Project No. 380, Proceedings of 2nd Meeting* Göttingen, Germany (Eds. Neuweiler, F., Reitner, J., and Monty, C.). *Facies*, 36, 219–223.

Wilkinson, B.H., Drummond, C.N., Diedrich, N.W., and Rotman, E.D. (1999) Poisson processes of carbonate accumulation on Paleozoic and Holocene platforms. *Journal of Sedimentary Research*, 69, 338–350.

Willian, C.S., Uchupi, E., Ballard, R.D., and Dettweiler, T.K. (1989) Sea-Floor Observations in the Tongue of the Ocean, Bahamas: An Argo/SeaMARC Survey. *Geo-Marine Letters*, 9, 171–178.

Wilson, J.L. (1975) Carbonate Facies in Geologic History. Springer, New York, 471 pp.

Wright, V.P., and Burgess, P.M. (2005) The carbonate factory continuum, facies mosaics and microfacies: an appraisal of some of the key concepts underpinning carbonate sedimentology. *Facies*, 51, 17–23.

Zhong, G., Geng, J., Kin Wong, H., Ma, Z., and Wu, N. (2004) A semi-quantitative method for the reconstruction of eustatic sea level history from seismic profiles and its

application to the southern South China Sea. *Earth and Planetary Science Letters*, 223, 443–459.